Technische Universität München

Technische Universität München

Fakultät für Medizin

The Role of Adipocyte-derived Extracellular Vesicles in Metabolic Diseases

Michaela Bauer

Vollständiger Abdruck der von der Fakultät für Medizin der Technischen Universität München zur Erlangung des akademischen Grades einer

Doktorin der Naturwissenschaften (Dr. rer. nat.)

genehmigten Dissertation.

Vorsitz: Prof. Dr. Lars Mägdefessel

Prüfende/-r der Dissertation: 1. Prof. Dr. Paul Th. Pfluger

2. apl. Prof. Dr. Johannes Beckers

Die Dissertation wurde am 14.11.2022 bei der Technischen Universität München eingereicht und durch die Fakultät für Medizin am 03.01.2023 angenommen.

Summary

Extracellular vesicles (EVs) are nano-sized vesicles that are secreted by nearly all cell types and can be found in various bodily fluids like blood, cerebrospinal fluid, saliva, urine or breast milk. Formerly solely considered as cellular trash bags, EVs emerged in recent years as novel mediators for intercellular and even inter-organ communication. EVs carry different macromolecules, including proteins, lipids, RNA and miRNA, providing a snapshot of the parental cell at the time of release. By transferring this cell-specific cargo to recipient cells, EVs can affect multiple signalling pathways simultaneously and thereby lead to potent functional effects. As they are systemically transported via the bloodstream and other bodily fluids, EVs can not only trigger paracrine effects but also target distinct organs in an endocrine fashion to help maintaining physiologic homeostasis. EVs secreted from diseased organs can moreover exacerbate pathological conditions like tumour metastasis, immunological disorders, neurodegenerative and cardiovascular diseases.

This thesis aimed to investigate the impact of EVs on metabolic diseases, specifically the role of adipocyte-derived EVs as novel endocrine signalling entity between the adipose tissue and different metabolic target organs. As especially adipose tissue is subjected to fundamental changes during the development of obesity, the first objective of this thesis was the investigation of the cargo of lean and obese adipocyte EVs and their potentially differing functional impact. Based on establishing a protocol for EV isolation from murine and human adipocytes that could fully avoid co-isolation of confounding EVs originating from the stromal vascular fraction, this thesis revealed that obesity induces distinct shifts in the proteome and miRNA profile in EVs from murine epididymal white adipose tissue (eWAT). Investigation of the EV biodistribution *in vivo* revealed an organ tropism towards metabolically active target organs such as liver, pancreas and eWAT. Functional assays investigating adipocyte differentiation, browning or macrophage polarization did not show an impact of adipocyte EVs. However, an influence of eWAT EVs on insulin secretion was observed, shown by an increased glucose stimulated insulin secretion from pancreatic islets after treatment with obese adipocyte EVs. By this mechanism, EVs may prime the metabolism to meet a higher insulin demand in a state of obesity and insulin resistance. Additional experiments investigating the systemic effects of the exosome secretion inhibitor GW4869 also suggested a glucoregulatory role for EVs. Taken together, this thesis showed that adipocyte-derived EVs originating from obese eWAT, being considered the more relevant adipose tissue depot in the context of metabolic diseases, serve as regulators of insulin secretion.

The second part of this thesis aimed to investigate the potential role of adipocyte EVs as biomarkers for metabolic diseases. A monoclonal antibody specific for adipocyte-derived EVs was generated, serving as technical tool as well as a possible source for the detection of biomarkers of adipocyte status. Following the development and screening accomplished in this thesis, the ultimate goal of this project is the investigation of human blood samples. By specifically analysing adipocyte EVs of patients with different metabolic states like lean, obese or healthy obese, adipocyte EVs could serve as liquid biopsies for adipose tissue health in future studies.

Zusammenfassung

Extrazelluläre Vesikel (EVs) sind Mikrovesikel im Nano-Bereich, die von fast allen Zelltypen sekretiert werden und in verschiedenen Körperflüssigkeiten wie Blut, Zerebrospinalflüssigkeit, Speichel, Urin oder Muttermilch nachgewiesen werden konnten. Ursprünglich wurden EVs als zelluläre Müllabfuhr betrachtet, in den letzten Jahren sind sie jedoch mehr und mehr als neuartige Signalüberträger zwischen Zellen und Organen in den Fokus gerückt. EVs transportieren verschiedene Makromoleküle wie Proteine, Lipide, RNA und miRNA und stellen dabei eine Momentaufnahme der Zelle zum Zeitpunkt der Freisetzung dar. Durch die Übertragung dieser Zell-spezifischen Moleküle auf Zielzellen können EVs simultan zahlreiche Signalwege ansprechen und so potente funktionale Effekte hervorrufen. Da EVs systemisch über die Blutzirkulation und andere Körperflüssigkeiten transportiert werden, können sie nicht nur parakrine Effekte verursachen, sondern auch endokrin auf weit entfernte Organe wirken. Neben der Aufrechterhaltung physiologischer Homöostase im gesunden Organismus können EVs aus erkrankten Organen pathologische Zustände verschärfen, wie zum Beispiel Metastasenbildung bei Krebserkrankungen oder immunologische sowie neurodegenerative und kardiovaskuläre Erkrankungen.

Ziel dieser Arbeit war die Untersuchung der Beeinflussung metabolischer Störungen durch EVs, im Speziellen die Rolle von EVs aus Adipozyten als neuartige endokrine Signalüberträger zwischen Fettgewebe und verschiedenen metabolischen Organen. Da insbesondere das Fettgewebe bei der Entstehung von Adipositas von substanziellen Veränderungen betroffen ist, war die erste Zielsetzung dieser Arbeit die Charakterisierung von EVs isoliert aus Adipozyten aus Fettgewebe von dünnen bzw. adipösen Mäusen. Zudem sollte gezeigt werden, ob diese Adipozyten-EVs aus dünnen verglichen mit dicken Tieren unterschiedliche Einflüsse auf Zielzellen und Gewebe haben können. Zunächst wurde ein Protokoll zur Isolierung von EVs aus murinen und humanen Adipozyten etabliert, das die störende Co-Isolation von EVs umgeht, die von der stromalen-vaskulären Fraktion des Fettgewebes sekretiert werden. Anschließende Studien konnten zeigen, dass Adipositas zu einer Verschiebung des Proteom- und miRNA-Profils von EVs, die von murinem epididymalem weißem Fettgewebe (eWAT) isoliert wurden, führte. Untersuchungen der EV-Bioverteilung *in vivo* zeigten eine organspezifische Akkumulation in metabolisch aktiven Zielorganen wie Leber, Pankreas und eWAT. Darauf basierende funktionale Studien in Adipozyten zur Differenzierung oder zur Entwicklung von braunen Fettzellmerkmalen konnten keinen Einfluss von Adipozyten-EVs feststellen, auch auf die Polarisierung von Makrophagen wurde kein Effekt beobachtet. Es konnte jedoch eine Beeinflussung der Insulinsekretion durch eWAT EVs entdeckt werden. Spezifisch konnte hierbei nach Behandlung mit Adipozyten-EVs aus adipösem Fettgewebe eine erhöhte

Glukose-stimulierte Insulinsekretion in pankreatischen Inselzellen festgestellt werden. Dieser spezifische, insulinotrope Effekt von EVs kann als Anpassung des Organismus an einen erhöhten Insulinbedarf gedeutet werden, der zur Aufrechterhaltung der Glukosehomöostase bei Adipositas mit etablierter Insulinresistenz benötigt wird. Zusätzliche systemische Experimente mit dem Exosomen-Sekretionsinhibitor GW4869 konnten ebenfalls eine Beteiligung von EVs an der Glukoseregulation feststellen. Zusammenfassend konnte diese Arbeit zeigen, dass EVs von Adipozyten aus adipösem eWAT, welches als relevantes Fettdepot für die Entwicklung metabolischer Erkrankungen gilt, als Einflussfaktoren auf die Insulinsekretion wirken.

Der zweite Teil dieser Arbeit war der Untersuchung von Adipozyten-EVs als mögliche Biomarker für metabolische Erkrankungen gewidmet. Dazu wurde ein monoklonaler Antikörper generiert, der spezifisch EVs aus Adipozyten bindet. Dieser könnte sowohl als technisches Werkzeug eingesetzt werden, als auch als mögliche Grundlage zur Identifizierung von Biomarkern für den metabolischen Status von Adipozyten dienen. Anschließend an die im Rahmen dieser Arbeit durchgeführte Antikörper-Entwicklung und das Screening, besteht die finale Zielsetzung dieses Projekts in der Untersuchung humaner Blutproben. Die Generierung des Antikörpers dient ultimativ der Nutzung von Adipozyten-EVs als Flüssigbiopsien zur Bestimmung der Fettgewebsgesundheit aus Blutproben und damit der Stratifizierung von Patienten mit verschiedenen metabolischen Zuständen wie normalgewichtig und gesund, krankhaft adipös mit Begleiterkrankungen sowie übergewichtig aber metabolisch gesund.

Table of Contents

List of Figures

List of Tables

List of Abbreviations

ABC	ammoniumbicarbonate
AT	adipose tissue
ATCC	American Type Culture Collection
AUC	area under the curve
BAT	brown adipose tissue
BCA	bicinchoninic acid
BMDM	bone marrow-derived macrophages
BMI	body mass index
BSA	bovine serum albumin
cDNA	complementary deoxyribonucleic acid
CNBr	cyoanogen bromide
CTB	Choleratoxin subunit B
DAPI	4',6-diamidino-2-phenylindole
DiR	1,1'-dioctadecyl-3,3,3',3'-tetramethylindotricarbocyanine iodide
DIO	diet-induced obese
DLS	dynamic light scattering
DMEM	Dulbecco's Modified Eagle Medium
DMEM/F-12	Dulbecco's Modified Eagle Medium/Nutrient Mixture F-12
DMSO	dimethyl sulfoxide
DNA	deoxyribonucleic acid
DSMZ	German Collection of Microorganisms and Cell Cultures
EDTA	Ethylenediaminetetraacetic acid
EGM	endothelial growth medium
ELISA	enzyme-linked immunosorbent assay
ER	endoplasmic reticulum
ESCRT	endosomal sorting complex required for transport
EV	extracellular vesicle
eWAT	epididymal white adipose tissue
FA	formic acid
FABP4	fatty acid binding protein 4

FBS	fetal bovine serum
gDNA	genomic deoxyribonucleic acid
GM1	ganglioside M1
GSIS	glucose-stimulated insulin secretion
HBSS	Hank's Balanced Salt Solution
HEPES	4-(2-hydroxyethyl)-1-piperazineethanesulfonic acid
HFD	high-fat diet
HOMA-IR	Homeostasis Model Assessment of Insulin Resistance
HRP	horse radish peroxidase
hSkMC	human skeletal muscle cells
HUVEC	human umbilical vein endothelial cells
IBMX	3-isobutyl-1-methylxanthine
IF	immunofluorescence
IFNγ	interferon gamma
IgG	immunoglobulin G
IL-4	interleukin 4
ILV	intraluminal vesicle
IMDM	Iscove's Modified Dulbecco's Medium
IP	immunoprecipitation
ip.	intraperitoneal
ipGTT	intraperitoneal glucose tolerance test
ISEV	International Society for Extracellular Vesicles
iv.	intravenous
iWAT	inguinal white adipose tissue
KRB	Krebs Ringer buffer
LC-MS/MS	Liquid chromatography – mass spectrometry
M-CSF	macrophage colony stimulating factor
MEM	Minimum Essential Media
MHC	major histocompatibility complex
min	minutes
MISEV	Minimal Information for Studies of Extracellular Vesicles

mRNA	messenger ribonucleic acid
miRNA	micro ribonucleic acid
MV	microvesicle
MVB	multivesicular body
nSMase	neutral sphingomyelinase
NTA	nanoparticle tracing analysis
ON	overnight
PBMC	peripheral blood mononuclear cells
PBS	phosphate buffered saline
PFA	paraformaldehyde
PCR	polymerase chain reaction
POMC	pro-opiomelanocortin
PVDF	polyvinylidene difluoride
qRT-PCR	quantitative real-time polymerase chain reaction
RIPA	radioimmunoprecipitation assay
RNA	ribonucleic acid
RPMI	Roswell Park Memorial Institute
RT	room temperature
RQ	respiratory quotient
SD	standard deviation
SDS	sodium dodecyl sulfate
sec	seconds
SGBS	Simpson-Golabi-Behmel syndrome
SVF	stromal vascular fraction
T2D	Type 2 Diabetes
T_3	Triiodothyronine
TBS-T	Tris-buffered saline with Tween
TEM	transmission electron microscopy
TNF	tumour necrosis factor
U	Unit

1 Introduction

1.1 Adipose tissue dysfunction in obesity

Obesity is a constantly growing world health problem and represents one of the most important but also preventable risk factors for the development of metabolic complications, including type 2 diabetes (T2D), cardiovascular diseases and certain types of cancers (1). The obesity epidemic has been continuously deteriorating over the last decades as shown by a nearly tripled increase in prevalence between 1975 and 2016. In 2016, 39% of the world's adult population were overweight and 13 % were obese, making it a major health problem worldwide (2). Due to the severe comorbidities, obesity causes also an increased mortality, with 2.8 million deaths per year worldwide as consequence of being overweight or obese (3). Obesity is defined by the World Health Organization as "abnormal or excessive fat accumulation that may impair health", particularly characterized by an excess of visceral adipose tissue in the abdominal cavity (1,2).

Under healthy and fairly lean conditions, white adipose tissue is found mainly in subcutaneous depots and serves predominantly as energy reservoir (4). Besides its role as main storage organ for triglycerides, adipose tissue (AT) has also been recognized as important endocrine organ that secretes various humoral factors named adipokines such as leptin, adiponectin or resistin, which play a critical role in inter-organ communication and metabolic homeostasis (4,5). Under obese conditions the AT mass extensively increases, especially in the visceral compartment. This accumulation is accompanied by chronic inflammation of AT with major changes in AT metabolism, leading to low-grade systemic inflammation and disbalances of various endocrine factors (4). An imbalance of adipokine profiles has been tightly linked to obesity-associated complications like insulin resistance and T2D, as well as cardiovascular diseases (6,7).

Recently, besides adipokines, a new signalling entity originating from AT has moved into the centre of attention (8): Extracellular vesicles (EVs), which are small signalosomes carrying a complex array of signalling molecules. They represent lipid bilayer-encased particles that are naturally released from almost all types of cells and circulate in bodily fluids. By transporting proteins, lipids and different RNA species, these vesicles may not only contribute to trans-organ signalling but also serve as diagnostic resources. With their special structure as membrane-enclosed compartments, EVs could also be used as therapeutic tools and deliver specific cargo protected from degradation to distinct recipient cells. EVs are also secreted from adipocytes and are discussed to contribute to the development of metabolic complications (8).

1.2 EV classification

The conventional EV classification is based on their subcellular origin and biophysical properties and distinguishes EVs into three major sub-populations: exosomes, microvesicles, and apoptotic bodies (9,10), also depicted in Figure 1. The following sections describe the biogenesis and main characteristics of the three major vesicle classes.

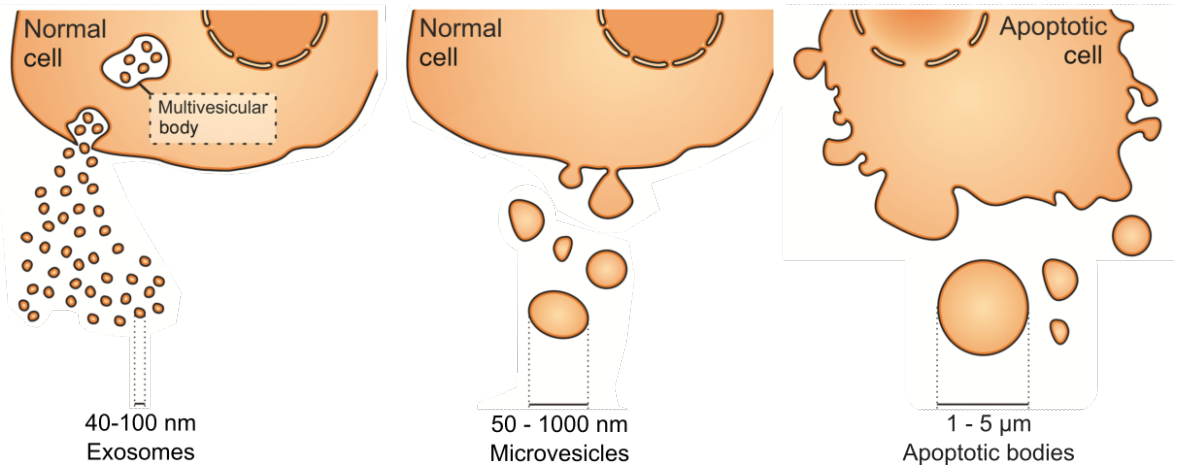

Figure 1: Overview of the different EV-subtypes secreted by normal and apoptotic cells. *Viable cells secrete two types of EVs: exosomes (left section) that are formed via the endosomal pathway and released by fusion of multivesicular bodies with the plasma membrane, and microvesicles (middle section) which are formed by outward budding and fission of the plasma membrane. During cell death the much larger apoptotic bodies (right section) are released from cells undergoing apoptosis (adapted from (10–13)).*

1.2.1 Exosomes

Exosomes are determined by their size ranging from 40 to 100 nm (10–15). Visualization of exosomes with transmission electron microscopy (TEM) shows rounded vesicles with lipid bilayers. They are generated by the endosomal pathway, starting with the invagination of the cellular membrane and the formation of the early endosome (16). Subsequent endosomal membrane invaginations result in the accumulation of intraluminal vesicles (ILVs) (Figure 2). The mature late endosome, also termed multivesicular body (MVB) can either fuse with the lysosome followed by ILV degradation, or alternatively, the ILV can be released as exosomes towards the extracellular space.

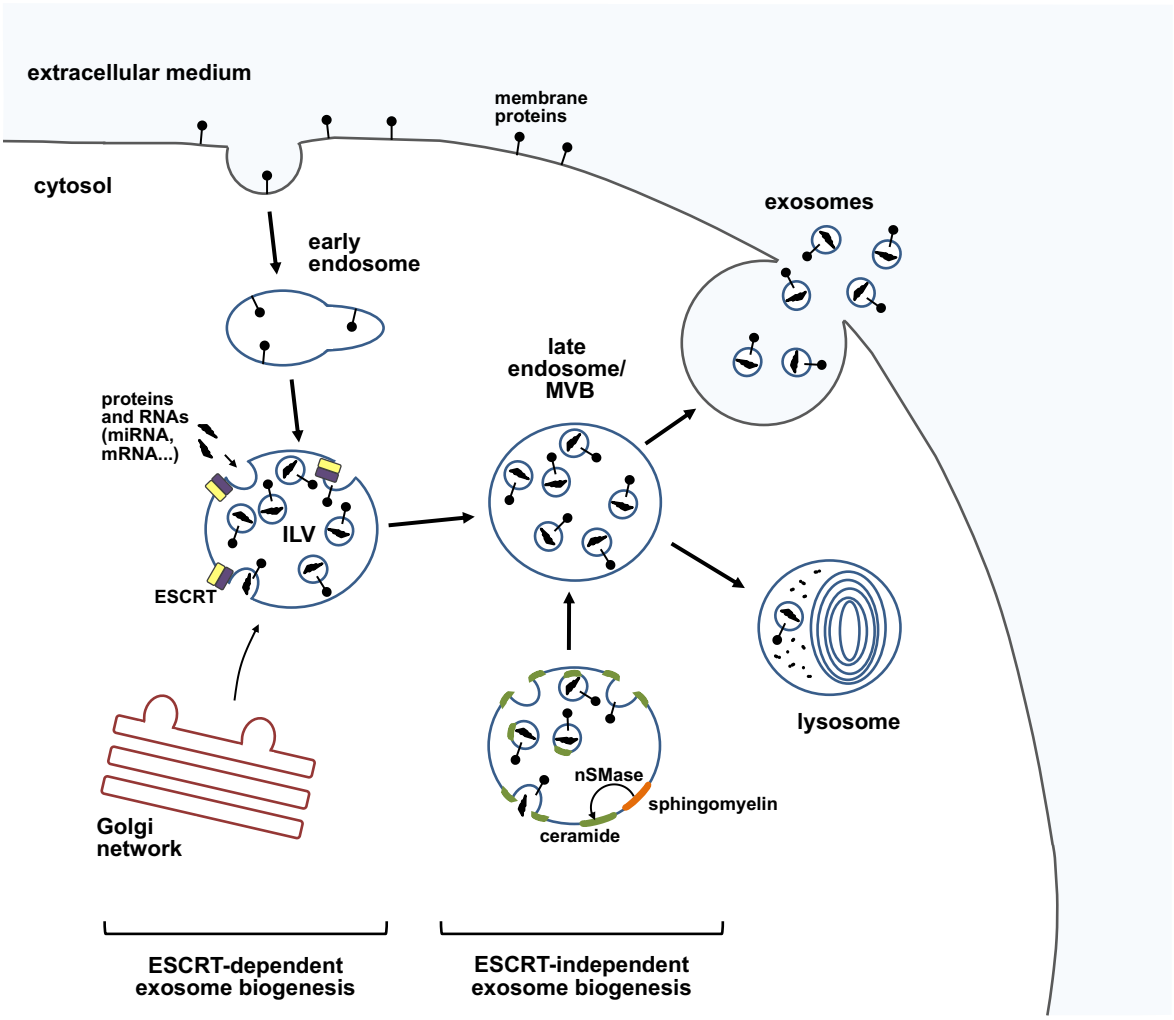

Figure 2: Schematic illustration of exosome biogenesis and secretion. *Exosomes originate from the endosomal pathway and are created as intraluminal vesicles (ILVs) by inward budding into the early endosome. The so formed multivesicular body (MVB) can either release the exosomes into the extracellular space by fusion with the plasma membrane or undergo degradation in the lysosomal pathway. Two pathways of ILV formation have been identified so far, dependent or independent of the endosomal sorting complex required for transport (ESCRT) machinery. Without involvement of the ESCRT complex, ILV formation is mediated by ceramide domains that are generated via the conversion of sphingomyelin by the enzyme neutral sphingomyelinase (nSMase) (adapted from (17–19)).*

The formation, trafficking and secretion of exosomes requires an orchestrated interaction of several protein complexes and has been described in detail (10,19,20). Briefly, the biogenesis of MVBs is driven by at least two discrete pathways, one requiring the endosomal sorting complex required for transport (ESCRT) machinery and the second one independent of the ESCRT-complexes (19). This alternative pathway is mainly driven by ceramides and has not been considered much in the EV field. Lipid rafts in the endosomal membrane contain high levels of sphingomyelin which can be converted to ceramide by the enzyme neutral sphingomyelinase (nSMase), resulting in the formation of larger ceramide domains that can promote membrane budding (16,21).

After formation, the MVBs are transported through the cell and fuse with the plasma membrane to release the exosomes. This process requires interaction with actin and microtubules of the cytoskeleton and is dependent on several proteins, most important the RAB GTPases. Different members of this family have been reported to be involved in EV secretion, e.g. RAB27A, RAB27B, RAB11 or RAB35 (16). Interestingly, RAB protein isoforms are not consistently expressed in all cell types, implicating a cell specific recruitment of the secretory machinery (10). Additionally, inactivation of specific RAB isoforms has been shown to only partially inhibit exosome release, which indicates a complementary or overlapping function of different RAB proteins (22). Beside RAB proteins also SNARE protein family members are involved in the final step of exosome secretion (10).

1.2.2 Microvesicles

Microvesicles (MVs) are generated by plasma membrane outward budding. Compared to exosomes, MVs are described to be larger and more heterogeneous in size (50 – 1000 nm) (10–15). The mechanisms involved in MV formation are less well characterized. Changes in membrane lipid composition and rearrangement of the cytoskeleton seem to be required for MV biogenesis. Processes that enhance asymmetry in the cell membrane are important mediators of membrane budding, for example the exposition of phosphatidylserine from the inner membrane leaflet to the cell surface by enzymes like flippases, floppases, scramblases or calpain, possibly triggered by Ca^{2+}-influx (10). Furthermore, lipid-rafts are involved in MV budding with cholesterol playing a key role (16). Interestingly, in a process comparable to ESCRT-independent exosome biogenesis, the conversion of sphingomyelin to ceramide by SMases is also involved in MV formation, resulting in membrane curvature and facilitating MV release (16). Besides membrane lipids, cytoskeletal elements are also important players in MV biogenesis. The RHO-GTPase family members and their associated proteins like ROCK regulate actin dynamics and enhance myosin contractility, which favours budding and fission of MVs (10,16).

1.2.3 Apoptotic bodies

The largest vesicles are apoptotic bodies, with a size from 1 up to 5 µm (10–15). While exosomes and MVs are generated from healthy and diseased cells, apoptotic bodies result from the degradation of apoptotic cells, which is characterized by three major steps: apoptotic membrane blebbing, membrane protrusion formation, and ultimately fragmentation into apoptotic bodies (23,24). One of their major functions is to ensure the efficient clearance of apoptotic cellular debris and thereby preventing unwanted inflammatory responses. Secondly, similar to other EV types, apoptotic bodies were shown to carry a range of biomolecules like DNA, RNA and proteins, which additionally

proposes an involvement in intercellular communication (25). Increasing evidence suggests that apoptotic bodies are not only the final product of cellular disassembly but also have important immune regulatory functions (24). Their role in trans-organ signalling, however, largely remains elusive.

1.2.4 Additional vesicle classes

Technical advances and gain of knowledge in the EV field over the last years has questioned the traditional classification of EVs in these three major groups. Novel vesicle classes with unique properties like mitovesicles originating from mitochondria (26), amphisomes as DNA carrying EVs (27) or oncosomes transferring oncogenic macromolecules (28) were discovered. By carrying distinct signalling molecules and also differently expressing classical EV markers, these additional classes add more complexity to EV research and have to be taken into account in future studies. Consequently, more detailed efforts are needed to better understand EV heterogeneity and to develop a reasonable consent about EV classification in the research community.

1.3 Composition of the EV cargo

The membrane-encased EV cargo is fundamental for the cellular response of the recipient cells upon EV delivery and further serves as rich source for diagnostic biomarkers. An overview of EV composition is depicted in Figure 3 and described below.

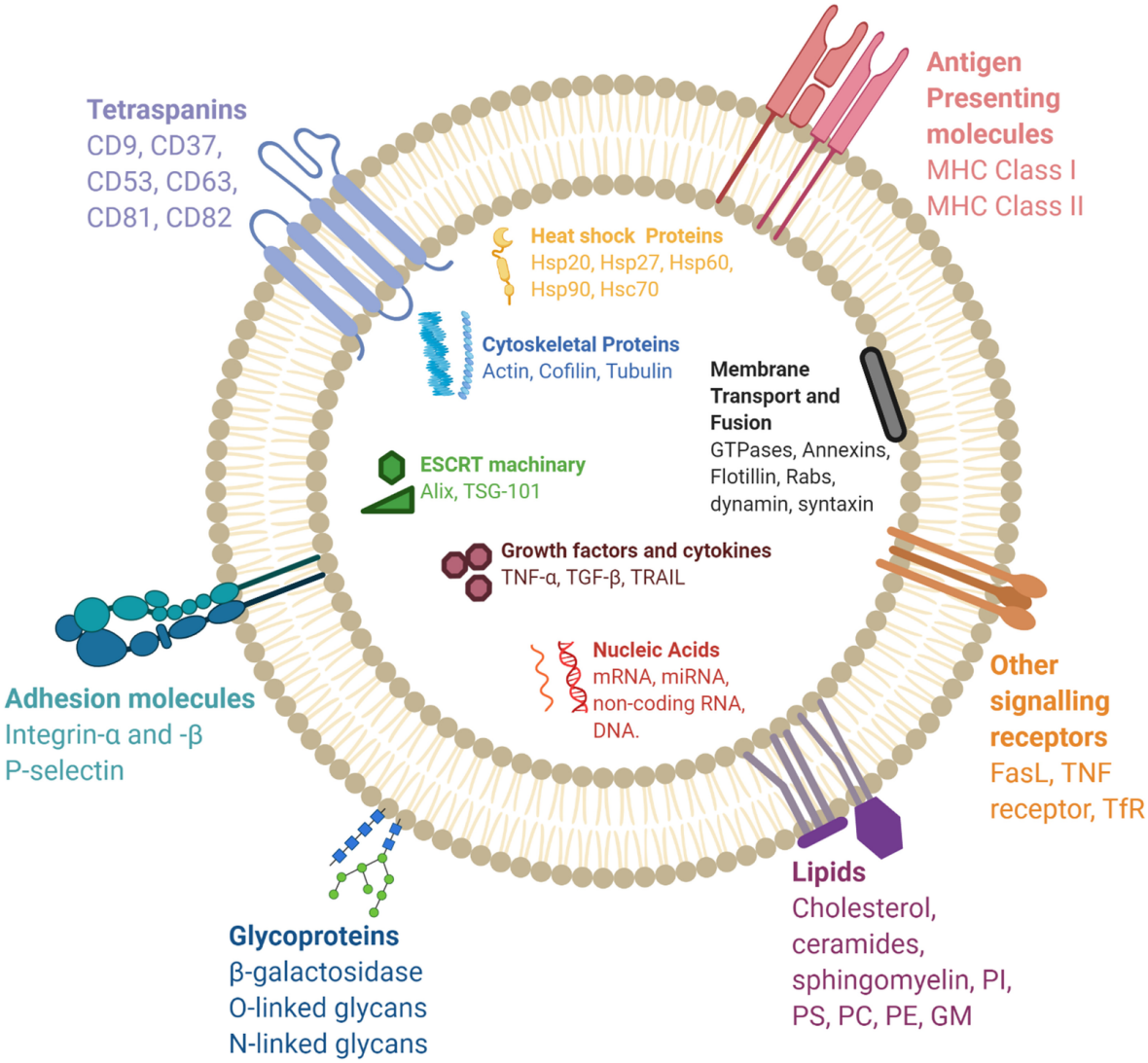

Figure 3: Overview of EV composition and cargo. *EVs are composed of various bioactive macromolecules including proteins, lipids and nucleic acids. Proteins are either transmembrane proteins like tetraspanins, adhesion molecules, glycoproteins, antigen presenting molecules and other signalling receptors or intraluminal like heat shock proteins (Hsp), proteins from the cytoskeleton or ESCRT machinery, membrane transport and fusion proteins as well as growth factors and cytokines. Lipids found in EVs include cholesterol, ceramides, sphingomyelin, phosphatidylinositol (PI), phosphatidylserine (PS), phosphatidylcholine (PC), phosphatidylethanolamine (PE) and gangliosides (GM). EVs also contain nucleic acids in their lumen such as DNA, mRNA, miRNA and other non-coding RNAs. Hsc: heat shock cognate; TSG: tumour susceptibility gene; TNF: tumour necrosis factor; TGF: transforming growth factor; TRAIL: TNF-related apoptosis-inducing ligand; FasL: Fas ligand; TfR: transferrin receptor (adapted from (29)).*

1.3.1 General EV markers

A large part of the EV cargo depends on the biochemical pathways involved in EV formation, which are often used as markers for EV characterization (14,30,31). Accordingly, exosomes contain cytosolic and membrane bound proteins involved in ESCRT, such as Alix and TSG101, membrane transport and fusion proteins (RAB proteins, Annexins, flotillin), members of the tetraspanin family (CD9, CD63, CD81, CD82) as well as heat shock proteins (HSC70, HSP90) (29). These markers are most widely used to isolate and identify EVs in experimental approaches. In contrast, knowledge about specific MV markers is still limited. Due to their route of biogenesis by budding and fission of the plasma membrane, cytoskeletal proteins like tubulin, actinin-4 and cytokeratin-18 are suggested as MV-specific markers (32–34). Recently, by in-depth analysis of different EV subpopulations, annexin A1 has also been identified as a specific marker for classical MVs (27).

However, further provoked by the continuing development of isolation and characterization techniques, the standardly used vesicle markers are under debate (33). For example, detailed proteome analysis identified several exosomal subsets that completely or partially lack the standard EV markers of the tetraspanin family (CD63, CD9 or CD81) (33,35,36). These advances add more complexity to the conduction and interpretation of EV research, and especially make it challenging in research projects having to adapt to changing standards over the time course of a project. Therefore, the definition of reasonable basic requirements for EV research is of urgence but also complicated in this rapidly developing research field.

1.3.2 Cell specific EV content

Many studies have highlighted that the EV cargo harbours selected macromolecules like proteins, nucleic acids and lipids rather than random cellular components and that this cargo varies substantially between different cell types (10,14,37). In 2007 novel findings by the group of Jan Lötvall opened a new field in EV research which has been intensively studied since then: The authors reported that EVs contain significant amounts of mRNA, miRNA as well as other non-coding RNAs. By *in vitro* translation of extracted RNA to full-length proteins they could show that EVs are capable of transferring functional genetic information to recipient cells (38). Additionally, EV-associated mRNA was found to be enriched compared to the mRNA content of the parental cell, suggesting a specific packaging of distinct mRNA sequences into the released vesicles (12). This breakthrough triggered an exponentially increasing research interest in EVs by numerous groups worldwide (39). Some evidence for EV-encapsulated miRNAs as functional signal mediators also exists for AT. Thomou and colleagues transplanted white and brown

adipose tissue (BAT) into ADicerKO mice lacking the critical miRNA-processing enzyme Dicer in the AT and demonstrate the release of miRNAs from transplanted fat pads via exosomes into circulation. Subsequently, BAT-derived miRNAs were associated with improved glucose tolerance and reductions in liver and circulating FGF21 levels (40). In a recent study, Ying et al. demonstrate that miRNA containing exosomes from AT macrophages can modulate systemic insulin and glucose tolerance (41). Furthermore, changing miRNA levels in circulating adipocyte-derived EVs were detected even prior to the onset of metabolic disorders, making them an interesting candidate for disease risk prediction and prevention (42).

Besides RNA, also the cell-specific protein content of EVs has been intensively studied over the last decades. Specific EV cargo has been reported for various cell types, including immune cells (43), several types of cancer cells (44,45), stem (46) or neural cells (47). An impressive body of knowledge about cell-specific EV proteins, RNAs and lipids has been compiled in online databases like ExoCarta (48) and Vesiclepedia (49) to facilitate the retrieval of information and to connect EV research worldwide.

Because of their mode of formation EVs are enclosed by a lipid bilayer, primarily originating from the plasma membrane. EVs are enriched in several raft-associated lipids like cholesterols, sphingolipids, ceramides and phosphoglycerides (21,50), which results in a higher rigidity of the EV membrane compared to the cell membrane and may therefore contribute to vesicle fusion and their resistance to degradation (11). Moreover, lipid mediators contained in EVs, such as prostaglandins and leukotrienes, have been implicated in signalling processes (51,52).

1.4 EV isolation and characterization

Several different methods have been developed to isolate secreted EVs from different sample types, including cell culture media, tissue cultures or bodily fluids such as blood plasma, urine, cerebrospinal fluid, breast milk, or saliva (12,14). An overview of the mostly applied isolation techniques for EVs together with their advantages and limitations is summarized in Table 1.

Table 1: Overview of the currently used methods for EV isolation and their main advantages and limitations. *Modified after (53–55).*

Principle of purification	Description	Advantages	Limitations
Differential ultra-centrifugation	Multiple centrifugation steps at different g- forces are used to separate EVs in a stepwise manner by pelleting	Low processing cost	Labour intensive
		Isolation from large sample volumes	Expensive equipment required
		No additional chemicals needed	Complexity
			Relatively low purity
	Based on differing buoyant density of EVs vs. other sample components		Efficiency dependent on the type of rotor
			Possible damage and aggregation of EVs due to high forces
Density gradient centrifugation	Centrifugation with a gradient medium like sucrose or iodixanol, EVs concentrate at a density of 1.1-1.2 g/ml	High purity	Labour intensive
		Standardized protocol	Expensive equipment required
			Complexity
	Based on differing buoyant density of EVs vs. other sample components		Loss of sample
			Removal of gradient medium necessary
Size-exclusion chromato-graphy	Filtration of the sample through a column with porous beads and collection of specific fractions	High purity	Labour intensive
		Preserves vesicle integrity and prevents aggregation	Specialized equipment
	Based on the differing hydrodynamic radius of the biomolecules	No additional chemicals needed	Co-isolation of proteins with similar size as EVs
Precipitation with polymers	Incubation with hydrophilic polymers (e.g. polyethylene glycol) results in EV precipitation	Simple and fast procedure	Cost (if commercial kits are used and for diluted samples)
		No additional equipment needed	Retention of the polymer
	After low-speed centrifugation pellet can be resuspended and further analysed	Preservation of EV integrity	Low purity, contamination with non-EV proteins
		Low cost	
Immuno-precipitation	Isolation of EVs using antibodies coupled to a solid phase (e.g. beads), bound EVs can later be eluted	High purity	No general but selective isolation of distinct EV classes due to use of specific antibodies
			Cost (antibodies)
	Based on antibodies against common EV surface proteins (e.g. CD9, CD63, CD81 or TSG101)		Difficulties with detachment of EVs from antibodies
			Non-specific binding of protein contaminants to the solid phase
Ultrafiltration	Filtration through nanomembranes or filters with a specific pore diameter (0.8 – 0.1 µm)	Simple procedure	Protein contamination
		No limitations on sample volume	Possible filter plugging and loss of sample (large sample volumes
	Based on the differing hydrodynamic radius of the biomolecules	Scalable	Deformation of vesicles
Field-flow fractionation	Separation of particles due to their differing migration capacities in special flow streams applied to a flow channel	High purity and yields	Expensive equipment required
		Rapid procedure	Complexity of devices
	Based on the differing hydrodynamic radius of the biomolecules	Scalable	Extensive optimization required
		No additional chemicals needed	

In the past, most studies have used differential ultracentrifugation to isolate EVs and it has been considered the gold standard technique for the last years. With the ongoing development of other purification methods, the advantages of other isolation techniques or the combination of several procedures emerged. For example, the combination of ultracentrifugation with a density gradient enables to isolate and separate all EV subpopulations and to distinguish them by their distinct protein signatures and RNA profiles (56). But nonetheless, the optimal methodology for studying EVs depends on the source/sample matrix of EVs, the available amount of sample and the intended downstream analysis of a specific experiment and has to be defined after individual assessment. Here, the limitations of the different methods must be considered in the experimental setup, as they may artificially influence EV properties and subsequent readouts.

Following isolation, the purity of EVs can be verified by their physical and molecular properties. Currently applied standard techniques include the measurement of vesicle size distribution by dynamic light scattering (DLS) or nanoparticle tracking analysis (NTA) which is based on the Brownian motion of EVs in solution. Another important method for EV characterization is the analysis by TEM, allowing the visual verification of vesicle size and morphology as well as purity of the isolated EVs by providing a high-resolution image. Also, for the examination of vesicle integrity TEM reflects a useful tool. Another approach of vesicle characterization is the analysis of specific EV-marker proteins like the tetraspanins (CD9, CD63, CD81) or ESCRT-related proteins, such as Alix and TSG101 by immunoblotting or proteomic profiling.

However, despite the intensively growing interest in EVs there is still major inconsistency in the methodology for EV isolation and characterization. Additionally, EV subtype-specific isolation methods and characteristic features of exosomes and microvesicles remain to be standardized. As more and more research in the EV field is published, the discussion about data quality and the need for standardized methodology is rising enormously. An intensive effort has been taken by the International Society for Extracellular Vesicles (ISEV) by proposing the “Minimal Information for Studies of Extracellular Vesicles (MISEV)” guidelines (9) and updating them based on novel insights and techniques. These standard recommendations aim to determine basic quality criteria for conducting EV research and should facilitate the interpretation and comparison of published EV studies. Amongst others, one suggestion of the ISEV consortium is to harmonize the EV nomenclature from exosomes to the more general term small EVs and from MVs to large EVs. Additionally, the online platform EV-TRACK (57) is a knowledgebase dedicated to enhance reporting transparency and improve interpretation of EV experiments. A similar

approach is pursued by the online database ExoCarta which catalogs information about exosomal proteins, RNA and lipids together with purification and characterization methods used in the underlying investigations (58). More generally speaking, overlapping sizes and densities of the different EV categories and variability in their molecular cargo have to be considered when comparing the available literature on EVs. Different studies applying varying isolation techniques may describe heterogenous vesicle populations with possibly different cellular origin and composition which also translates in potential diverging functional characteristics (9).

1.5 EVs in trans-organ signalling

Due to their diverse and variable cargo, EVs are considered as vectorial signalosomes. EVs carrying distinct cellular markers from different organs have been identified in the bloodstream (59). However, how these EVs can cross endothelial barriers in order to reach and exit the circulation is still widely unclear. More attention has turned toward examining the biodistribution of EVs *in vivo*, which closes the gap between functional *in vitro* effects and physiological significance.

1.5.1 EV biodistribution and cell or tissue tropism

A specific delivery of EV cargo to distant target cells is mediated by organ tropism that depends on specific EV surface markers, but also on physical parameters such as vesicle size and physiological parameters such as organ blood flow (60). Currently available *in vivo* studies investigating EV biodistribution are heterogeneous and vary in their approaches, with large differences in timing, dosing, route of injection and target organs investigated. In addition, in the absence of genetic models, these studies apply different labelling methods such as fluorescent or bioluminescent dyes and radiolabels, which may influence the outcome of the studies.

A recent review (61) summarizing available biodistribution studies has demonstrated that EVs primarily home into the liver, lungs, kidneys, and spleen, which may depend on physiological parameters such as endothelial fenestration and differences in organ blood flow. However, the finding that EVs are also capable to cross the blood brain or blood placenta barrier in a transcytosis-mediated manner, also suggests an active transport into distinct organs (62–66).

Additional studies have shown that the size of the EVs is another determinant for their biodistribution. For example, for EV subsets isolated from the melanoma cell line B16-F10 and *iv.* injected into mice, a higher targeting to lymph nodes was detected for large compared to small EVs, apart from a main accumulation in the liver for all vesicle

subclasses (67). Whether this tropism is mainly determined by the vesicle size, or represents a more secondary effect because of their differing molecular composition remains to be determined

The trafficking of EVs to their target site is also influenced by the EV surface composition. Specific proteins, such as integrins and tetraspanins, are known to alter EV targeting behaviours. Distinct integrin complexes can direct EVs either to the liver ($\alpha_V\beta_1$) or lungs ($\alpha_6\beta_4$ and $\alpha_6\beta_1$) (68). For tetraspanins, CD63-positive EVs were shown to target whole neurons and glial cells while CD63-negative EVs exhibited a specificity towards neuronal dendrites (69). Additionally, the presence of a complex of the tetraspanin Tspan8 and integrin α_4 on EVs has been shown to direct EVs selectively to the pancreas (70). The EV lipid composition may also influence the biodistribution as shown for the recognition of phosphatidylserine by macrophages (71). This interaction may also be mediated by the negative charge of phosphatidylserine, reflecting an additional targeting mechanism. Last, also sugars such as glycans have been identified as modulators of EV tropism, for example by interaction with lectin receptors (72).

1.5.2 EV uptake and contribution to cellular signalling

After reaching their target site several modes of interaction between EVs and their recipient cell have been proposed. EVs can either directly induce downstream signalling by interacting with extracellular receptors, fuse with the plasma membrane and release their content in the recipient cell or get internalized as a whole by different mechanisms (29). An overview of the mechanistic pathways involved in EV internalization is shown in Figure 4. Each possible internalization route requires the interaction between EVs and target cell by surface molecules such as tetraspanins, integrins, immunoglobulins, proteoglycans, lectins or phosphatidylserine, and seems to be highly cell and EV type specific (73).

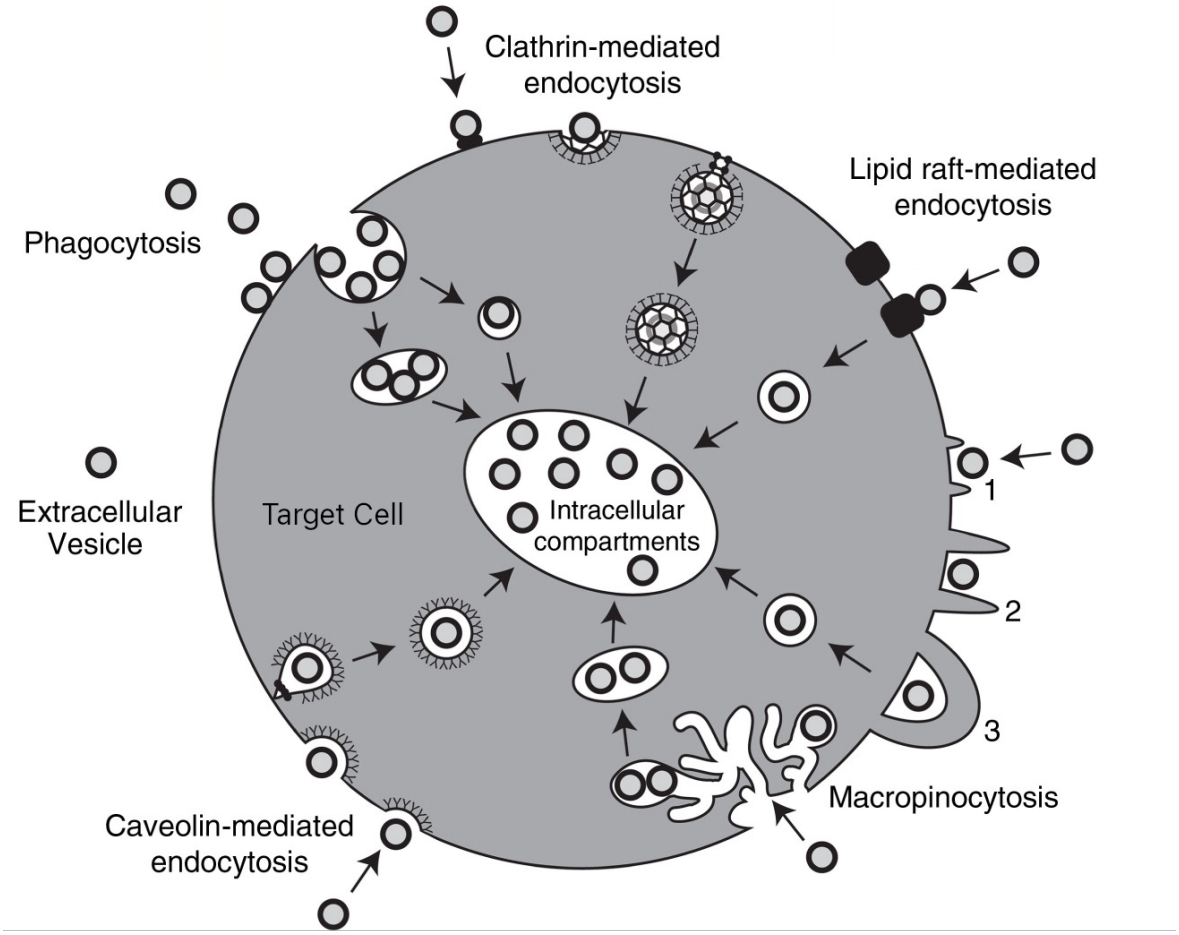

Figure 4: Overview of the EV internalization pathways. *EVs can be internalized into their target cell by clathrin- and caveolin-mediated endocytosis, phagocytosis or mechanisms facilitated by lipid rafts. In macropinocytosis EVs are taken up by the formation of membrane protusions or ruffles enclosing extracellular fluid followed by vesicle internalization. Internalized EVs are transported to the endosomal compartment for further distribution or degradative processes (adapted from (73)).*

The direct signalling is depending on ligand-receptor interactions present on the EV and cellular surface which induces the activation of specific signalling cascades in the target cell. For example, immunomodulatory or apoptotic processes like the activation of T-lymphocytes through MHC-peptide complexes or binding to TNF receptors have been shown to utilize this mechanism (74,75).

The fusion of EVs with the plasma membrane of the target cell requires interaction with surface molecules like lipid raft domains, integrins or adhesion molecules to mediate spatial proximity and finally the fusion process (29). Protein families known from cell membrane fusion studies such as SNARE and Rab-Proteins are suggested to facilitate this mechanism (76). For the internalization of whole EVs several mechanisms have been reported so far: clathrin-mediated endocytosis, phagocytosis, lipid raft-mediated endocytosis, macropinocytosis and calveolin-mediated endocytosis.

The proposed mechanisms of EV uptake have been described in detail (29,60,73). It includes the internalization of EVs in clathrin-mediated endocytosis which is characterized by a stepwise assembly of clathrin-coated vesicles involving various transmembrane receptors and ligands, followed by membrane deformation and pinching off the plasma membrane. Internalized vesicles then undergo clathrin uncoating and fuse with the endosomal compartment. The alternative process of phagocytosis is known from the uptake of large particles like bacteria or fragments of apoptotic cells but can also be utilized to internalize small particles like EVs. In this receptor-mediated mechanism, cell membrane deformations progressively surround the EVs destined for internalization and form phagosomes that are directed to the endosome or lysosomal pathways. Lipid-rafts have also been shown to facilitate EV internalization. These specific free-floating membrane microdomains are rich in sphingolipids and cholesterol and serve as organizing centres for protein receptors and signalling molecules in the cell membrane. Lipid-raft mediated endocytosis has been shown to involve Annexin A2 or Flotillin as mediators of internalization. An additional route of internalization is the calveolin-dependent endocytosis. Comparable to clathrin, calveolin forms coated membrane invaginations which are internalized into the cell, uncoated and fuse with the endosome. Macropinocytosis is characterized by the engulfment of extracellular matter including EVs and is in contrast to phagocytosis independent of receptor interaction. This process involves the actin-driven formation of membrane protrusions to finally enclose extracellular fluid and macromolecules containing vesicles that are taken up from the recipient cell. Alternatively, EVs can also be internalized in a macropinocytosis-mediated manner after being trapped in membrane ruffles. The applicable routes of EV internalization are diverse and likely depend on the cell type of the donor and target cell, on their physiological state or the conditions present in the microenvironment (11).

Following internalization, the intracellular fate of EVs is mostly defined by the endosomal pathway. After sorting into early endosomes, EVs can either be sorted in late endosomes/MVBs or be redirected promptly to the plasma membrane in recycling endosomes (77). This direct recycling process might mediate the transport of intact EVs through multiple cellular layers necessary for paracrine signalling (78). Classically, the endosomal pathway results in the degradation of the internalized contents in the lysosome, which also applies for internalized EVs. However, EVs need to have the ability to at least partially escape lysosomal degradation to exert their function in the target cell, as various studies demonstrate functional modulation after EV uptake. Interestingly, EVs have been shown to use a similar method as human immunodeficiency virus to avoid degradative pathways after uptake into mature dendritic cells (79). Besides fusion with the limited endosomal membrane and subsequent release of the EV content into the cytosol, EVs

have also been shown to travel to other cellular compartments. For example, EV-containing endosomes have been proposed to directly interact with the endoplasmic reticulum (ER) (80), but the precise mechanism is still unknown. Especially for EV-transported miRNAs this interaction would be a possible route to explain observed effects on altered gene expression. Also interaction of late endosomes with nuclear envelope-associated invaginations was observed, proposing a mechanism for nuclear EV cargo (81). However, the exact mechanisms of internalization and the following intercellular fate of EVs and their cargo are still under investigation. It is also under debate if imaging and tracking techniques may directly influence the observed findings. For example, commonly used fluorescent lipophilic dyes can form nanoparticles which are hardly distinguishable from EVs and even colocalize with them in cellular compartments, making a clear conclusion impossible (82). Technical advances in live-imaging and super-resolution methods will help to understand these processes in more detail and solve contradictory results reported in the literature up to date.

1.6 Application of EVs as diagnostic and therapeutic tools

Numerous studies showed that EVs carry a specific cargo which is characteristic for the secreting cell. Like a fingerprint, EVs can mirror the releasing cell and its physiological or pathophysiological state. Therefore, EVs also emerged as diagnostic tools and represent a rich source of biomarkers to monitor health and disease states. According to the National Institutes of Health a biomarker is defined as “characteristic that is objectively measured and evaluated as an indicator of normal biological processes, pathogenic processes, or pharmacologic responses to a therapeutic intervention” (83). The utilization of EVs as biomarkers has several advantages: First, EVs are distributed systemically and can be isolated from various bodily fluids, making them easily accessible. Second, due to the specific structure, EVs can transport cargo like miRNA protected against degradation; and third, by carrying a complex array of different macromolecules like proteins, miRNAs and lipids, EV-based biomarker detection could rely on a multifaceted signal rather than a single factor. The availability of EVs in a blood sample gives the opportunity to use EVs as liquid biopsies and makes them a valuable diagnostic tool where the accessibility to a tissue biopsy is limited, especially in tumours of the brain and central nervous system disorders. The application of EVs as biomarkers has been explored in various studies and is also investigated in numerous clinical trials (84). The potential role of adipocyte EVs as source of biomarkers in the context of metabolic diseases is introduced in a separate section found below (chapter 1.7.2). The EV-based biomarker approach has been most intensively studied in cancer and tumour EVs are recognized as promising targets for

disease diagnosis and monitoring (85). Interestingly, one study revealed that EVs are advantageous in early diagnosis and may represent a more sensitive readout, as the investigated marker protein in EVs was detectable before a tumour mass could be diagnosed with standard imaging techniques (86). Therefore, EVs may serve as valuable biomarkers for cancer diagnosis, the prediction of treatment response and early detection of relapse (85). One application already found its way into the clinical setting: the EV-based liquid biopsy test for prostate cancer patients “ExoDx™ Prostate IntelliScore” (Exosome Diagnostics, Waltham, USA) is designed to avoid unnecessary biopsy procedures (87) and was awarded from the U.S. Food and Drug Administration with a Breakthrough Device Designation. Additionally, studies in other fields suggested the diagnostic potential of EVs, as for example EVs isolated from urine were shown to reflect acute kidney injury (88) or predict kidney dysfunction after transplantation (89). The major difficulty in the detection of EV-based biomarkers in biofluids is the specific selection of EVs of distinct cellular origin. As cancer cells carry specific markers and differ substantially from healthy body cells (85), a caption of tumour-derived biomarkers in bodily fluids could be facilitated. High effort is made not only in the field of cancer research to detect novel biomarkers, as seen by numerous investigations dedicated to the discovery of new targets.

Besides the application as biomarkers, EVs also bear the potential to be used as therapeutic tools in a clinical setting (90,91). Due to their structure, EVs can transport various therapeutic substances, independent of polarity and in a stable surrounding, protected from environmental factors and degradation, thereby increasing bioavailability. Additionally, the EV-mediated transfer of a complex signalling cargo consisting of proteins, miRNAs and lipids can stimulate multiple pathways simultaneously and lead to potent effects compared to the single compounds. Furthermore, EVs can also be experimentally loaded with specific drugs, increasing the potential area of application. As EVs are distributed via the circulation and can even cross the blood brain barrier, therapeutic agents can be delivered by EVs to otherwise difficult to reach target sites. By specific targeting of distinct cell types, side effects can be strongly decreased compared to systemic administration. As most currently EV-based therapies use EVs derived from human cell lines or primary cells, the immunogenic potential and subsequent side effects of this therapeutic approach is comparatively low, combined with a high biocompatibility. Investigated areas of EV-mediated therapeutics include targeted delivery of cancer chemotherapeutics (92,93), cancer vaccination or immunotherapy (94,95) or regenerative medicine applications for example in chronic or degenerative diseases (96,97). However, for the isolation and characterization of EVs in therapeutic purposes, well-defined and very high, evaluated quality standards are needed to meet the requirements of a medical

product. Engineered nanoparticles have also been studied as EV-like therapeutic vehicles, helping to overcome obstacles like batch-to-batch variation or sterility issues but lacking the beneficial factors of a biological formed vesicle (91). Undoubtedly, one of the major challenges in EV-based treatment strategies is the specific targeting of a certain organ or cell type to deliver the EV cargo. So far only few cell-specific signalling factors have been proposed (68,70,72) and knowledge about discrete targeting pathways is limited. However, a detailed understanding of the signalling mechanisms underlying organ or cell tropism is crucial to safely direct therapeutic EVs to their site of action.

1.7 EVs in metabolic diseases

Metabolic diseases is an umbrella term for dysfunctions including abdominal obesity, insulin resistance or diabetes, hyperlipidaemia and hypertension. Particularly a combination of these disorders also named as metabolic syndrome is exceedingly detrimental and can lead to severe medical complications (98,99). The major driver of these diseases is the increase in AT mass upon the development of obesity, predominantly an accumulation of visceral AT (100). This massive AT expansion leads to complex remodelling processes, which also impair adipocyte signalling and function (101). As a consequence of cellular stress, EV secretion from adipocytes and sorting of specific cargo was suggested to be altered, translating into functional differences in EV signalling. A functional role of adipocyte-derived EVs in metabolic diseases is currently investigated and suggests an involvement in inflammation or metabolic dysfunctions like insulin resistance.

1.7.1 Functional role of AT-derived EVs in disease progression

AT EVs have been recognized as important entity of the AT secretome and were shown to influence cells resident or infiltrating in AT such as macrophages, endothelial cells, preadipocytes and mature adipocytes. Besides this paracrine function, AT EVs were also proposed to impact distant organs like the liver, skeletal muscle, heart or brain by a systemic distribution over the circulation (8). Over the last years, an increasing body of knowledge about the composition and function of AT EVs has emerged. However, with interpretation and comparison of these studies, careful attention must be taken on the exact source of EVs. Especially in studies investigating whole AT EVs, a potentially strong signalling effect from EVs secreted by other AT resident cells like macrophages might overlay the signal from adipocyte EVs and could result in misleading conclusions.

The EV-based communication between adipocytes and macrophages has been investigated in several studies. This axis is of great importance in the context of metabolic

diseases, as inflammatory macrophage activation was shown to be a major trigger in the development of obesity related comorbidities (102). Adipocyte EVs were shown to induce macrophage polarization into the proinflammatory M1-state leading to insulin resistance in myoblasts *in vitro* (103–105). Additional to activation, macrophages also showed an increased lipid accumulation stimulated by adipocyte EVs which is also associated with insulin resistance (106). Interestingly, a recent study reported the transfer of mitochondria from adipocytes to macrophages which is impaired in an obese state (107). EVs have recently been suggested to transfer mitochondrial components (108), but whether the transport between adipocytes and macrophages occurs by this mechanism warrants further study. Apart from the adipocyte-macrophage communication axis, less is known about the crosstalk with other AT resident cells like adipocyte progenitors, mature adipocytes and endothelial cells. Adipocyte EVs were shown to promote preadipocyte differentiation (105,109) or induce stem cell differentiation into the adipocyte lineage (110) and to be involved in beiging processes (111). The proposed EV-mediated crosstalk between mature adipocytes is likely serving the purpose to synchronize the neighbouring cells. For example, isolated EVs from hypoxic adipocytes were able to induce insulin resistance in adipocytes cultured under normoxic conditions (112), or EVs transferred from large adipocytes could induce lipid accumulation and increase the cell size of small adipocytes (113). There is also evidence that endothelial cells are a target of adipocyte EVs, and their signalling can contribute to cardiovascular complications. EVs from insulin resistant cultured adipocytes were shown to induce processes involved in atherosclerotic plaque rupture in endothelial cells and lead to a reduced plaque stability in mice (114). Besides paracrine signalling in AT, adipocyte EVs can also influence distant organs in an endocrine fashion. Metabolically active organs like liver and skeletal muscle have been suggested as signalling targets for adipocyte EVs. By the treatment with obese AT EVs or EVs from *in vitro* stressed adipocytes, studies showed an induction of insulin resistance in HepG2 hepatocytes (115) and skeletal muscle cells (116), as well as a stimulation of non-alcoholic fatty liver disease-related signalling in hepatocytes (117). A miRNA-mediated gene suppression by stressed adipocyte EVs was also shown in the context of cardiovascular diseases, worsening the phenotype of myocardial injury in diabetic mice (118). Having the ability to cross the blood-brain barrier, adipocyte EVs can also influence targets in the brain: adipocyte EVs from visceral AT of obese mice were shown enhance food intake by miRNA-mediated stimulation of POMC neurons in the hypothalamus (119). Interestingly, EVs from lean AT could reverse the effect and showed the opposite of a reduced food intake.

The available literature suggests that in the context of obesity, adipocyte EVs can trigger local and systemic inflammation and induce insulin resistance. However, it is not entirely

clear if this is a consequence of the direct signalling of AT EVs to metabolic organs or a more indirect effect mediated by the recruitment and activation of immune cells (120). Which route reflects the more important driver of the aggravation of metabolic complications still needs to be determined. Furthermore, the conditions of the metabolic syndrome including cytokine-mediated inflammation, hypoxia, high glucose or high insulin levels and distinct fatty acids have been shown to stimulate the release of EVs from AT (8). These factors of cellular stress do not only lead to an induced secretion, but most likely also change the adipocyte EV cargo. However, the precise molecular mechanisms underlying these adaptions and also the physiological relevance of these changes have not been elucidated in detail so far.

1.7.2 Adipocyte EVs as diagnostic tools for the metabolic syndrome

As AT undergoes major functional remodelling processes with the development of obesity (101,121,122), the investigation of adipocyte-derived EVs in the context of obesity and related metabolic disorders seems a plausible rationale. Especially an early diagnosis of metabolic dysfunctions as already shown for EVs in the early detection of pancreatic cancer in advance to visible tumour growth (86) would be favourable to implement specific treatment strategies before the onset of major complications. However, only limited knowledge exists in this area so far. It has been shown that adipocyte EVs are present in the circulation (40) and their levels are increased in obese humans and mice (123) or decreased after caloric restriction and bariatric surgery (124). Interestingly, by analysing the miRNA composition of EVs positive for the adipocyte specific protein fatty acid binding protein 4 (FABP4) in human serum samples, distinct profiles could be identified for obese and lean individuals, supporting a potential application as disease biomarker. The influence of metabolic diseases on adipocyte EVs and their potential application as biomarkers is currently investigated in several clinical trials, but only two studies are specifically investigating AT EVs (125,126). One major challenge in the field of biomarker-based approaches is the specific isolation and analysis of a particular EV type of origin from the complex mixture present in plasma. Known AT or adipocyte-specific markers such as Perilipin-1 (Plin1) and FABP4 have been proposed as potential marker proteins for adipocyte EVs (105,127). However, enrichment methods relying on distinct marker proteins may select a specific subpopulation of EVs and thus confound the obtained results. Furthermore, profiling of miRNAs from plasma EVs could also serve as approach for biomarker detection and was already applied in the context of obesity and metabolic disorders (127). Overall, further research interest is needed to fully elucidate the biomarker potential of adipocyte specific EVs and their diagnostic value in the field of metabolic diseases.

1.8 Aims of this thesis

EVs are nano-sized vesicles that are secreted by nearly all cell types and can be found in various bodily fluids like blood, saliva, urine or breast milk. For decades, EVs were solely considered as cellular trash bags without major biological relevance. In recent years however, EVs emerged as novel mediators for intercellular and even inter-organ communication. EVs carry different macromolecules, including proteins, lipids, RNA and miRNA, providing a snapshot of the parental cell at the time of release. By transferring this cell- specific cargo to recipient cells, EVs can affect multiple signalling pathways at once and can therefore lead to potent effects inside a target cell. As they are also transported via the bloodstream and other bodily fluids, EVs are able to trigger not only paracrine effects in neighbouring tissue but can also target even distinct organs throughout the entire organism in an endocrine fashion. With a content specific for the releasing cell, EVs can also transfer information from diseased donors and therefore not only contribute to physiologic homeostasis but also to pathological conditions like tumour metastasis (68,128,129), immunological disorders (19,130), neurodegenerative (131) and cardiovascular diseases (132).

Based on these findings the **first aim** of this thesis was to elucidate if EVs can serve as novel endocrine signalling element between the AT and different metabolic target organs. As especially AT is subjected to fundamental changes during the development of obesity I aimed to investigate if the cargo of adipocyte-derived EVs and also their functional impact on target cells is altered in the state of obesity. This interest was aroused on the basis of a number of recent studies that link EVs with metabolic disorders. EVs isolated from adipocyte cell lines were demonstrated to play a role in monocyte differentiation (133), adipocyte differentiation and lipogenesis (109,113,134). Furthermore, EVs isolated from AT of lean and obese subjects were shown to induce differential insulin signalling responses in HepG2 hepatocytes and C2C12 muscle cells (115). First *in vivo* evidence was provided by Deng and colleagues by showing that AT-derived EVs from leptin deficient Lep^{ob} mice lead to monocyte activation and insulin resistance in wild type mice (103). More recently, transfer of distinct miRNAs via exosomes from BAT (40) and from macrophages residing in the AT (41) was linked with the modulation of insulin resistance and glucose tolerance in mice. To study the possible link between AT EVs and metabolic target organs, first adipocyte-EVs were characterized in detail and their distribution *in vivo* was assessed. Additionally, several functional assays were developed to investigate the effect of adipocyte-derived EVs on other cell types and their function, like paracrine effects on adipocytes, macrophage polarization or insulin secretion from pancreatic ß-cells.

Secondly, this thesis aimed to investigate the potential role of AT-derived EVs as biomarkers for metabolic diseases. Especially in the field of cancer research, the possible applicability of EVs as biomarkers has intensively been studied. In numerous types of malignancies EVs have been shown to modulate tumour growth, metastasis and even treatment response, which makes them a valuable tool for diagnosis and prediction of disease progression (85). In a key discovery Melo and colleagues suggested a benefit of EVs in early disease diagnosis by detection of an EV-associated tumour marker protein prior to detection of the tumour mass itself by conventional imaging techniques (86). But not only in cancer, also in other pathologies like cardiovascular disease, liver or neurodegenerative diseases EVs were propagated as diagnostic tools and biomarkers (135–137). In the field of metabolic diseases, first evidence links urinary EVs from Type 1 and Type 2 diabetic patients with a deterioration of nephropathological complications (138,139). To study the potential application of adipocyte-derived EVs as biomarker for metabolic diseases, this thesis generated a novel antibody targeting adipocyte EVs and tested the specificity in various assays.

2 Materials and Methods

2.1 Cell culture

2.1.1 Cell lines and cell culture maintenance

The cell lines investigated in this thesis were maintained at 37°C with a concentration of 20% O_2 and 5% CO_2 in a humidified atmosphere. Hypoxia experiments were conducted in 3% O_2, while keeping the CO_2 concentration constant.

2.1.1.1 SGBS pre-adipocytes

The human pre-adipocyte Simpson-Golabi-Behmel Syndrome (SGBS) cell strain, established at the University of Ulm in the 1990s from a patient's AT specimen (140,141), was kindly provided by Prof. Wabitsch, Universitätsklinikum Ulm. SGBS cells are characterized by a high capacity for adipogenic differentiation and retain this ability up to generation 50 without being neither transformed nor immortalized. Once differentiated, the cells' function and behaviour is comparable to primary human adipocytes (142). SGBS cells were cultured in SGBS growth medium. In order to retain the ability for differentiation, cells were only grown until ~70% confluency and subcultured as required. To induce differentiation of SGBS pre-adipocytes into functional adipocytes, the cells were cultured as previously described (142). Briefly, the cells were grown to confluence in normal growth medium, washed with phosphate buffered saline (PBS) and incubated with differentiation medium I under serum-free conditions for four days. At day 4 the medium was replaced by serum-free differentiation medium II and the cells were incubated until fully differentiated.

Basal medium:	Dulbecco's Modified Eagle Medium/ Nutrient Mixture F-12 (1:1) (DMEM/F12) GlutaMAX™ + 100 U/ml Penicillin, 100 µg/ml Streptomycin + 17 µM Pantothenate + 33 µM Biotin
SGBS growth medium:	Basal medium + 10% fetal bovine serum (FBS)
Differentiation medium I: (day 0 - day 4)	Basal medium + 10 µg/ml Transferrin + 2 µg/ml Insulin (human) + 100 nM Cortisol

	+ 0.2 nM T_3
	+ 25 nM Dexamethasone
	+ 250 µM IBMX
	+ 2 µM Rosiglitazone
Differentiation medium II:	Basal medium
(day 4 - end)	+ 10 µg/ml Transferrin
	+ 2 µg/ml Insulin (human)
	+ 100 nM Cortisol
	+ 0.2 nM T_3

2.1.1.2 HepG2 cells

The HepG2 cell line is an immortalized human liver carcinoma cell line, derived from a liver hepatocellular carcinoma of a 15-year-old Caucasian male in 1975 (143,144). The cells were purchased from the Leibniz Institute German Collection of Microorganisms and Cell Cultures (DSMZ, Germany). HepG2 cells were cultured in Dulbecco's Modified Eagle Medium (DMEM, high glucose, GlutaMAX™, 1 mM pyruvate) supplemented with 100 U/ml penicillin, 100 µg/ml streptomycin and 10% FBS (heat inactivated). As HepG2 cells tend to grow in small aggregates (145), they were subcultured regularly.

2.1.1.3 Caco2 cells

The Caco2 cell line was established from a colorectal adenocarcinoma of a 72-year-old Caucasian male in 1974 (146,147). Because of their ability to differentiate into an epithelial cell monolayer that resembles the enterocytes in the small intestine, Caco2 cells are widely used as *in vitro* model for pharmacokinetic studies to investigate drug absorption (148). The cells were purchased from the American Type Culture Collection (ATCC®, Nr. HTB-37). The medium to culture Caco2 cells consisted of Iscove's Modified Dulbecco's Medium (IMDM) supplemented with 1x Minimum Essential Medium (MEM) non-essential amino acids, 4 mM L-glutamine, 40 µg/ml gentamicin and 10% FBS (heat inactivated).

2.1.1.4 PANC-1 cells

The human epithelial pancreatic cell line PANC-1 was isolated in 1972 from the ductal cells of a pancreatic carcinoma from a 56-year-old Caucasian male (149). The cells were purchased from the DSMZ, Germany. PANC-1 cells were cultured in DMEM (high glucose, 1 mM pyruvate, 4 mM L-glutamine) supplemented with 100 U/ml penicillin, 100 µg/ml streptomycin and 10% FBS (heat inactivated) and subcultured as required.

2.1.1.5 Panc02 cells

Murine Panc02 cells are commonly used as a model for pancreatic ductal adenocarcinoma and were established almost 35 years ago by Corbett et al. from C57BL/6 mice after treating the animals with 3-methyl-cholanthrene (150). Panc02 cells were cultured in DMEM (high glucose, 1 mM pyruvate, 4 mM L-glutamine) supplemented with 100 U/ml penicillin, 100 µg/ml streptomycin and 10% FBS (heat inactivated) and were subcultured as required. Cells were a gift from PD Dr. Ivo Partecke, Chirurgisches Forschungslabor Universitätsmedizin Greifswald, Klinik und Poliklinik für Chirurgie, Abt. für Allgemeine Chirurgie, Viszeral-, Thorax- und Gefäßchirurgie.

2.1.1.6 Saos-2 cells

The Saos-2 cell line is a human osteoblastic cell line, derived from the primary osteogenic sarcoma of an 11-year-old Caucasian girl in 1973 and is one of a large series of human tumour cell lines isolated and characterized by J. Fogh and colleagues (146).

Saos-2 cells were purchased from the DSMZ, Germany, and were cultured in McCoy's 5A medium supplemented with 15% FBS (heat inactivated).

2.1.1.7 MCF-7 cells

The breast cancer cell line MCF-7 was established from the pleural effusion of a 69-year-old Caucasian female with metastatic mammary carcinoma in 1970 (151) and became the most widely used *in vitro* model for breast cancer research worldwide. Because this cell line also expresses the estrogen receptor alpha, MCF-7 cells have become an important system to study the majority of invasive human breast cancers, which are characterized by estrogen receptor expression (152). The cells were purchased from the DSMZ, Germany. MCF-7 cells were grown in Roswell Park Memorial Institute (RPMI) 1640 medium supplemented with 1x MEM non-essential amino acids, 1 mM sodium pyruvate, 10 µg/ml human insulin, 100 U/ml penicillin, 100 µg/ml streptomycin and 10% FBS (heat inactivated).

2.1.1.8 Human skeletal muscle cells

Non-immortalized, primary human skeletal muscle cells (hSkMC), isolated from healthy adult limb skeletal muscle were obtained from Cell Applications along with the necessary media and cultured as described in the manufacturer's protocol. Briefly, hSkMC were expanded in normal growth medium and subcultured not more than four passages. To induce differentiation into myotubes, the cells were seeded at a density of $3.2x10^6$ cells/cm^2 in collagen coated flasks and differentiation was induced the following day by adding differentiation medium. HSkMC were differentiated for nine days, with a medium change every other day.

2.1.1.9 Human Umbilical Vein Endothelial Cells

Primary human umbilical vein endothelial cells (HUVEC) are isolated from the vein of the umbilical cord and are commonly used in functional studies, particularly in angiogenesis assays (153). The cells were purchased from Lonza, together with EGM™-2 Medium required for culturing HUVEC. The cells were cultured and expanded in normal growth medium as described in the manufacturer's protocol.

2.1.1.10 L929 cells

The murine fibroblast cell line L929 is widely used in *in vitro* experiments, primarily in immunology research due to the ability to secrete considerable amounts of macrophage colony stimulating factor (M-CSF) into the culture medium. Therefore, L929 conditioned medium can be used to differentiate bone marrow cells into bone marrow-derived macrophages (154,155). L929 cells were purchased from the DSMZ, Germany. To generate L929-conditioned medium the cells were cultured in growth medium (DMEM high glucose, 4 mM L-glutamine, supplemented with 100 U/ml penicillin, 100 µg/ml streptomycin and 10% FBS (not inactivated)) until 90% confluency. Subsequently, fresh growth medium was added and incubated for three days. The conditioned medium was harvested, filter sterilized and stored at -20°C until further usage. For a second harvest, fresh growth medium was added once more to the L929 cells and again incubated for three days, followed by harvesting the medium and discarding the cells.

2.1.2 Isolation and cultivation of primary cells

2.1.2.1 Murine white pre-adipocytes

Murine pre-adipocytes from white fad pads were isolated from inguinal white adipose tissue (iWAT) samples of 6- to 8-week-old male C57BL/6J mice. The tissue was excised, washed in DMEM/F12 GlutaMAX™, minced and digested using 0.15% Collagenase IV and 2% bovine serum albumin (BSA, low endotoxin). Samples were incubated for 50 min at 37°C under gentle shaking on a heated shaker at 100 rpm. The digested tissue was passed through a 100 µm mesh to remove undigested parts and floating adipocytes were separated by centrifugation at 400×g for 10 min using a Heraeus™ Multifuge™ X3R Centrifuge. Adipocytes and medium supernatant were removed and the pelleted stromal vascular fraction (SVF) containing the pre-adipocytes was re-suspended and incubated in erythrocyte lysis buffer (154 mM NH_4Cl, 10 mM $KHCO_3$, 0.1 mM EDTA) to lyse contaminating red blood cells. After 20 min of incubation at room temperature (RT), the SVF was pelleted by another centrifugation step at 400×g for 10 min, re-suspended in culture medium (DMEM/F12 GlutaMAX™, 10% FBS (not inactivated), 100 U/ml penicillin and 100 µg/ml streptomycin), passed through a 40 µm mesh and seeded in culture medium at a density of $1x10^5$ cells/cm^2. The differentiation into adipocytes was induced by

changing the medium to induction medium (culture medium supplemented with 1 µM dexamethasone, 0.5 mM IBMX, 1 µM rosiglitazone and 5 µg/ml insulin) when the cells reached 90% confluence. Two days post induction, the medium was changed to differentiation medium (culture medium supplemented with 5 µg/ml insulin). At day five of differentiation the cells were shifted to EV medium (DMEM/F12 GlutaMAX™, 100 U/ml penicillin, 100 µg/ml streptomycin and 0.5% fatty acid free BSA) containing lean or obese iWAT adipocyte EVs or vehicle (EV buffer only). After 24 h of treatment, the cells were either washed with PBS and lysed for RNA isolation or further exposed to 10 µM isoproterenol for 6 h to induce adipocyte browning, also followed by lysis for RNA extraction.

2.1.2.2 Murine bone marrow-derived macrophages (BMDM)

Bone marrow cell suspensions were isolated under sterile conditions by flushing femurs and tibias of 8- to 10- week-old C57BL/6J mice with RPMI 1640 containing 2% FBS (not inactivated). To eliminate erythrocyte contaminations, the cells were incubated with erythrocyte lysis buffer (154 mM NH_4Cl, 10 mM $KHCO_3$, 0.1 mM EDTA) and washed with PBS. Additionally, a density gradient centrifugation with Ficoll-Paque for 30 min at 400×g was performed using a Heraeus™ Multifuge™ X3R Centrifuge. Subsequently, the isolated bone marrow mononuclear cells representing the middle fraction after centrifugation were washed once in PBS to remove residual Ficoll-Paque. For macrophage selection, cell suspensions were seeded onto non–tissue culture treated petri dishes in BMDM differentiation medium (DMEM high glucose with 2 mM L-glutamine supplemented with 20% FBS (not inactivated), 30% L929 supernatant, 100 U/ml penicillin, 100 µg/ml streptomycin and 50 µg/ml normocin) using L929-conditioned medium as source of M-CSF. BMDMs were differentiated for five days with a change of medium every two days. Fully differentiated BMDMs were detached and seeded for treatment with EVs and cytokines (see chapter 2.13.1.1 for details).

2.1.2.3 Murine pancreatic islets

Islets of Langerhans were isolated from 3-month-old male C57BL/6J mice by collagenase digestion. Briefly, after killing the mice by cervical dislocation the pancreas was perfused with 1 mg/ml Collagenase P, dissolved in G-solution (HBSS with 25 mM HEPES, pH 7.4, supplemented with 0.5% BSA) via injection into the common bile duct. To ensure a correct perfusion of the entire pancreas, the duodenum was clamped at the ampulla of Vater with a serrefine. The perfused pancreas was carefully removed and digested in a water bath at 37°C for 14 min. Islets were hand-picked multiple times to ensure a high purity and were maintained overnight (ON) in suspension dishes with culture medium (RPMI 1640, 10% FBS (not inactivated), 100 U/ml penicillin, 100 µg/ml streptomycin) to recover from

the isolation procedure. On the following day, the islets were treated with EVs and insulin secretion was measured (see chapter 2.13.2 for details).

2.1.2.4 Human blood cells and peripheral blood mononuclear cells

Three distinct cellular components of human blood, namely erythrocytes, peripheral blood mononuclear cells (PBMC) and a mixed cell population consisting of leukocytes and thrombocytes were isolated using three different protocols. For all protocols, human blood was drawn by venepuncture and collected in heparinized monovettes.

To isolate the erythrocyte fraction, a protocol adapted from Hanson et al. (156) was applied. Briefly, whole blood was centrifuged at 500×g for 10 min and the upper layer of plasma and the buffy coat was aspirated. The pelleted erythrocytes were washed three times with wash buffer (PBS supplemented with 2 mM EDTA) to remove remaining plasma and were incubated in RPMI 1640 supplemented with 10% FBS (heat inactivated), 100 U/ml penicillin and 100 µg/ml streptomycin.

The isolation of PBMC was performed according to a protocol provided from Miltenyi Biotech, Germany (157) using a density gradient centrifugation. Whole blood was diluted with three volumes of wash buffer (PBS supplemented with 2 mM EDTA) and carefully layered on Ficoll-Paque, followed by a centrifugation at 400×g for 10 min at 20°C. The upper layer consisting of plasma was aspirated and the middle layer containing the mononuclear cells (lymphocytes, monocytes, and thrombocytes) was transferred to a new tube. After a washing step with wash buffer, platelets were separated by two centrifugation steps at 200×g, with platelets remaining in the supernatant. Finally, isolated PBMCs were resuspended and cultured in RPMI 1640 supplemented with 10% FBS (heat inactivated), 100 U/ml penicillin and 100 µg/ml streptomycin.

Leukocytes and thrombocytes were isolated from the whole blood cellular compartment by lysis of the erythrocytes. Therefore, whole blood was incubated with erythrocyte lysis buffer (154 mM NH_4Cl, 10 mM $KHCO_3$, 0.1 mM EDTA) for 20 min under gentle shaking. The remaining leukocytes and thrombocytes were washed with PBS and directly lysed in radioimmunoprecipitation assay (RIPA) buffer for protein isolation.

2.2 Protein isolation, quantification and analysis

2.2.1 Generation of cell lysates and protein extraction

To generate cell lysates from cultured cells, cell pellets or flasks were thawed on ice and 1-2 ml of ice-cold RIPA buffer supplemented with 5 mM EDTA and 1x Halt™ protease and phosphatase inhibitor cocktail was added. Cells in flasks were detached using a cell

scraper, whereas cell pellets were processed directly. The samples were sonicated twice for 10 s using the Ultrasonic Homogenizer 150 VT to obtain complete cell disruption, followed by centrifugation for 15 min at 2,000×g and 4°C to pellet debris and non-lysed cell contents. The supernatant containing the extracted proteins was collected and either used for experiments immediately or stored at -80°C until further usage.

RIPA buffer:
- 50 mM Tris-HCl (pH 8)
- 150 mM sodium chloride
- 1% (v/v) NP-40
- 0.5% (v/v) sodium deoxycholate
- 0.1% (v/v) sodium dodecyl sulfate (SDS)
- 5 mM EDTA (add fresh)
- Halt™ Protease & Phosphatase Inhibitor Cocktail (add fresh)

Proteins from human AT were extracted with a different protocol using EBC lysis buffer (50 mM Tris-HCl, 120 mM NaCl, 0.5% NP-40 and 5 mM EDTA, pH 8.0) supplemented with cOmplete Mini protease inhibitor cocktail tablets (EDTA-free). To lyse the tissue, 1 ml ice cold EBC lysis buffer was added to 400 mg of AT on ice and homogenized using the TissueLyser for 1 min at the frequency 30/min. This homogenization was repeated twice with the samples being placed on ice in between to avoid protein degradation. Subsequently, the samples were incubated on ice for 30 min and vortexed shortly in between, followed by a centrifugation for 10 min at 1,000×g and 4°C to pellet non-lysed tissue parts and separate lipid components. The supernatant was again centrifuged for 20 min at 15,000×g and 4°C for further purification and stored at -80°C until further usage.

Because the ingredients of both, RIPA and EBC buffer disturb the proteomic analysis, AT lysates used for mass spectrometry experiments were generated using a less complex lysis buffer consisting of 100 mM Tris-HCl pH 7.6 supplemented with cOmplete Mini protease inhibitor cocktail tablets (EDTA-free). The applied protocol was consistent to the isolation procedure described above, except an additional final centrifugation step of 5 min at 15,000×g and 4°C, which was added to improve purity.

2.2.2 Determination of protein concentration

The concentration of protein was measured using the bicinchoninic acid (BCA) assay. This colorimetric assay is based on the detection of peptide bonds in a sample, directly proportional to the protein content. Dependent on the individual protein content, the samples were measured either undiluted or in different dilution ranges, always using the original sample buffer as diluent. For quantification, a calibration curve of BSA standard

also using the sample buffer as diluent was measured simultaneously with the samples. According to the manufacturer's instructions 200 µl of BCA reagent (BCA Protein Assay Reagent A and B) was added to 5 µl of the samples, incubated for 30 min at 37°C and the absorption at 562 nm was measured using the PHERAStar FS microplate reader.

2.2.3 Marker analysis by dot blot and immunostaining

To characterize the isolated EV fractions, the presence of several EV markers was investigated by dot blot and immunostaining. Therefore, 5 µl of EV suspensions or cell lysates were spotted on nitrocellulose membranes using a Whatman® Minifold I Dot-Blot System. The membrane and filter papers were equilibrated in Milli-Q water and the blotting chamber was assembled according to the manufacturer's instructions, followed by 5 min vacuum application to transfer the samples onto the membrane. After blocking for 1 h at RT in blocking buffer (Tris-buffered saline with Tween (TBS-T, 50 mM Tris, 150 mM NaCl, 0.1% Tween 20, pH 7.5) supplemented with 3% skimmed milk), the blots were incubated ON at 4°C with antibodies against the classical EV markers CD9, CD63, CD81 (58) or cholera toxin subunit B (CTB). CTB stains ganglioside M1 (GM1) positive lipid rafts that are enriched in EV membranes (158). Antibody details and dilutions are shown in Table 2. Following three washes with TBS-T, membranes were incubated for 1 h at RT with the appropriate horse radish peroxidase (HRP)-conjugated secondary antibodies diluted 1:10 000 in blocking buffer, except for CTB, which was already HRP-labelled and could therefore directly be imaged. Subsequently, the blots were washed three times with TBS-T, then Clarity™ Western ECL Substrate was added and incubated according to the manufacturer's recommendations. Finally, the chemiluminescent signal was detected using the Odyssey® Fc Imaging System. Following imaging, the blots were washed with TBS-T and stained with Ponceau S (see chapter 2.2.5) for normalization purposes.

Table 2: Antibodies used for dot blot imaging

Antibody	clone/ product No.	manufacturer	host species	blocking buffer (in TBS-T)	antibody dilution
CD9	MM2/57 (CBL162)	Chemicon	mouse	3% skimmed milk	1:500
CD63	bs-1523R	Bioss	rabbit	3% skimmed milk	1:500
CD81	bs-6934R	Bioss	rabbit	3% skimmed milk	1:500
Cholera toxin B (HRP conjugate)	C34780	Thermo Fisher	-	3% skimmed milk	1:5000

2.2.4 Marker analysis by Western blot and immunostaining

The purity and isolation quality of SGBS EVs was also evaluated by western blot and immunostaining. 10 µg of EVs and cell lysates from differentiated SGBS cells were mixed with NuPAGE™ LDS Sample Buffer and incubated at 95°C for 10 min. To achieve reducing conditions, the sample buffer was supplemented with 5% β-mercaptoethanol. For non-reducing conditions required for tetraspanin analysis, sample buffer was used without supplements. Samples were loaded on a Criterion™ TGX™ 12% precast gel and gel electrophoresis was performed using a Criterion™ Vertical Electrophoresis Cell with Tris/Glycine/SDS-electrophoresis buffer. The run was operated at 100 V until the loading front was absorbed into the gel and finished at 150 V. For size standardization, a PageRuler™ prestained protein ladder was run together with the samples. The separated proteins were transferred to a PVDF membrane with 0.45 µm pore size (Immobilon™-P) applying a wet transfer with a Criterion™ Blotter filled with transfer buffer (25 mM Tris-HCl, 190 mM glycine, 20% methanol). The transfer was operated at 70 V for 2 h 40 min. During the transfer process the device was constantly operated on ice to avoid excessive heat generation. After blocking the membranes for 1 h at RT in blocking buffer (TBS-T supplemented with 3% skimmed milk or 3% BSA), the blots were incubated ON at 4°C with antibodies against the classical EV markers Alix, CD9, CD63, CD81 and TSG101 (58) or Calnexin, a protein found in ER membranes as negative marker (159). Antibody details and dilutions are shown in Table 3. Following three washes with TBS-T, membranes were incubated for 1 h at RT with the appropriate HRP-conjugated secondary antibodies diluted 1:10 000 in blocking buffer. Subsequently, the blots were washed three times with TBS-T, then Clarity™ Western ECL Substrate was added and incubated according to the manufacturer's recommendations. Finally, the chemiluminescent signal was detected using the Odyssey® Fc Imaging System. Following imaging, the blots were washed with TBS-T and stained with Ponceau S (see chapter 2.2.5) for normalization purposes.

To be able to reprobe a blot with a new primary antibody, the former antibody complex was retrieved from the membrane by incubation with stripping buffer (200 mM glycine, 0.1% SDS, 1% Tween 20, pH 2.2). Therefore, membranes were incubated twice with pre-warmed (55°C) stripping buffer for 10 min. Before being ready for blocking and incubation with a new primary antibody, blots were washed two times with PBS for 10 min, followed by two 5 min-washes with TBS-T.

Table 3: Antibodies used for western blot imaging

Antibody	clone/ product No.	manufacturer	host species	reducing/ non-reducing	blocking buffer (in TBS-T)	antibody dilution
Alix	3A9 (634501)	BioLegend	mouse	reducing	3% BSA	1:1000
Calnexin	AF18 (sc-23954)	Santa Cruz	mouse	reducing	3% skimmed milk	1:200
CD9	MM2/57 (CBL162)	Chemicon	mouse	non-reducing	3% skimmed milk	1:1000
CD63	MX-49.129.5 (sc-5275)	Santa Cruz	mouse	non-reducing	3% skimmed milk	1:200
CD81	5A6 (349501)	BioLegend	mouse	non-reducing	3% BSA	1:500
TSG101	HPA006161	Sigma Aldrich	rabbit	reducing	3% skimmed milk	1:1000

2.2.5 Ponceau S Staining

For a better visualization or normalization purposes, blotted membranes of dot blots or western blots were stained with a Ponceau S solution, a protein staining diazo dye, which does not influence the membrane bound proteins and can easily be reversed by water washes. The membranes were incubated with staining solution (0.5% (w/v) Ponceau S in 1% acetic acid) for 1 min, followed by a destaining in distilled H_2O for 3 min to destain the background. Subsequent blocking or washes in TBS-T fully removed the remaining Ponceau S stain.

2.3 Gene expression analysis

2.3.1 RNA isolation and quantification

To extract RNA, the Rneasy® Mini Kit was used according to the manufacturer's instructions. This kit uses silica-membrane Rneasy® spin columns with different lysis and washing buffers for purification of RNA. To isolate RNA from cultured cells the kit could directly be used, RNA from tissue first had to be isolated by homogenization with TRIzol followed by an extraction with chloroform as described in standard protocols (160). Purified RNA was eluted with nuclease free water and either processed immediately or stored at -80°C.

RNA concentration was determined by measuring its absorption at 260 nm with the NanoDrop 2000 Spectrophotometer, with an OD260 of 1 relating to 40 µg/ml RNA. Additionally, the absorption at 280 nm was measured to quantify possible protein contaminations. A ratio of the absorbance at 260nm/280nm with a value of 1.8 to 2 indicates a pure RNA isolation without contamination.

2.3.2 cDNA synthesis and quantitative Real-Time Polymerase Chain Reaction

For gene expression analysis, the extracted total RNA was transcribed to cDNA using the QuantiTect® Reverse Transcription Kit according to manufacturer's instructions. This kit provides a fast procedure for cDNA synthesis with integrated genomic DNA removal. Briefly, contamination of the RNA samples with genomic DNA was eliminated by incubating with gDNA wipeout buffer, followed by cDNA synthesis using reverse transcriptase, RT Buffer and a RT primer mix according to the provided protocol. Both steps were run in the thermocycler Mastercycler® pro. For all gene expression analyses, 1 µg of total RNA was transcribed to cDNA. After synthesis, the cDNA was either stored at -20°C until further usage or directly diluted with nuclease free water in different ranges depending on target gene abundance.

To determine the expression levels of target genes, quantitative real-time PCR (qRT-PCR) was performed either using specific primer pairs with SYBR-Green or TaqMan probes. For quantification with SYBR-Green, a ready-to-use SYBR Green PCR Master Mix and target gene specific primer pairs were used. The primers were retrieved from a public primer bank (http://pga.mgh.harvard.edu/primerbank/) and additionally tested for specificity using Primer-BLAST (http://www.ncbi.nlm.nih.gov/tools/primer-blast/). The primer sequences of target and housekeeping genes are listed in Table 4. Prior to the actual analysis of target gene expression, the primers were validated in a separate primer test PCR. To calculate the exact PCR efficiencies, a standard curve for each primer pair was included in the SYBR-Green qPCRs. The relative expression of a target gene was calculated using the ΔΔCt method according to Pfaffl (161) and normalized to the expression of the housekeeping genes hypoxanthine phosphoribosyltransferase (*HPRT1 or Hprt1*) – a key enzyme in purine metabolism, the ribosomal phosphoprotein P0 (*36B4*) or the cytosolic enzyme cyclophilin A (*CypA*). The PCR reaction mix consisted of 5 µl SYBR Green PCR Master Mix, 0.5 µl of forward and reverse primer each (both 10 µM), 2 µl nuclease free water and 2 µl of diluted cDNA sample, giving a total reaction volume of 10 µl. In assays using the TaqMan-System, predesigned target specific TaqMan probes were used for target and housekeeping gene expression analysis. The probes are listed in Table 5. The PCR-Mix was combined according to the manufacturer's instructions, consisting of 5 µl TaqMan Universal PCR Master Mix, 0.5 µl TaqMan probe, 0.5 µl nuclease free water and

4 µl of diluted cDNA sample, with a total reaction volume of 10 µl. In SYBR-Green qPCR assays, a final melting curve was included to ensure a target gene specific amplification. All qPCR reactions were performed in the ViiA™ 7 Real-Time PCR System using 384 well PCR plates sealed with MicroAmp® Adhesive Film. The qRT-PCR conditions are displayed in Table 6.

Table 4: Primers used for gene expression analysis with SYBR-Green qRT-PCR

Gene	Gene synonym	Accession number	Primer sequence
human ribosomal protein, large, P0 (Rplp0)	*36B4*	NM_001002	Fw 5'- GCAGCATCTACAACCCTGAAG -3' Rev 5'- CACTGGCAACATTGCGGAC -3'
human fatty acid binding protein 4	*FABP4*	NM_001442	Fw 5'- ACTGGGCCAGGAATTTGACG -3' Rev 5'- CTCGTGGAAGTGACGCCTT -3'
human hypoxanthine phosphoribosyl transferase 1	*HPRT*	NM_000194	Fw 5'- CCTGGCGTCGTGATTAGTGAT -3' Rev 5'- AGACGTTCAGTCCTGTCCATAA -3'
human peroxisome proliferator-activated receptor gamma	*PPARG*	NM_138711	Fw 5'- TACTGTCGGTTTCAGAAATGCC -3' Rev 5'- GTCAGCGGACTCTGGATTCAG -3'
murine arginase	*Arg1*	NM_007482	Fw 5'- CTCCAAGCCAAAGTCCTTAGAG -3' Rev 5'- AGGAGCTGTCATTAGGGACATC -3'
murine C-type lectin domain family 10 member A	*Clec10a*	NM_001204252	Fw 5'- CTCTGGAGAGCACAGTGGAG -3' Rev 5'- ACTTCCGAGCCGTTGTTCT -3'
murine cyclophilin A / peptidylprolyl isomerase A	*CypA*	NM_008907	Fw 5'- ATGGTCAACCCCACCGTGT -3' Rev 5'- TTTCTGCTGTCTTTGGAACTTTGTC -3'
murine found in inflammatory zone -1 / resistin like alpha	*Fizz1*	NM_020509	Fw 5'- CCCTCCACTGTAACGAAGACT -3' Rev 5'- CAGTGGTCCAGTCAACGAGT -3'
murine hypoxanthine phosphoribosyltransferase 1	*Hprt*	NM_013556	Fw 5'- TCAGTCAACGGGGGACATAAA -3' Rev 5'- GGGGCTGTACTGCTTAACCAG -3'
murine nitric oxide synthase 2	*Nos2*	NM_001313922	Fw 5'- CCCCGCTACTACTCCATCAG -3' Rev 5'- CCACTGACACTTCGCACAAA -3'
murine peroxisome proliferator-activated receptor gamma, coactivator 1 alpha	*Ppargc1a*	NM_008904	Fw 5'- AGCCGTGACCACTGACAACGAG -3' Rev 5'- GCTGCATGGTTCTGAGTGCTAAG -3'
murine uncoupling protein 1	*Ucp1*	NM_009463	Fw 5'- GGCCTCTACGACTCAGTCCA -3' Rev 5'- TAAGCCGGCTGAGATCTTGT -3'

Table 5: TaqMan-Probes used for gene expression analysis with TaqMan qRT-PCR

Gene	Gene synonym	Assay ID
murine peptidylprolyl isomerase B	*Ppib*	Mm00478295_m1
murine sphingomyelin phosphodiesterase 2, neutral	*Smpd2*	Mm01188195_g1
murine sphingomyelin phosphodiesterase 3, neutral	*Smpd3*	Mm00491359_m1

Table 6: qRT-PCR conditions

temperature	time
50°C	2 min
95°C	10 min
repeat for 40 cycles:	
95°C	15 sec
60°C	1 min
melt curve (SYBR-Green qRT-PCR only):	
95°C	15 sec
60°C	1 min
95°C	15 sec

2.4 EV isolation from cell culture medium supernatants

2.4.1 Preparation of EV-depleted FBS

Almost all cell types show the ability to secrete EVs into the extracellular milieu (162). Amongst others, differential centrifugation is one potent method to isolate secreted EVs from the medium. To avoid a possible contamination with bovine EVs originating from FBS present in cell culture media, EV-depleted complete media was freshly prepared prior to the experiments. Therefore, one volume of growth medium supplemented with 40% FBS was prepared and centrifuged ON at 100,000×g and 4°C using the Beckman Coulter Optima^{TM} L-70 ultracentrifuge with appropriate 25 ml ultracentrifugation tubes. The EV-containing pellet was discarded and the supernatant was diluted in three volumes of

growth medium without FBS to achieve a final FBS concentration of 10%, followed by sterile filtration. Alternatively, if only small volumes of medium were needed, the whole growth medium was centrifuged without adding extra FBS, also followed by sterile filtration at 0.2 µm. These preparations only had to be carried out for cells dependent on FBS-containing media, as for example differentiated SGBS cells are cultured under serum-free conditions already.

2.4.2 Isolation of EVs from cell culture medium supernatants

To isolate EVs from cultured cells, they were grown or differentiated as required (see chapter 2.1 for details) under standard culture conditions. The cells were washed with PBS and the medium was changed to either pre-centrifuged EV-depleted medium or differentiation medium II for FBS-dependent cultures or differentiated SGBS cells, respectively. The medium was incubated for 48 h to allow a sufficient EV secretion. Subsequently, the EV-containing medium was collected and centrifuged to isolate EVs. The remaining cells were washed once with PBS to remove medium residues and stored at -80°C for later protein isolation.

For purification of EVs from cell culture medium supernatants a protocol using differential centrifugation was applied. This method makes use of the specific density of cellular components which allows separation by pelleting at different g-forces. All steps were operated at 4°C in pre-cooled centrifuges and rotors and the samples were always kept on ice in between. A flow chart of the EV isolation procedure is depicted in Figure 5. In the first step to remove dead cells and debris the medium was centrifuged for 10 min at 300×g using the Heraeus™ Multifuge™ X3R Centrifuge. Subsequently, the supernatant was transferred to ultracentrifugation tubes suitable for the Optima™ L-70 ultracentrifuge and centrifuged for 30 min at 10,000×g to further remove cell debris and larger vesicles. EVs were pelleted at 100,000×g for 70 min using the Optima™ MAX-XP ultracentrifuge. For further purification, the EV-containing pellet was re-suspended in PBS and spun down again at 100,000×g for 2 h 10 min. The isolated EV-enriched fractions were finally re-suspended in EV buffer (recipe see below) and either immediately used for protein determination, TEM and exposure experiments or stored at -80°C for further studies.

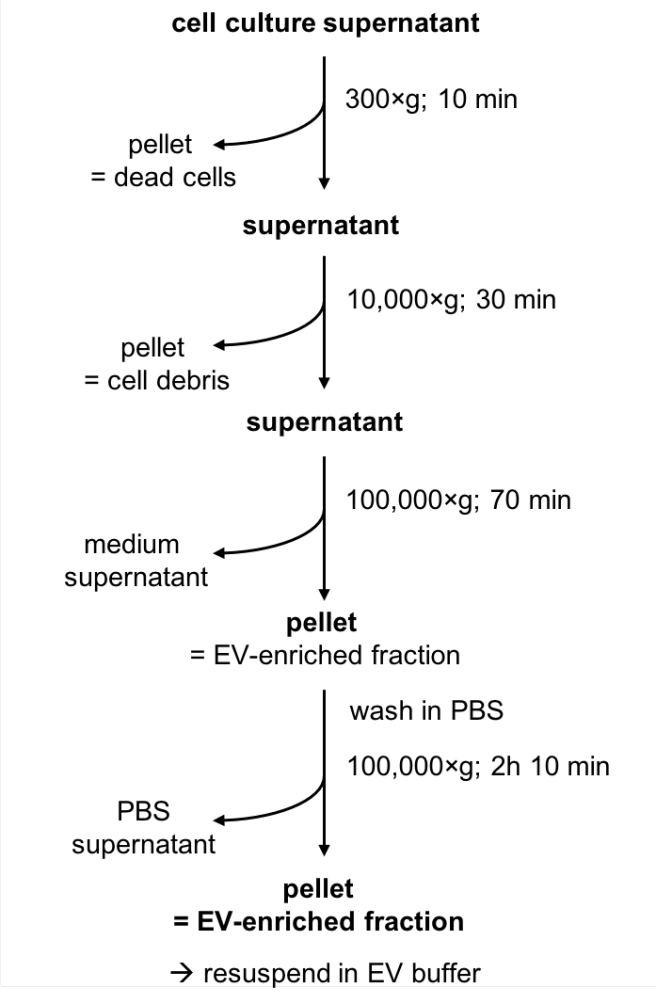

Figure 5: Flow chart of the EV isolation process. *EVs were isolated using differential centrifugation, speed and length of each step are indicated right of the arrows. As the pellets resulting from the first two centrifugations contain mainly dead cells and debris they were discarded, the pellets formed after the ultracentrifugation steps represent the EV-enriched fraction.*

EV buffer: 10 mM Tris-HCl
250 mM Sucrose
1 mM EDTA
140 mM NaCl
pH 7.4
cOmplete Mini protease inhibitor cocktail tablets (EDTA-free)

2.5 Isolation of EVs from murine white AT

Male C57BL/6J mice (Janvier, France; 8-10 weeks of age) were *ad libitum* fed a high-fat diet (HFD), 58% calories from fat (D12331, Research Diets Inc., USA) or chow (#1310, Altromin, Germany) for at least 16 weeks. For the isolation of EVs from AT, mice were sacrificed by cervical dislocation and epididymal white adipose tissue (eWAT) or iWAT were excised and transferred to pre-warmed DMEM (4.5 g/l glucose, GlutaMAX™)

supplemented with 100 U/ml penicillin and 100 µg/ml streptomycin. Finely minced fat pads were incubated in 0.075% Collagenase IV and 1% BSA (low endotoxin) solved in DMEM with penicillin/ streptomycin on a heated shaker at 37°C and 50 rpm. After 40 min incubation for eWAT or 50 min for iWAT two volumes of plain DMEM with penicillin/streptomycin were added to the digestion mix to dilute the collagenase cocktail. Subsequently, the digested tissue was passed through a 100 µm mesh to remove undigested parts and connective tissue. Adipocytes were separated from the SVF by centrifugation at 100×g for 10 min using a Heraeus™ Multifuge™ X3R Centrifuge. The upper layer containing the adipocytes was then carefully removed and incubated in pre-equilibrated medium (DMEM 4.5 g/l glucose, GlutaMAX™, with penicillin/streptomycin) supplemented with 0.2% BSA (low endotoxin) at 37°C in a humidified atmosphere. After 2 h of incubation the conditioned media were collected and secreted EVs were isolated by differential centrifugation at 4°C. First, a 10 min centrifugation step at 1,000×g was performed to remove cellular debris and dead cells followed by a 30 min step at 10,000×g to remove remaining fragments. While transferring the EV-containing media to fresh tubes, it was always taken great care not to disturb or transfer the upper layer of contaminating adipocyte fragments and lipids in order to retain a clean fraction. Subsequently, EVs were spun down at 100,000×g for 70 min, washed in PBS and centrifuged again at 100,000×g for 70 min using the Optima™ MAX-XP ultracentrifuge with the appropriate ultracentrifugation tubes. EV-enriched fractions were re-suspended in EV buffer (recipe see 2.4.2) and either immediately used for exposure and TEM experiments or stored at -80°C for marker analyses.

2.6 Isolation of EVs from human AT specimen

Human AT samples were obtained in collaboration with plastic surgeons from patients undergoing liposuction or abdominoplasty. All patients were informed and gave their written consent for the use of the tissue for scientific purposes. After the surgical procedures, the tissue was transported in sterile vessels containing medium (DMEM/F12, GlutaMAX™) to the laboratory, washed once with fresh medium and stored ON at 4°C in sterile containers supplied with DMEM/F12 GlutaMAX™. Before further processing on the following day, the tissue was kept at RT for 1 h. To isolate EVs from human AT a modified protocol based on the isolation of EVs from murine white AT was developed. Human tissue samples originating from liposuctions could be directly processed whereas whole tissue pieces from abdominoplasties had to be cleaned from blood vessels and connective tissue first and were then finely minced. To remove blood contaminants and medium residues the tissue was washed with PBS, followed by an incubation in 0.075%

Collagenase IV and 1% BSA (low endotoxin) solved in DMEM supplemented with penicillin/ streptomycin at 37°C and 55 rpm on a heated shaker. The incubation time was dependent of the origin of tissue, with liposuction samples being digested for 25 min and samples from abdominoplasty for 70 min. Following digestion, the experimental procedures to isolate EVs were performed according to the EV isolation protocol for murine white AT (see chapter 2.5 for details). Briefly, isolated human adipocytes were incubated in medium for 2 h and the EVs secreted into the medium were isolated using differential centrifugation. For isolation of EVs originating from the SVF, the pellet obtained after the first centrifugation step following AT digestion (10 min at 100×g) was incubated with erythrocyte lysis buffer (154 mM NH_4Cl, 10 mM $KHCO_3$, 0.1 mM EDTA) for 5 min to lyse contaminating red blood cells. After washing with PBS the SVF was incubated in medium (DMEM 4.5 g/l glucose, GlutaMAX™, with penicillin/ streptomycin, and 0.2% BSA (low endotoxin)) for 2 h and the same differential centrifugation steps as for the adipocyte EVs were applied. Finally, the isolated EV-enriched fractions were re-suspended in EV buffer (recipe see 2.4.2) and either used immediately for TEM analyses or stored at -80°C for further experiments.

2.7 Isolation of EVs from murine and human serum

EVs from fresh murine or human serum were collected with the ExoQuick® reagent according to the manufacturers protocol with the following modifications: Before incubating with ExoQuick®, serum was centrifuged for 30 min at 10,000×g to remove debris and larger vesicles. Additionally, resulting EVs were dissolved in PBS and centrifuged for 70 min at 100,000×g and 4°C to remove excess reagent and potential impurities. EV protein concentrations were determined by BCA assay.

2.8 Measurement of the size distribution of EVs

EV numbers and sizes were determined by NTA as well as DLS. For measurements using NTA, EVs were diluted in PBS in a range between 1:1000 to 1:8000 to ensure an optimal measurement concentration and measured with the ZetaView® Nanoparticle Tracking Analyzer PMX 110 and its corresponding software (ZetaView 8.03.08). For DLS measurements, EVs were diluted in PBS 1:20 for eWAT EVs or 1:50 for serum EVs, sonicated to separate aggregates and analysed using the Zetasizer Nano ZS with the corresponding software (Zetasizer Ver. 7.10).

2.9 Transmission electron microscopy imaging

TEM imaging was used to verify the presence and appearance of EVs in the isolated fractions. EV suspensions (5 µl) were deposited on formvar- carbon coated EM grids (200 mesh Copper) for 1 min. The grids were transferred to a 5 µl drop of 0.5% uranyl acetate in 70% ethanol solution for 2x 10 sec and then air dried for 10 min. The samples were examined by TEM using the Zeiss Libra 120 Plus. Pictures were acquired using a Slow Scan CCD-camera in combination with the iTEM software.

2.10 Liquid chromatography–mass spectrometry (LC-MS/MS) of isolated EVs

2.10.1 Sample preparation for mass spectrometric analysis

Isolated EVs from serum or AT (10 µg each) were subjected to tryptic digestion using a modified filter aided sample preparation (FASP) procedure (163,164). Human adipocyte, SVF and serum EVs were additionally purified before digestion using the Exo-spin™ columns according to the manufacturer's instructions. Subsequently, samples were diluted to 100 µl with 50 mM ammoniumbicarbonate (ABC), prior to cysteine reduction with 10 µl of 100 mM dithiothreitol for 30 min at 60°C. After cooling the samples to RT, they were diluted 2-fold with 8 M urea in 0.1 M Tris/HCl pH 8.5 and cysteines were alkylated with 10 µl of 300 mM iodoacetamide for 30 min at RT in the dark. Samples were centrifuged on a 30 kDa cut-off filter device, washed thrice with 8 M urea in 0.1 M Tris/HCl pH 8.5 and twice with 50 mM ABC. Flow-through solutions were discarded. Denatured proteins on the filter were digested in 70 µl of 50 mM ABC for 2 h at RT using 1 µg Lys-C and for additional 16 h at 37°C using 2 µg trypsin. Peptides were collected by centrifugation at 14,000×g for 2 min and filters were again eluted with 20 µl of 50 mM ABC/ 2% acetonitrile. Combined eluates were acidified with 0.5% trifluoroacetic acid and stored at -20°C until the mass spectrometric analysis.

2.10.2 Mass spectrometry

Before loading, the samples were centrifuged for 5 min at 4°C. LC-MS/MS analysis was performed as described previously on an LTQ-OrbitrapXL coupled to an Ultimate 3000 nano-HPLC (165,166). Approximately 0.5 µg of every sample was automatically injected and loaded onto the trap column (300 µm i.d.×5 mm, packed with Acclaim PepMap100 C18, 5 µm/100 Å; LC Packings) at a flow rate of 30 µl/min in 5% I/ 0.1% formic acid (FA). After 5 min the peptides were eluted from the trap column and separated on the analytical column (PepMap, 15cm, 75µm i.d., 3 µm/100 Å pore size, LC Packings) by a 135 min gradient from 7 to 32% I in 0.1% FA at a flow rate of 300 nl/min followed by a short gradient from 32 to 93% I in 0.1% FA in 5 min. Between each sample, the gradient was

set back to 7% I in 0.1% FA and left to equilibrate for 20 min. From the MS prescan, the ten most abundant peptide ions were selected for fragmentation in the linear ion trap if they exceeded an intensity of at least 200 counts and if they were at least doubly charged, with a dynamic exclusion of 60 s. During fragment analysis a high-resolution (60,000 full-width half maximum) MS spectrum was acquired in the Orbitrap with a mass range from 300 to 1500 Da.

2.10.3 Label-free analysis using Progenesis LC-MS

The acquired spectra were loaded to the Progenesis LC-MS software (version 2.5, Nonlinear) for label free quantification and analysed as previously described (165,166). Briefly, profile data of the MS and MS/MS scans were transformed to peak lists with respective peak m/z values, intensities, abundances (areas under the peaks) and m/z width. After reference selection, the retention times of the other samples were aligned by automatic alignment to a maximum overlay of all features. MS/MS spectra of features with charges of +2 to +7 were exported as mascot generic file and used for peptide identification with Mascot (version 2.3) in the Ensembl mouse protein database (release 72, 23210570 residues, 51372 sequences). Search parameters used were: 10 ppm peptide mass tolerance and 0.6 Da fragment mass tolerance, one missed cleavage allowed, carbamidomethylation was set as fixed modification, methionine oxidation and asparagine or glutamine deamidation were allowed as variable modifications. Searches were filtered with a mascot percolator score cut-off of 15 and an appropriate significance threshold p, in order to reach a false discovery rate of <1%. Peptide identifications were re-imported into the Progenesis LC-MS software. Summed normalized abundances of the proteins were exported and used for calculation of fold-changes and significance between groups.

2.11 EV microRNA isolation and profiling

The experiments to isolate and characterize EV-encapsulated microRNAs (miRNAs) were conducted at Exiqon, Denmark. In detail, isolated EVs (3 – 7 µg) were lysed in QIAzol lysis reagent and pre-purified by phenol (QIAzol)/chloroform extraction. Nucleic acids in the aqueous phase were precipitated with 100% ethanol and total RNA was extracted using the Qiagen miRNeasy® Mini Kit according to standard protocols. 10 µl RNA was reverse transcribed in 50 µl reactions using the miRCURY LNA™ Universal RT microRNA PCR system including a polyadenylation and cDNA synthesis kit (Exiqon, Denmark). cDNA was diluted 50x and assayed in 10 µl PCR reactions according to the protocol for the miRCURY LNA™ Universal RT microRNA PCR system; each microRNA was assayed once by qPCR on the microRNA Ready-to-Use PCR Mouse and Rat panel I using

ExiLENT SYBR® Green master mix (both Exiqon, Denkmark). Negative controls excluding template from the reverse transcription reaction were included and profiled like the samples. The amplification was performed in a LightCycler® 480 Real-Time PCR System in 384 well plates. The amplification curves were analysed using the LightCycler® 480 software, both for the determination of Cq (by the 2nd derivative method) and the melting curve analysis. The amplification efficiency was calculated using algorithms similar to the LinReg software. All assays were inspected for distinct melting curves and the melting temperature was checked to be within known specifications for the assay. Furthermore, assays had to be detected with 5 Cqs less than the negative control and had to have a Cq < 37 to be included in the data analysis. Data that did not pass these criteria were omitted from any further analysis. Using NormFinder (167), the best normalizer was found to be the average of assays detected in all samples. Accordingly, all data was normalized to the average of assays detected in all samples (average – assay Cq).

2.12 Staining and *in vivo* tracking of EVs

To visualize the organ distribution of eWAT EVs *in vivo*, stained EVs were injected and the EV assimilation was measured by analysing the fluorescence signal in different layers of the body. Briefly, freshly isolated EVs (20 – 50 µg in EV buffer) were incubated with the near-infrared fluorescent cyanine dye 1,1'-dioctadecyl-3,3,3',3'-tetramethylindotricarbocyanine iodide (DiR, dissolved in DMSO at 5 mg/ml) in a 1:500 dilution in PBS for 30 min at 37°C and 400 rpm on a thermal shaker (Thermomixer comfort). Subsequently, the stained EVs were washed with PBS and pelleted at 100,000×g for 2 h 10 min at 4°C using the Optima™ MAX-XP ultracentrifuge with the appropriate ultracentrifugation tubes. Stained EVs were re-suspended in EV buffer, quantified by BCA and immediately used for experiments. EV buffer subjected to the same labelling protocol served as a vehicle control. For *in vivo*-tracking studies, 10 µg of DiR-stained EVs or vehicle control were diluted in PBS (total volume 100 µl) and injected intraperitoneally (*ip.*) or intravenously (*iv.*) into 11 to 16-week-old male C57BL/6J mice. To obtain EV uptake kinetics, mice were sacrificed 4, 24 or 48 h after EV injection via CO_2 asphyxiation followed by shaving and freezing of the mouse carcass at -20°C. After embedding in Tissue-Tek® O.C.T. (Sakura, USA), the mouse was cryo-sliced along the long axis at steps of 100 µm, and co-registered colour and fluorescence cross-sectional images were acquired at each step in epi-illumination mode. For cryo-slicing and imaging a modified Leica CM 1950 cryotome, equipped with a motorized multi-wavelength filter wheel and a CCD-camera was used (168). Fluorescence images were captured at the peak emission wavelength of DiR (≈ 800 nm). Each image stack was further normalized

against the average maximum fluorescence intensity of the stack corresponding to the controls. Three representative slices per animal were selected. Regions of interest were defined to cover the complete cross-section of the organ from which the relative fluorescence intensity was calculated.

2.13 Functional assays with EV treatment *in vitro*

2.13.1 Functional impact of EVs on BMDMs

2.13.1.1 EV treatment of BMDMs and analysis of gene expression

To investigate if eWAT EVs are capable to influence inflammatory processes, BMDMs were isolated as described in chapter 2.1.2.2 and treated with different concentrations of eWAT EVs isolated from lean and obese mice. Therefore, fully differentiated BMDMs were seeded in 6 well plates with $1.5x10^6$ cells per well in serum-free medium (DMEM with 4.5 g/l glucose and 2 mM L-glutamine) supplemented with 100 U/ml penicillin and 100 µg/ml streptomycin. Six hours after seeding, cells were treated with 1 µg/ml or 5 µg/ml of EVs isolated from lean and obese eWAT. To induce M1 and M2 polarization, BMDMs were additionally treated with interferon gamma (IFNγ, 20 ng/ml) and interleukin 4 (IL-4, 10 ng/ml), respectively. After 24 h of incubation, the cells were harvested for gene expression analysis and therefore lysed, followed by RNA isolation and transcription to cDNA. M1/M2 marker gene expression was measured using qPCR with SYBR-Green (see chapter 2.3 for experimental details).

2.13.1.2 Measurement of macrophage phagocytosis

In addition to gene expression also the functional impact of adipocyte EVs on macrophages was assessed by measuring phagocytotic activity. Therefore, a phagocytosis assay with pHrodo™ BioParticles® Conjugates was performed according to the manufacturer's protocol. Briefly, $1x10^5$ cells were seeded in a 96 well plate in serum free-medium (DMEM with 4.5 g/l glucose and 2 mM L-glutamine) supplemented with 100 U/ml penicillin and 100 µg/ml streptomycin. Six hours after seeding, BMDMs were treated for 24 h with EVs from lean vs. obese adipocytes in absence or presence of IFNγ (20 ng/ml) and IL-4 (10 ng/ml). Furthermore, 1 h before the phagocytosis assay, additional control wells were treated with 1 µM Cytochalasin D, an inhibitor of cytoskeletal network formation to serve as negative control. Following treatment, pHrodo™ particles were added and fluorescence was measured after 1.5 h of incubation. For normalization cells were fixed in 4% paraformaldehyde (PFA) and stained with DAPI.

2.13.2 EV treatment of murine pancreatic islets and insulin secretion assay

Islets of Langerhans were isolated as described in chapter 2.1.2.3 and cultured ON to recover from the isolation procedure. For the following treatment with EVs isolated from eWAT of lean or obese mice, islets were hand-picked in 3.5 cm suspension dishes with 50 islets per condition. Treatments with 1, 5 or 10 µg of EVs were performed in culture medium depleted from FBS-derived EVs by ON centrifugation at 100,000×g and 4°C. After 6 h of treatment the islets were picked in groups of nine in a 96-well V-bottom plate and glucose stimulated insulin secretion (GSIS) was assayed using a static incubation. Therefore, islets were washed and pre-incubated for 1 h in modified Krebs Ringer buffer (KRB) (120 mM NaCl, 4.8 mM KCl, 2.5 mM $CaCl_2$, 1.2 mM $MgCl_2$, 5 mM HEPES, 24 mM $NaHCO_3$, 0.1% BSA) containing 2 mM glucose. The buffer was then replaced by KRB containing 2 mM glucose for 1 h (low glucose), followed by an 1 h incubation period in KRB containing 16.7 mM glucose (high glucose). To ensure a continuous treatment with EVs, all incubation steps were performed in EV containing buffers. Insulin contents of supernatants were determined by an enzyme-linked immunosorbent assay (ELISA) according to the manufacturer's instructions. For normalization, islets were lysed in RIPA buffer supplemented with protease inhibitor (Halt™ protease & phosphatase inhibitor cocktail) and total insulin and protein contents were measured by ELISA and BCA assays, respectively.

2.14 *In vivo* studies

2.14.1 Mouse husbandry

Male C57BL/6J mice (Janvier, France; 6 weeks of age) were housed three per cage under specific-pathogen-free conditions in individually ventilated cages. After one week of acclimatization, mice were *ad libitum* fed a HFD, 58% calories from fat, 5.56 kcal/g (D12331, Research Diets, USA) or chow, 3.34 kcal/g (1310, Altromin, Germany) for at least 16 weeks. For tissue sampling and blood collection mice were sacrificed by cervical dislocation or CO_2 followed by heart puncture.

2.14.2 Intraperitoneal glucose tolerance test (ipGTT)

Chow or HFD-fed male C57BL/6J animals were fasted for 6 h before receiving an intraperitoneal (*ip.*) glucose bolus of 1.7 mg/g body weight. Mice of the GW4869 study cohort received a bolus of 2 mg/g body weight. Blood glucose levels were measured before (0 min) and at 15, 30, 60, and 120 min after glucose administration using Freestyle Freedom Lite glucometers using tail vein blood. For EV-treatment, mice received 4 h prior to the glucose injection an *ip.* injection of 10 µg freshly prepared eWAT EVs from lean

mice, in a total volume of 100 µl diluted in PBS. Vehicle treated animals received the same amount of EV buffer only, diluted with PBS to a total volume of 100 µl.

2.14.3 Inhibition of EV secretion *in vivo* by GW4869 administration

2.14.3.1 Preparation of GW4869 for injection

The small molecule inhibitor GW4869 is a cell-permeable, specific and non-competitive inhibitor of nSMase (169) and is widely used to study EV secretion *in vitro* and *in vivo*. By blocking the formation of ceramide, GW4869 inhibits the invagination of vesicles into MVBs and therefore inhibits one possible route of EV formation (170,171). The maximum solubility of GW4869 given by the manufacturer is 0.2 mg/ml in 100 % dimethyl sulfoxide (DMSO). However, in previous studies concentrations up to 60-fold higher were used without mentioning any concerns regarding solubility or DMSO administration (172–175). Therefore, a stock solution with 2 mg/ml in DMSO was prepared to achieve an injection with 1 mg GW4869/kg body weight taking into account the regulations of a maximum injection volume of 10 ml/kg body weight and a maximum percentage of 5 % DMSO in the final injection volume.

2.14.3.2 Combined indirect calorimetry and metabolic phenotyping

Male C57BL/6J mice (Janvier, France) at an age of 5 weeks were given *ad libitum* access to HFD or chow diet for 24 weeks. Subsequently, mice were subjected to a combined indirect calorimetry system (TSE PhenoMaster) that allows the simultaneous measurement of food intake, energy expenditure, respiratory exchange ratio, and locomotor activity. After three days of acclimatization to the air-tight cages, groups of chow and diet-induced obese (DIO) mice (n=8) were intraperitoneally (*ip.*) injected with 1 mg/kg GW4869, or vehicle (5% DMSO in 0.9% NaCl). Injections were performed once daily in the first hours of the light phase for 16 days. Fat and lean masses were analysed at day 16 by nuclear magnetic resonance (EchoMRI). To investigate glucose homeostasis, an ipGTT was performed on day 13 (for experimental details see chapter 2.14.2). After 16 days of treatment mice were sacrificed by cervical dislocation. Epididymal fat pads and serum were collected for EV isolation and quantification as described above.

2.14.3.3 Measurement of the HOMA-IR

As a measurement for insulin resistance the Homeostasis Model Assessment of Insulin Resistance (HOMA-IR) index was determined prior to the treatment start and at day 13. Therefore, after an initial fast of six hours, glucose levels were measured with Freestyle Freedom Lite glucometers and a blood sample was drawn from the tail vein using EDTA-coated microvettes. A commercially available ELISA kit was used to quantify serum insulin (Ultra Sensitive Mouse Insulin ELISA kit) according to the manufacturer's instructions. The

HOMA-IR was calculated using the following formula with a conversion factor for insulin of 1 U = 0.0347 mg (176):

HOMA-IR = fasting insulin (mIU/l) × fasting glucose (mg/dl) / 405

2.15 Generation and evaluation of a monoclonal antibody

2.15.1 Immunization and isolation procedure

Purified EVs originating from SGBS cells (10 µg) were emulsified in an equal volume of incomplete Freund's adjuvant and 5 nmol CpG oligonucleotides and injected subcutaneously (*sc.*) and intraperitoneally (*ip.*) into two Lou/C rats and one C57BL/6 mouse. The immune response was boosted after six weeks by an additional *ip.* and *sc.* injection with EVs and CpG oligonucleotides in absence of Freund's adjuvant. Three days after the boosting injection, cells of the mouse myeloma cell line P3X63-Ag8.653 were fused with spleen cells from immunized animals according to the standard procedure described by Köhler and Milstein (177). The cells were plated and cultured in 96-well plates (24 plates for rat spleen, 8 plates for mouse spleen) in RPMI 1640 medium supplemented with 20% FBS, 100 U/ml penicillin, 100 µg/ml streptomycin, 1% sodium pyruvate, 1% non-essential amino acids, 2% hybridoma cloning factor and 2% hypoxantin-aminopterin supplement.

Ten days after fusion, cell supernatants were tested in a solid-phase ELISA for the presence of rat or mouse immunoglobulin Gs (IgGs). ELISA plates were coated with purified monoclonal mouse-anti-rat or rat anti-mouse κ- and λ-light chain antibodies (3 µg/ml each) in 0.2 M carbonate buffer with pH 9.5. After blocking with 2% FBS in PBS for 1 h at RT, the plates were washed once with PBS and hybridoma supernatants were added and incubated for 30 min. After another wash with PBS, bound antibodies were detected using a mixture of HRP-conjugated monoclonal mouse antibodies against the four rat or mouse IgG subclasses. HRP was visualized with ready-to-use TMB substrate solution (1-Step™ Ultra TMB-ELISA substrate) and the absorbance was measured at 650nm with a Tecan microplate reader.

2.15.2 Plate based immunofluorescence screening assay

Supernatants from IgG-positive clones were further validated by an immunofluorescence screening assay. Because of the limitations in available material and the lack of suitable methods for a screening assay, isolated EVs could not be used in the first screening approaches. Therefore, the primary source of the EVs, differentiated SGBS cells were used. As EVs due to their formation in the endosomal pathway share the outer membrane

with their cells of origin, antibodies can detect extracellular domains on both, EVs and parental cells.

To allow simultaneous testing of a high amount of hybridoma supernatants, a 96-well plate-based assay using immunofluorescence was developed. The assay uses three layers of antibodies: first, the antibody in the primary hybridoma supernatant to test binds the cells. Second, a subclass-specific antibody is used to bind the Fc region of the first antibody, and third, for detection a fluorophore-labelled antibody is used by binding the Fc-part of the secondary antibody. A scheme of the assay principle is depicted in Figure 6.

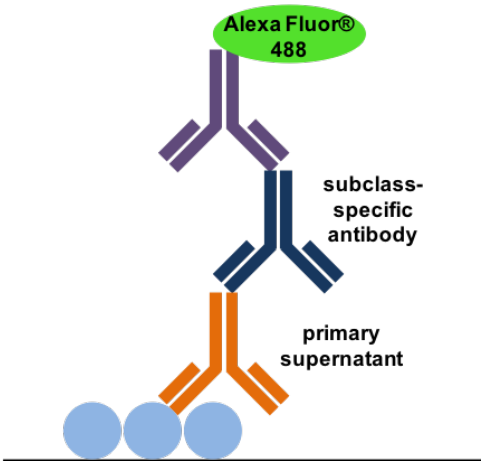

Figure 6: Schematic illustration of the assay principle used for the screening of hybridoma supernatants. *The antibody of the primary hybridoma supernatant binds the cultured cells, a secondary subclass-specific antibody binds the Fc region of the first antibody and a third fluorophore-labelled antibody is used for detection.*

In the first round of screening differentiated SGBS cells were used as positive control and the signal was compared to HepG2 cells serving as negative control. Only supernatants single positive in differentiated SGBS cells were further tested, all others were discarded. To further narrow down the number of specific supernatants, a second round of screening was performed, also using differentiated SGBS cells as positive control together with undifferentiated SGBS cells as negative control. Again, only supernatants single positive in differentiated SGBS cells were selected for further analysis. The cells were seeded in black 96-well plates with glass bottom to avoid confounders like plastic labware or the fluorescence of neighbouring wells. SGBS cells were seeded at a density of $6x10^3$ cells per well and differentiated until day 13 as described in 2.1.1.1. HepG2 cells were seeded 4 days prior to the assay at a density of $1x10^4$ cells per well. For the second round of screening undifferentiated SGBS cells were used as negative control and were therefore seeded in a density of $6x10^3$ cells per well, 6 days prior to the screening experiment. In

the screening assay, the cells were first washed once with PBS, followed by an incubation with the hybridoma supernatants for 30 min on ice. The plates were washed once with assay buffer (PBS supplemented with 1% FCS and 0.1% sodium azide) and the subclass mix consisting of hybridoma supernatants with antibodies against all IgG subclasses diluted 1:10 in assay buffer was added. After an incubation for 30 min on ice, the cells were washed once with assay buffer and the fluorophore-labelled antibody Alexa Fluor 488 (rat anti-mouse or mouse anti-rat, depending on the subclass mix) diluted 1:400 in assay buffer was added, followed by another 30 min incubation on ice, protected from light. Subsequently, the plates were washed twice with assay buffer and fluorescence was measured using a PHERAStar plate reader with an excitation at 485 nm and an emission at 520 nm. The signal of selected wells was also confirmed by fluorescence microscopy with the Keyence BZ-9000E microscope.

Cells from all positively tested supernatants were expanded, supernatant was collected and one vial of viable cells was frozen in FBS supplemented with 10% DMSO in liquid nitrogen. The IgG subclass in the supernatant was identified in an ELISA assay using mouse anti-rat or rat anti-mouse light chain antibodies as capture antibodies. For subclass determination, individual HRP-coupled mouse anti-rat or rat anti-mouse IgG subclass-specific antibodies were used as detection antibodies as described above. Additionally, the identified subclasses were confirmed in the immunofluorescence assay using differentiated SGBS cells. The assay was performed as described above, but instead of a mixture of all subclasses, single subclass antibodies were used as secondary antibody. At this stage most clones were oligoclonal and needed to be subcloned in order to obtain stable monoclonal hybridoma clones which can be used for large scale antibody production.

2.15.3 Target identification by immunoprecipitation and mass spectrometry

To identify the target proteins bound by the selected antibody clones, an immunoprecipitation (IP) together with a mass spectrometric analysis of the bound epitopes was performed. A scheme of the experimental procedure is depicted in Figure 7.

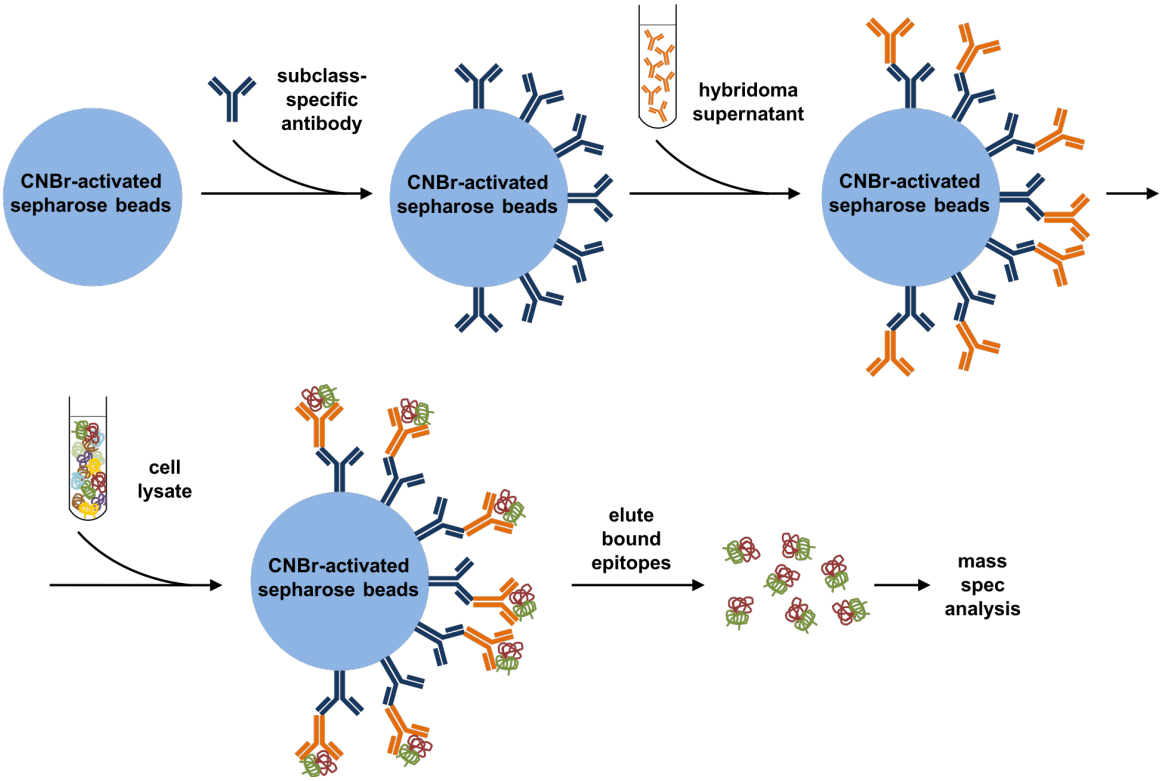

Figure 7: Experimental procedure of the immunoprecipitation assay. *Sepharose beads were coupled with subclass-specific antibodies and served as binding partners for antibodies in the hybridoma supernatants. The coupled beads were incubated with cell lysate, the bound epitopes eluted from the beads and analysed by mass spectrometry.*

For the IP assay, cyoanogen bromide (CNBr)-activated sepharose™ 4 fast flow beads were used according to the manufacturer's instructions. Briefly, the beads were activated with ice cold 1mM HCl and incubated ON at 4°C with 2.5 mg of subclass specific antibody (anti-R2a, anti-R2b or anti-M2a, according to the subclass of the hybridoma clone) in coupling buffer (0.1 M $NaHCO_3$, 0.5 M NaCl, pH 8.3). After washing with coupling buffer, remaining active groups were blocked with 1 M ethanolamine, pH 8 at RT for 2 h. The beads were washed three times each with wash buffer (0.1 M Tris-HCl, 0.5 M NaCl, pH 8) and acetate buffer (0.1 M NaAc, 0.5 M NaCl, pH 4), followed by another washing cycle of 3x washing buffer and 3x acetate buffer. Subsequently, the beads were washed three times with PBS and incubated with the hybridoma supernatants ON at 4°C. After 3 washes with PBS, the beads were incubated with SGBS cell lysate (generated in RIPA buffer without SDS, protocol see 2.2.1) ON at 4°C. To remove unbound protein fragments, the beads were washed once with RIPA buffer without SDS, followed by to washing steps with PBS supplemented with 0.5% N-Laurylsarcosine and 0.1% SDS and two additional washes with PBS. The bound epitopes were eluted from the beads with Laemmli buffer (22 mM Tris-HCl, pH 6.8, 3% glycerol, 0.8% SDS and 1.7% β-mercaptoethanol) and analysed by mass spectrometry.

2.15.4 Specificity testing by dot blot and immunostaining

Supernatants from positively tested clones were further validated by a dot blot with immunostaining to determine their specificity for EVs and cell lysates of different sources. Therefore, 2 µg or 10 µg of EVs from cell culture or serum, respectively, and 10 µg of cell lysates were spotted on a PVDF membrane as described above (see chapter 2.2.3), blocked for 1 h at RT in blocking buffer (TBS-T supplemented with 5% BSA) and incubated ON at 4°C with hybridoma supernatants diluted 1:10 in blocking buffer. After three 10 min washes with TBS-T, the blots were incubated with secondary antibody (anti-R2a, anti-R2b or anti-M2a, according to the subclass of the primary antibody) 1:1 000 in blocking buffer. Subsequently, the blots were washed three times with TBS-T, Clarity™ Western ECL Substrate was added and incubated according to the manufacturer's recommendations. Finally, the chemiluminescent signal was detected using the Odyssey® Fc Imaging System. Following imaging, the blots were washed with TBS-T and stained with Ponceau S (see chapter 2.2.5) for normalization purposes.

2.15.5 Subcloning and purification

After validation, cells from selected oligoclones were thawed and subcloned twice by limiting dilution to obtain stable monoclonal hybridoma cell clones. In each cloning round, specificity of up to ten subclones was determined by ELISA (IgG) and additionally verified in an immunofluorescence assay (for details see 2.15.1 and 2.15.2). Furthermore, the target specificity of the established clones was further validated by repeating the IP assay with mass spec analysis (2.15.3).

Antibodies were purified from 500 ml hybridoma supernatant on Protein G-Sepharose 4 Fast Flow columns. Bound IgGs were eluted with 0.1 M citrate buffer, pH 2.7 and the eluate was collected in a dialysis tube. To neutralize the pH, the eluate was dialyzed three times against PBS. The protein concentrations of the purified antibodies were determined at 235 and 280 nm using a NanoDrop spectrophotometer.

2.15.6 Antibody sequencing

To fully characterize the selected antibody clones, the sequences of the variable regions of the light and heavy chains were determined. First, RNA was isolated from frozen hybridoma cell pellets using the TRIzol chloroform method. RNA was transcribed to cDNA and amplified using the 5' Rapid amplification of cDNA ends (RACE)- PCR kit together with gene specific primers for heavy and light chain isotypes as previously described (178). For further purification, the resulting PCR product was applied to a 2 % agarose gel and separated. Fragments of approximately 750 bp of size were excised from the gel and purified using the QIAquick® Gel Extraction kit. Purified DNA was sequenced by Eurofins,

Germany, using Sanger sequencing. The DNA sequences were analysed with the online platform www.abysis.org.

2.16 Statistical analysis

Statistical analyses were performed using the GraphPad Prism 6.0 software (GraphPad Software Inc., USA) or the statistical programming environment R (R Development Core Team (179)) implemented in CARMAweb (180). Proteome analyses were done using MATLAB R2017a (MathWorks, USA) with Bioinformatics and Statistics toolbox. KEGG pathway enrichments were estimated using a hypergeometric distribution test. Data are shown as mean ± standard deviation (SD) unless otherwise stated. A p-value < 0.05 was considered statistically significant and p-values are displayed in the figures as * $p<0.05$, ** $p<0.01$, *** $p<0.001$.

2.17 Animal Ethics

The Animal Use and Care Committee of the state of Bavaria, Germany, approved all procedures.

2.18 Contributions from Collaborations

Parts of this work were not conducted solely by myself but were a result of fruitful collaborations. With these joint projects it was possible to increase the impact of this work to an international level and to gain novel insights in the rapidly developing field of EV research. Here, I therefore want to acknowledge the contributions of external experts to the presented results:

The imaging of EVs by TEM was performed together with Dr. Michaela Aichler and Gabi Mettenleitner (Helmholtz Zentrum München, AAP).

The proteome analysis of murine and human EVs was conducted at the Core Facility Proteomics (Helmholtz Zentrum München, PROT) by Dr. Stefanie Hauck and Dr. Juliane Merl-Pham. Additional help with data analysis was provided by Dr. Dominik Lutter (Helmholtz Zentrum München, IDO).

Particle size and distribution was measured using the ZetaView system in collaboration with Prof. Dr. Reinhard Zeidler and Dr. Kathrin Gärtner (Helmholtz Zentrum München, AGV).

The isolation and analysis of miRNAs originating from EVs was performed by Exiqon, Denmark.

The cryoslice experiments were conducted in collaboration with Prof. Dr. Vasilis Ntziachristos and Dr. Josefine Reber (Helmholtz Zentrum München, IBMI), who performed the slicing experiments and data analysis.

The development of a monoclonal antibody was performed in collaboration with the Monoclonal Antibody Core Facility (Helmholtz Zentrum München, MAB), especially with Dr. Regina Feederle, Andrew Flatley and Dr. Elisabeth Kremmer. The core facility performed the immunization, generation of hybridomas, ELISA testing, subcloning and purification of antibodies and also provided purified and HRP-labelled subclass antibodies.

3 Results

3.1 Murine adipocyte EVs – characterization and functional studies

3.1.1 Isolated vesicles show characteristic EV features

At the beginning of this thesis, published EV isolation protocols were mainly described for cell culture supernatants or biological fluids, only few reports existed for AT explant samples (133,181–183). The majority of these studies described EV isolation protocols for whole AT samples including the SVF. The SVF consists of several EV-secreting cell types like mesenchymal stem cells, endothelial cells, fibroblasts and a variety of immune cells (184,185) and therefore contributes to the EV-fraction released from whole tissue explant samples. Additionally, the cell number of immune cells like macrophages dramatically increases during the development of obesity from 5% to up to 50% of all AT cells (186), making non-adipocyte-derived EVs a highly confounding effect. To avoid co-isolation, my thesis aimed to establish a protocol to isolate EVs from the adipocyte fraction of the eWAT and iWAT excluding the SVF. In the course of this thesis, I use the term eWAT-EVs or iWAT-EVs for EVs stemming from the adipocyte fractions of the epididymal or the inguinal white adipose tissue, respectively.

TEM imaging of isolated eWAT- (Figure 8A), iWAT- (Figure 9E) and serum EVs (Figure 8B) of lean and DIO mice revealed a cup-shaped morphology typical for EVs. Size measurements by NTA showed that eWAT adipocytes of lean and obese mice released comparable vesicle populations ranging from 15 to 405 nm of size (Figure 8C), with a mean particle size ± SD of 157.2 ± 12.4 nm for lean eWAT EVs and 160.4 ± 7.6 nm for obese eWAT EVs (Figure 8E). Vesicles isolated of serum from lean and obese mice (Figure 8D) displayed a mean particle size ± SD of 123.2 ± 12.0 nm and 140.6 ± 15.0 nm, respectively, with a significant difference between diet groups (two-tailed Student's t-test, $p=0.02$; Figure 8E). The measured size ranges suggest that the isolated eWAT and serum EVs are a mixed population containing both small EVs like exosomes and large EVs like MVs. No additional particles were detected in the size range between 700 nm and 6000 nm (data not shown), indicating the absence of apoptotic bodies which are characterized by a size ranging from 1000 to 5000 nm (13).

In addition, the EV secretion rates from eWAT adipocytes and serum EV levels of chow and HFD-fed mice were determined by EV protein quantification. The measurements were normalized to the wet tissue mass or original volume of serum used for EV isolation, respectively. By quantifying total EV protein, a significantly increased EV secretion from eWAT explants of DIO mice compared to lean controls (Figure 8F) was found. Higher

secretion rates together with increased AT mass in DIO mice therefore should translate to an overall higher eWAT EV secretion and elevated circulating AT EVs under obese conditions. However, total EV protein levels measured in serum (Figure 8G) were not influenced by the dietary challenge of HFD-feeding.

To further characterize the isolated vesicles from iWAT or eWAT, the presence of classical exosomal markers like the tetraspanins CD9, CD63 and CD81 and the endosome-associated protein annexin A5 (ANXA5) was analysed by immunoblotting or mass spectrometry. In addition, Choleratoxin B (CTB) was used to stain ganglioside M1 (GM1) positive lipid rafts, which are enriched in exosomal membranes. Immunostaining of GM1 and CD63 (Figure 9A-D) confirmed the presence of EVs and indicated a tissue and diet-specific expression profile. Similar patterning was observed by mass spectrometric analysis of the exosomal markers CD9, CD81 and ANXA5 (Figure 9F, upper panels). Furthermore, the protein abundances of FABP4, adiponectin and leptin were significantly changed in eWAT and partially iWAT EVs from lean and DIO mice (Figure 9F, lower panels). Taken together, this indicates that adipocyte-derived EVs undergo a substantial change in composition upon a dietary intervention and that they dynamically reflect the metabolic state of their tissue of origin.

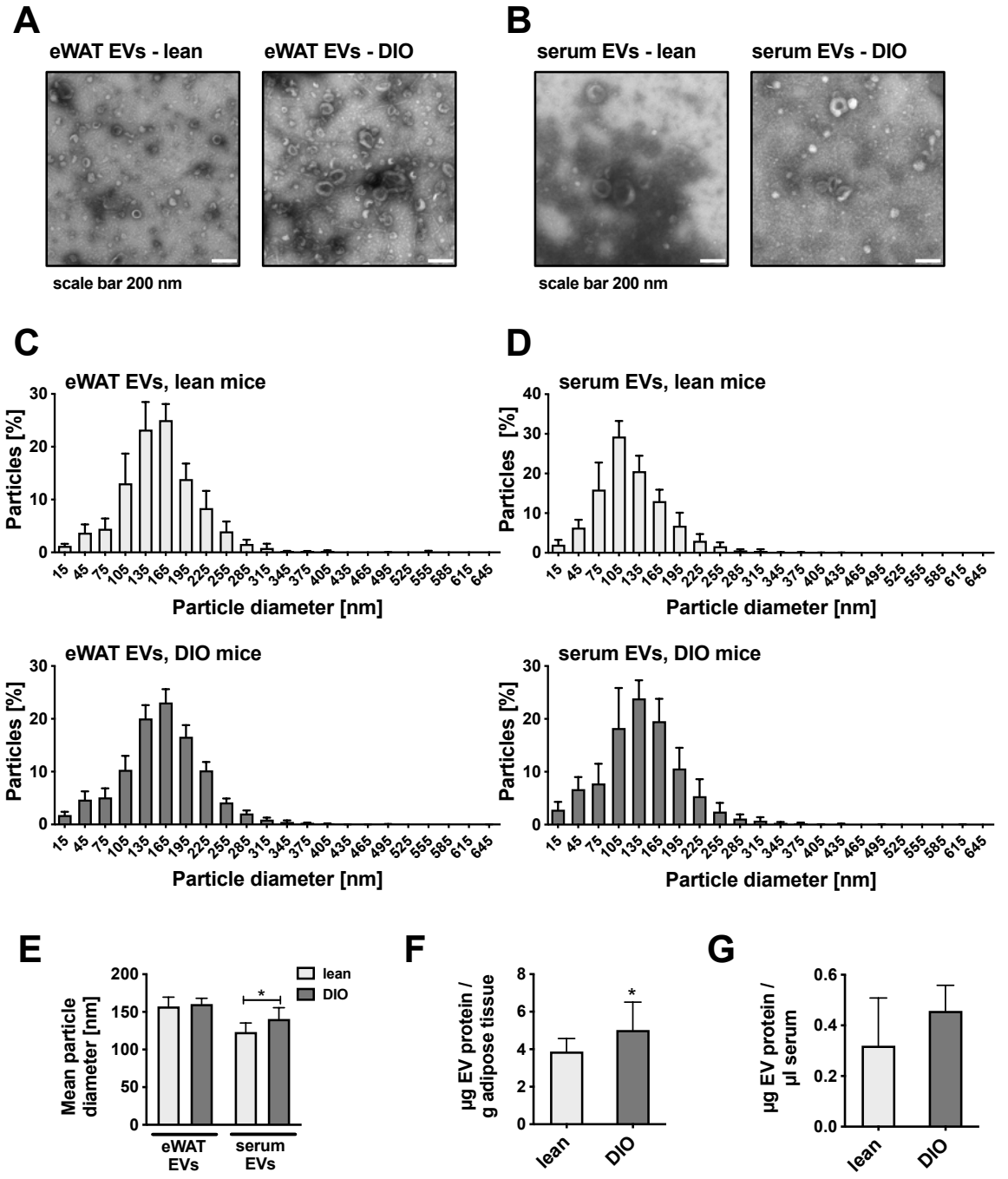

Figure 8: Vesicles isolated from eWAT and serum show characteristic EV properties. *(**A-B**) Representative transmission electron microscopy of EVs isolated from eWAT adipocytes (**A**) or serum (**B**) of lean (left panel) and diet-induced obese (DIO, right panel) mice (scale bar: 200 nm). (**C-D**) Size distribution of EVs secreted by eWAT adipocytes (**C**) and isolated from serum (**D**) of chow (upper panel) and HFD-fed (lower panel) mice, determined by nanoparticle tracking analysis (n=8, serum DIO n=7). (**E**) Mean particle size of eWAT and serum EVs isolated from chow and HFD-fed mice (n=8, serum DIO n=7) (**F**) EV secretion rates from eWAT adipocyte explants normalized to wet tissue weight (lean n=13, DIO n=10, pooled from 78 or 22 mice, respectively) and (**F**) EV levels from serum normalized to original serum volume used for EV isolation (lean n=8, DIO n=7). Data are shown as mean ± SD. Statistical significance was determined by two-tailed Student's t-test, * p<0.05.*

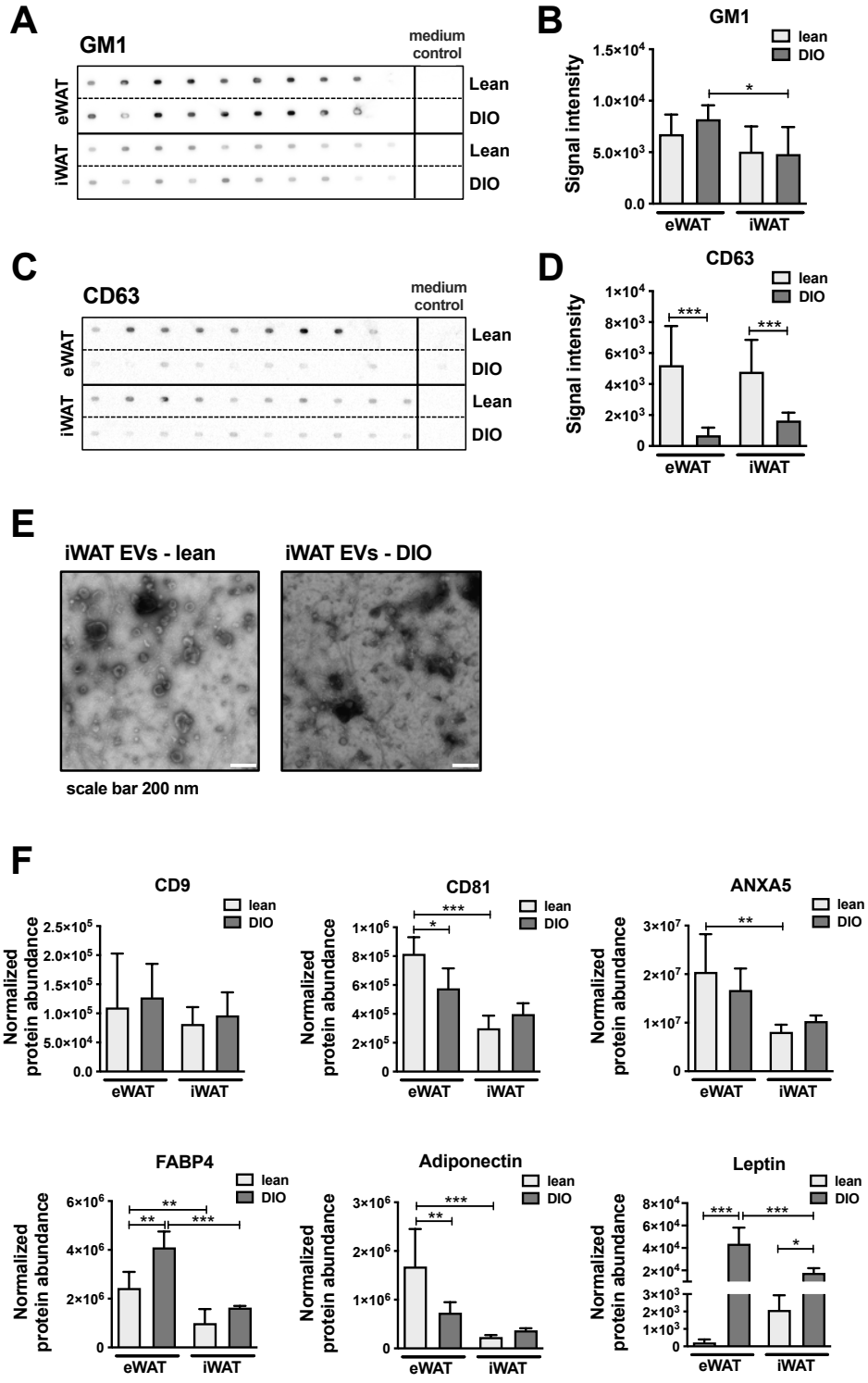

Figure 9: EVs can be isolated from visceral and subcutaneous adipose tissue. *(**A-D**) Dot blots of EVs derived from eWAT (upper panels) and iWAT (lower panels) of lean and DIO mice (eWAT n=9, iWAT n=10) and corresponding signal intensities of GM1 (**A**, **B**) and CD63 (**C**, **D**), medium subjected to the same isolation protocol was used as control. (**E**) Representative transmission electron microscopy of EVs isolated from iWAT adipocytes of lean and DIO mice (scale bar: 200 nm). (**F**) Relative protein abundance of the three exosomal marker proteins CD9, CD81 and annexin A5 (ANXA5) (upper panels), and of the adipocyte specific proteins fatty acid binding protein 4 (FABP4), adiponectin and leptin (lower panels), determined by mass spectrometry (normalized to all proteins, n=5, pooled from 25 mice). Data are shown as mean ± SD. Statistical significance was analysed by One-Way ANOVA and Tukey's multiple comparisons test, * p<0.05, ** p<0.01, *** p<0.001.*

3.1.2 Proteomic and miRNA profiling of EVs reveal substantial differences

The next aim of this thesis was to investigate the differences of EV cargo compared to the cell of origin and if the metabolic challenge of HFD-feeding could induce a change in EV composition. EVs were isolated from eWAT and iWAT of the same cohort of lean and DIO mice with significantly different mean body weights ± SD of 33.3 ± 1.0 g and 47.5 ± 4.0 g, respectively (two-tailed Student's t-test, $p<0.001$). The proteome analysis was conducted at the Core Facility Proteomics (Helmholtz Zentrum München, PROT) by Dr. Stefanie Hauck and Dr. Juliane Merl-Pham. EV proteome analyses revealed distinct protein signatures in adipocyte EVs depending on the tissue of origin (eWAT vs. iWAT) and the dietary intervention (lean vs. DIO) (Figure 10A). Total protein recovery rates following mass spectrometry were slightly higher in eWAT EVs (detected proteins: lean: 931, DIO: 1108) than in iWAT EVs (detected proteins: lean: 749, DIO: 772). For further analysis, proteins with a minimum of 2 peptides were selected and used for quantitation in both tissues and diet groups. This resulted in 793 proteins in eWAT EVs and 577 proteins in iWAT EVs with a broad overlap of 521 proteins detected in both tissue types (Figure 10B), indicating a wide similarity between AT EVs. When comparing diet groups, 80 proteins in eWAT EVs and 33 proteins in iWAT EVs were significantly deregulated between chow and HFD-feeding, with only 6 proteins shared in both tissue types (Figure 10C). KEGG pathway enrichment analyses of deregulated proteins identified 14 significantly enriched pathways ($p<0.05$) with again a distinct patterning between tissue types (Figure 10D). Determined pathways were mainly related to adipocyte differentiation and lipid metabolism, including PPAR signalling, fat digestion and absorption, biosynthesis of unsaturated fatty acids and peroxisome function. Additionally, identification of proteins involved in the PI3K/Akt signalling pathway further suggests an impact on a variety of fundamental cell processes, especially on adipocyte differentiation, insulin-stimulated glucose uptake and lipolysis.

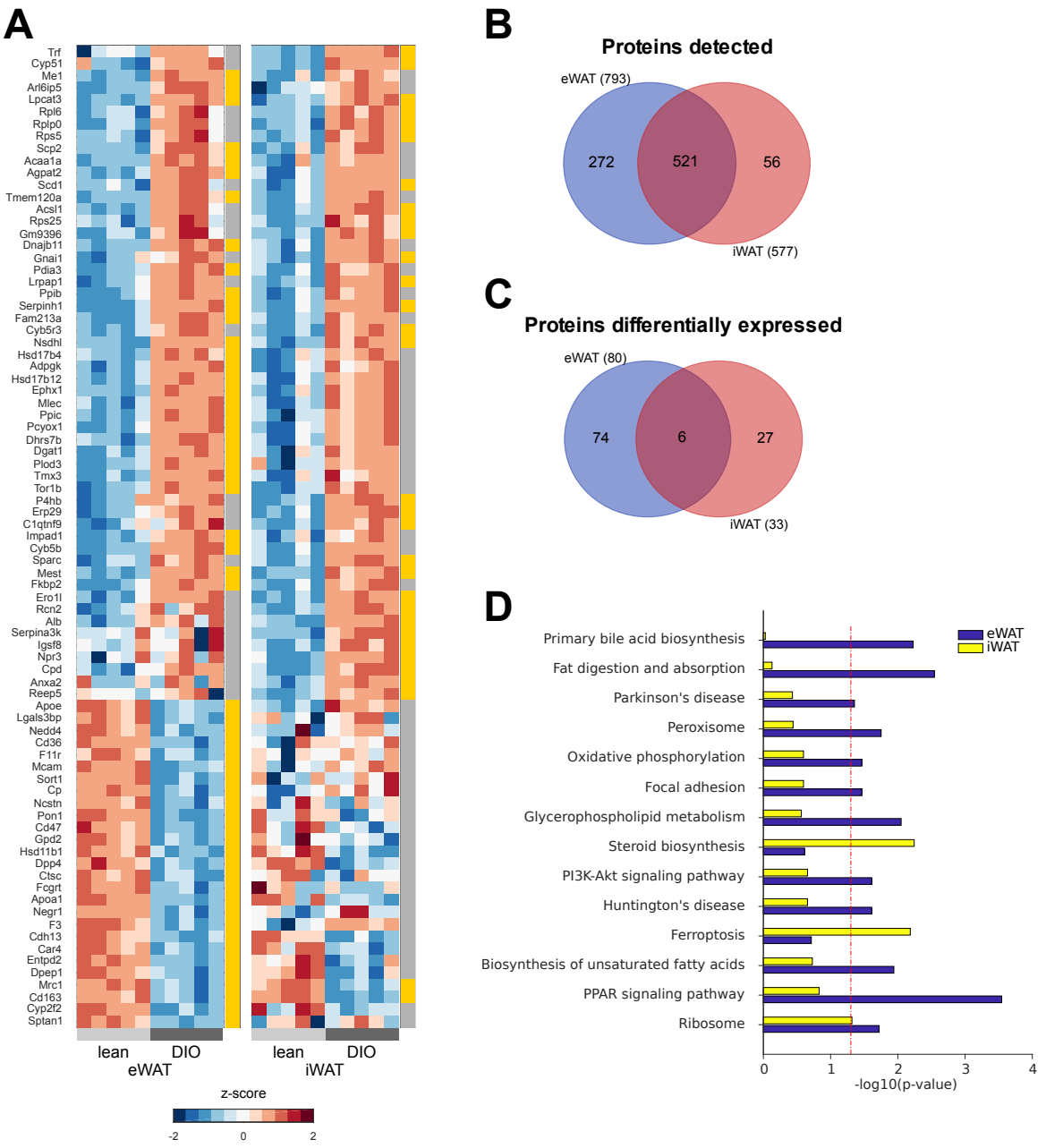

Figure 10: Proteome analysis of EVs from eWAT and iWAT reveals substantial differences in relation to diet and tissue of origin. *(**A**) Heatmap comparing significantly up- or downregulated EV proteins from eWAT and iWAT of lean and diet induced obese (DIO) mice (n=5). EVs from 5 mice were pooled for one sample replicate. Grey and yellow squares flanking the heat maps indicate non-significant and significant regulation between diet groups, respectively. (**B-C**) Venn diagrams displaying total numbers of detected proteins (**B**) and significantly deregulated proteins between diet groups (**C**) in eWAT and iWAT EVs and their overlap. (**D**) Analysis of significantly enriched KEGG pathways of protein contents in eWAT and iWAT EVs deregulated between diet groups. -Log10 p-values are shown as horizontal bars, the dashed line indicates a significance level of 0.05. Statistical significance was determined by ANOVA followed by Bonferroni correction using a p-value of 0.05, enrichment of KEGG pathways was assessed using hypergeometric distribution tests.*

To further elucidate if the EV protein cargo reflects the tissue of origin, the proteomes of eWAT EVs and eWAT tissue lysates were compared. Total protein recovery depended on the sample matrix and was slightly higher in eWAT tissue lysates (1125 detected proteins) compared to eWAT EVs (793 detected proteins) with an overlap of 405 proteins (Figure 11A). Spearman rank correlation testing was used to compare the log fold change (logFC) expression levels of all detected proteins (DIO vs. lean) between eWAT lysates and eWAT EVs. It confirmed a highly significant association between tissue lysates and eWAT EVs, indicating that eWAT EVs closely reflect the metabolic status of the secreting AT (Figure 11B). Additional KEGG analysis of the significantly deregulated proteins in lean and DIO mice predicted 53 significantly enriched pathways in eWAT EVs and 22 pathways in the tissue lysates ($p<0.05$, Table S 1). Interestingly, significantly enriched pathways involved in lipid metabolism, insulin and adipocytokine signalling were overrepresented in eWAT EVs compared to eWAT tissue lysates, indicated by higher numbers of deregulated genes per pathway (Figure 11C). Together, these findings suggest that adipocyte EVs reflect the status of their originating cell and furthermore that the eWAT EV proteome could represent a superior predictor for the metabolic state of adipocytes compared to the proteome of whole tissue lysate.

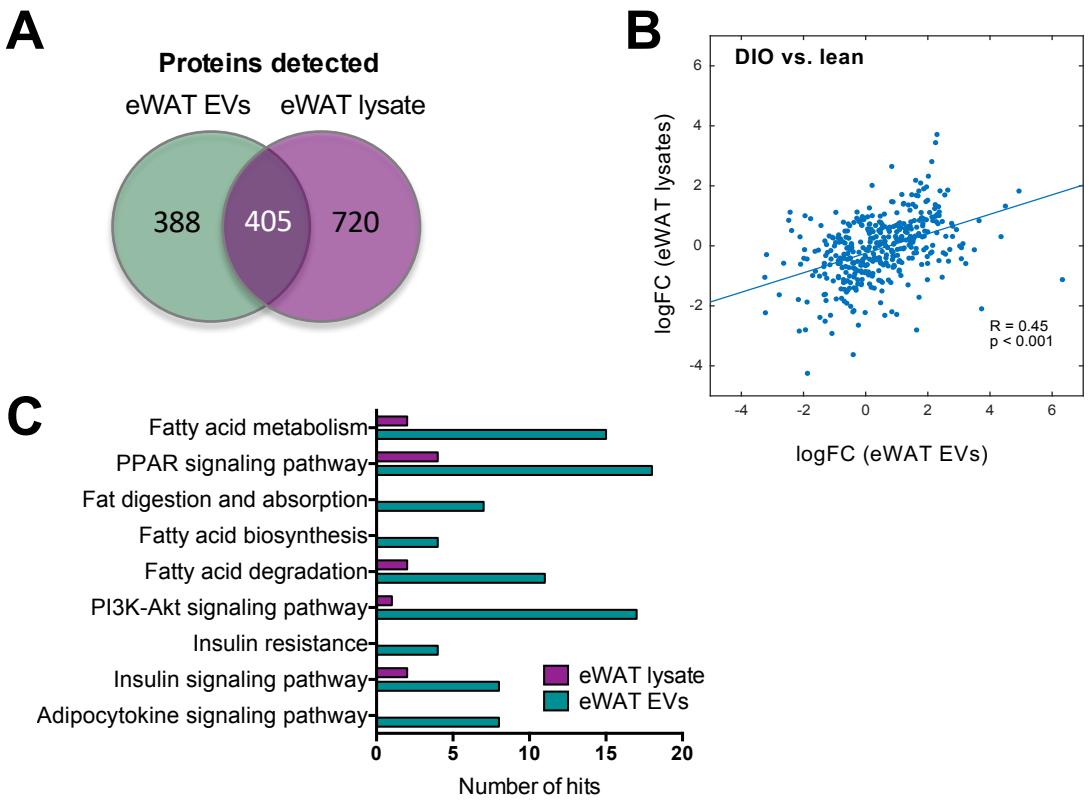

Figure 11: Comparison of the proteome of eWAT EVs and eWAT tissue lysate shows that EVs reflect their tissue of origin and can be used as surrogate markers. *(**A**) Venn diagram displaying number of proteins detected in eWAT EVs and tissue lysates together with their overlap. (**B**) Spearman rank correlation test comparing the log fold change (logFC) expression levels of all detected proteins (diet induced obese (DIO) vs. lean) between eWAT lysates and eWAT EVs. (**C**) Analysis of significantly enriched KEGG pathways of protein contents of eWAT EVs and tissue lysate deregulated between diet groups. Number of enriched genes are displayed as horizontal bars. Statistical significance was determined by ANOVA followed by Bonferroni correction using a p-value of 0.05, enrichment of KEGG pathways was assessed using hypergeometric distribution tests.*

In addition to proteins, various nucleic acids have recently been identified in EVs (40,41,58) and especially miRNAs have been reported to modulate EV target cells (38,187,188). To better specify how adipocyte EVs could affect distinct target organs, the miRNA contents from eWAT EVs of lean and obese mice were isolated and compared. Out of a panel of 372 miRNAs, 139 miRNAs were detected in both groups. Statistical analysis comparing the diet groups using a t-test with a p-value threshold of 0.05 identified 53 miRNAs to be differentially deregulated in eWAT adipocyte-derived EVs from lean vs. obese mice (Figure 12A). An additional Benjamini-Hochberg correction at a significance level of 0.05 narrowed down the number of deregulated miRNAs to 19 (Table 7). To further assess the regulatory roles of the differentially regulated miRNAs and their controlled pathways a KEGG pathway analysis was performed using DIANA-miRPath

v3.0 online software (189) applying a p-value cut-off of 0.001, whereby 30 enriched KEGG pathways could be identified. Amongst others these pathways included fatty acid metabolism as well as insulin signalling (Figure 12B).

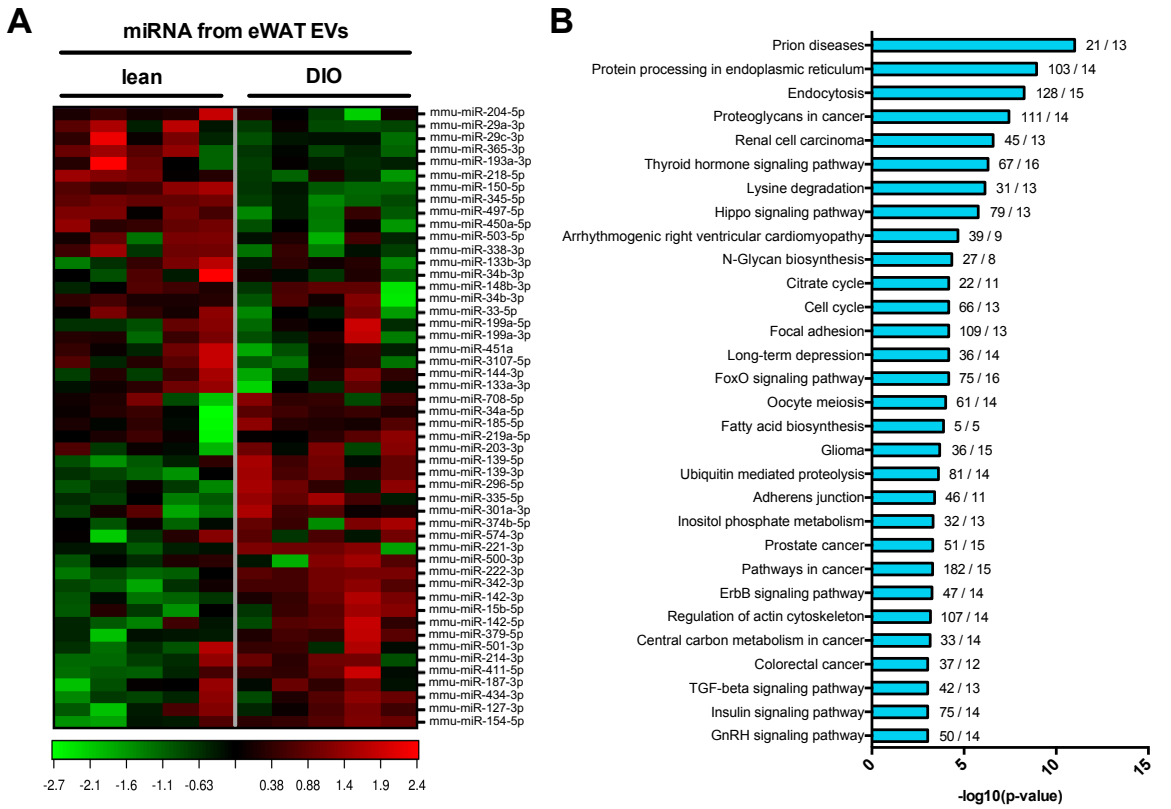

Figure 12: The miRNA profile of eWAT EVs is altered by HFD feeding. *(**A**) Heatmap displaying the result of the two-way hierarchical clustering of miRNAs and samples (n=5, EVs from 5 mice were pooled for one sample replicate). Each row represents one miRNA, each column represents one sample. The clustering was performed on all samples and on the top 50 miRNAs with highest standard deviations. (**B**) Significantly enriched KEGG pathways of 19 differentially expressed miRNAs in eWAT EVs from lean and obese mice, using DIANA-miRPath v3.0 online software with a p-value cut-off of 0.001. -Log10 p-values are shown as horizontal bars, numbers behind bars indicate number of regulated genes and involved miRNAs.*

Table 7: Significantly deregulated miRNAs in eWAT EVs isolated from lean and DIO mice *also showing the fold change (FC) between diet groups and p-values of t-test and Benjamini-Hochberg (BH) correction.*

miRNA	FC (DIO / lean)	t-test p-value	BH adj. p-value
mmu-miR-101a-3p	-1.6715	0.0001	0.0137
mmu-miR-143-3p	-1.6183	0.0002	0.0137
mmu-miR-222-3p	4.0947	0.0003	0.0137
mmu-miR-150-5p	-2.4025	0.0003	0.0137
mmu-miR-345-5p	-2.5334	0.0003	0.0137
mmu-miR-27b-3p	1.6139	0.0006	0.0183
mmu-miR-139-3p	5.6558	0.0007	0.0183
mmu-miR-181a-5p	-1.6744	0.0007	0.0183
mmu-miR-322-5p	-1.7413	0.0009	0.0189
mmu-miR-142-3p	2.4302	0.0009	0.0189
mmu-miR-126a-3p	-1.7111	0.0014	0.0262
mmu-miR-24-3p	1.5757	0.0016	0.0269
mmu-miR-376a-3p	3.3743	0.0029	0.0440
mmu-miR-342-3p	4.3555	0.0032	0.0440
mmu-miR-425-5p	-1.4712	0.0034	0.0440
mmu-miR-146b-5p	1.7666	0.0036	0.0440
mmu-miR-29b-3p	-1.4181	0.0038	0.0440
mmu-miR-18a-5p	1.7924	0.0038	0.0440
mmu-miR-450a-5p	-2.6134	0.0045	0.0487

Analysing the potential regulatory targets of the 53 significantly deregulated miRNAs identified by t-test with a p-value threshold of 0.05 revealed a broad spectrum of possible interference (Table 8). The identified miRNAs have been previously reported to be involved in adipogenesis, adipocyte browning, inflammation and macrophage polarization. Additionally, potential targeted pathways are exocytosis and insulin secretion as well as insulin gene regulation, suggesting not only a paracrine but also endocrine mode of action. The corresponding fold change between diet groups, however, was not clearly conclusive regarding the direction of modulation towards up- or downregulation.

Overall, these findings suggest that body weight and environmental factors like dietary interventions influence EV cargo, in particular the EV proteome and miRNA profiles.

Table 8: Differentially expressed miRNAs in eWAT EVs and their known involvement in selected pathways. *The last two columns show fold changes (FC) between lean and DIO mice and the respective p-values from t-tests. * p<0.05, ** p<0.01, *** p<0.001.*

Pathway	miRNA	Function	Reference	FC (DIO / lean)	t-test p-value
Adipogenesis	miR-143	Enhancer and inhibitor of adipogenesis (stage dependent)	(190)	-1.618	0.0002***
	miR-139	Inhibitor of adipogenesis	(191)	5.656	0.0007***
	miR-181a	Enhancer of adipogenesis	(192)	-1.674	0.0007***
	miR-342	Enhancer of adipogenesis	(193)	4.355	0.003**
	miR-425	Inhibitor of adipogenesis	(194)	-1.471	0.003**
	miR-146b	Promotor of adipogenesis	(195)	1.767	0.004**
	miR-29b	Promotor of adipogenesis	(196)	-1.418	0.004**
	miR-450a	Promotor of adipogenesis	(197)	-2.613	0.004**
	miR-145a	Promotor of adipogenesis	(198)	-1.445	0.008**
	miR-15b	Promotor of adipogenesis	(199)	2.043	0.031*
	miR-141	Promotor of adipogenesis	(200)	-4.250	0.038*
	miR-26b	Promotor of adipogenesis	(201)	-1.479	0.038*
	miR-193b	Enhancer of adiponectin secretion	(202)	-1.435	0.049*
Adipocyte browning	miR-150	Negative regulator of AT browning	(203)	-2.403	0.0003***
	miR-27b	Negative regulator of browning	(204)	1.614	0.0006***
	miR-338	Negative regulator of browning	(205)	-2.519	0.027*
Inflammation and macrophage polarization	miR-222	Adipocyte inflammation	(206)	4.095	0.0003***
	miR-345	Adipocyte inflammation	(206)	-2.533	0.0003***
	miR-142	Macrophage polarization	(207)	2.430	0.0009***
	miR-10a	Anti-inflammatory via IL6 and TNF suppression	(208)	-1.601	0.009**
	miR-342	Activation of inflammatory macrophages	(209)	4.985	0.017*
	miR-326	Inhibition of macrophage activation	(210)	1.487	0.020*
	miR-23b	Anti-inflammatory via suppression of IL17	(211)	1.440	0.021*
	miR-99a	Macrophage polarization	(212)	-1.253	0.027*
	miR-365	Anti-inflammatory via suppression of IL6	(213)	-1.716	0.044*
Exocytosis and insulin secretion	miR-322	Negative regulator of insulin secretion by repression of Stxbp1	(214)	-1.741	0.001***
	miR-218	Negative regulator of insulin secretion by repression of Stxbp1	(214)	-2.53	0.006**
	miR-335	Negative regulator of insulin secretion	(215)	4.192	0.007**
	miR-135a	Negative regulator of insulin signalling	(216)	-3.630	0.018*
	miR-29a	Negative regulator of insulin secretion by repression of Stx1a	(217)	-1.730	0.045*
Insulin gene regulation	miR-24	Positive regulator of insulin transcription	(218)	1.576	0.002**
	miR-26	Upregulation of insulin transcription	(218)	-1.594	0.005**
	miR-196b	Positive regulator of insulin transcription	(219)	-4.943	0.027*

3.1.3 Injected adipocyte EVs specifically locate in distinct target organs

The next aim was to investigate whether circulating eWAT EVs can function as a novel route of intercellular and even inter-organ communication. Specifically, I aimed to elucidate if eWAT EVs accumulate in distinct tissues with metabolic relevance.

Lean C57BL/6J mice received an intraperitoneal (*ip.*, Figure 13) or intravenous (*iv.*, Figure 14) injection of either eWAT EVs labelled with the lipophilic near-infrared fluorescent cyanine dye DiR or DiR-stained PBS as control, and were sacrificed 4, 24 or 48 h after the injections. Subsequent cryo-slicing of the whole murine torso along the axial planes followed by automated fluorescence analysis of each slice was used to quantify fluorescence intensities in different target organs. The cryo-slicing and data analysis were performed in collaboration with Prof. Dr. Vasilis Ntziachristos and Dr. Josefine Reber (Helmholtz Zentrum München, IBMI).

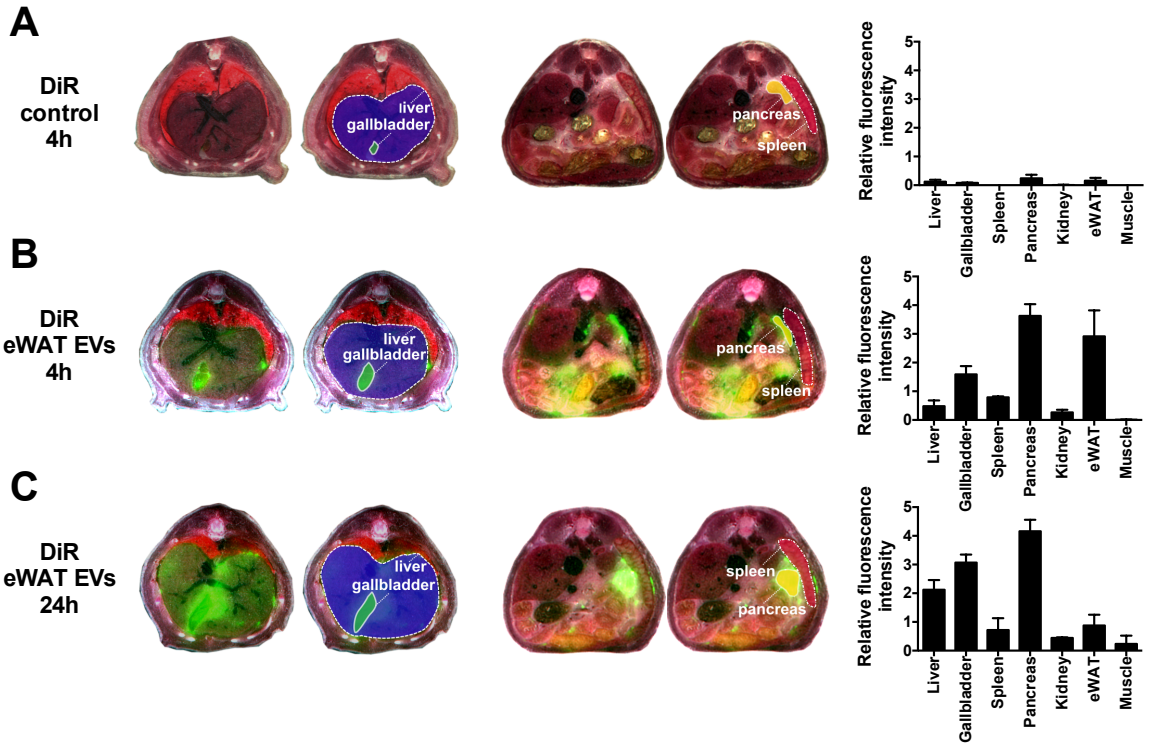

Figure 13: Tissue specific uptake of ip. injected fluorescently labelled eWAT EVs in mice. *Representative cross-sections of multiscale and multispectral images of the whole cryosliced mouse torso along the axial planes after colour and fluorescence image fusion (left/middle panels) together with relative quantifications of fluorescence intensities between the target organs (right panels) of mice ip. injected with (**A**) DiR-control 4 h after ip. injection and (**B**) DiR-labelled eWAT EVs 4 h after ip. injection and (**C**) DiR-labelled eWAT EVs 24 h after ip. injection. Images are shown as unlabelled (left) and overlaid with organ labels (right). Three representative slices per animal (n=2) were selected for quantification. Data represent organs with detectable signals only and are shown as mean ± SD.*

Image analysis revealed minor background staining in *ip.* injected control mice (Figure 13A and Figure S 1A) and a clear organ specific targeting of DiR-eWAT EVs 4 h after *ip.* injection (Figure 13B). The measured fluorescence intensity even increased 24 h after *ip.* injection (Figure 13C), suggesting time-dependent uptake kinetics. When evaluating the delivery pattern, the DiR-eWAT EV signal 4 h after *ip.* injection was highest in the pancreas followed by eWAT, gallbladder, spleen and kidney. No signal was found in iWAT and muscle. After 24 h, highest fluorescence intensities were detected in the pancreas, followed by gallbladder, liver, eWAT, spleen, kidney and muscle, while iWAT was still negative. To proof whether this delivery pattern is unique to eWAT EVs, DiR-labelled Panc02-EVs were also injected *ip.*, showing a lower uptake into the liver and an early uptake into the muscle compared to eWAT EVs (Figure S 1C).

Furthermore, comparing the *ip.* and *iv.* injections revealed that the route of EV-administration strongly influences the delivery pattern and uptake kinetics. Consistent with the observations in *ip.* injected mice, minor background fluorescence intensities were detected in the DiR-control *iv.* injections (Figure 14A and Figure S 1B). Interestingly, only weak signals were detected 4 h after *iv.* injection (Figure 14B) whereas *ip.* injected mice already showed an intense staining. 24 h after *iv.* injection, DiR-labelled eWAT EVs were detected in 11 organs with the highest signal in spleen, followed by liver, gallbladder, lung, iWAT, deep brain areas, pancreas, upper brain areas, kidney, eWAT and muscle (Figure 14C). Increasing the time to 48 h resulted in highest fluorescence intensities in spleen, followed by liver, gallbladder, lung, upper brain areas, deep brain areas, pancreas, kidney, eWAT, iWAT and muscle (Figure 14D).

Taken together, the observed organ-specific delivery pattern especially to metabolically active target organs such as liver, pancreas and eWAT points towards a contribution of eWAT EVs to cellular communication in the regulation of metabolism and metabolic diseases.

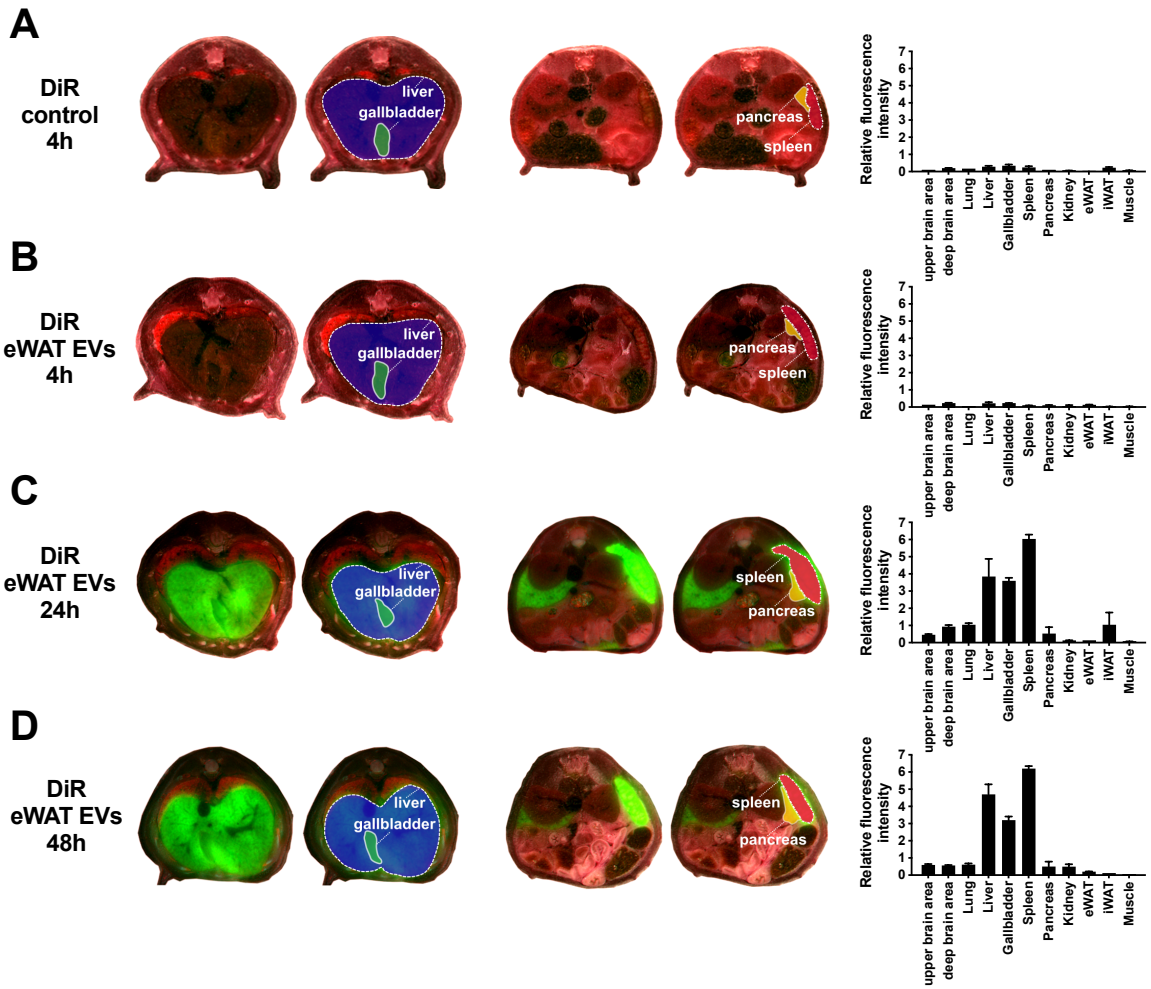

Figure 14: Tissue specific uptake of iv. injected fluorescently labelled eWAT EVs in mice. *Representative cross-sections of multiscale and multispectral images of the whole cryosliced mouse torso along the axial planes after colour and fluorescence image fusion (left/middle panels) together with relative quantifications of fluorescence intensities between the target organs (right panels) of mice iv. injected with (**A**) DiR-control 4 h after iv. injection and (**B**) DiR-labelled eWAT EVs 4 h after iv. injection, (**C**) DiR-labelled eWAT EVs 24 h after iv. injection and (**D**) DiR-labelled eWAT EVs 48 h after iv. injection. Images are shown as unlabelled (left) and overlaid with organ labels (right). Three representative slices per animal (n=2) were selected for quantification. Data represent organs with detectable signals only and are shown as mean ± SD.*

3.1.4 Hypoxia has no impact on EV secretion of adipocytes

With the ongoing expansion of AT mass upon the development of obesity, supplying the tissue with oxygen becomes an issue. Previous publications have shown that hypoxia is a major trigger of AT dysfunction and occurs particularly in obese AT leading to obesity-associated metabolic consequences (220–222). Additionally, EV secretion has been shown to be increased under hypoxic conditions for instance in cancer cells (223–225). I therefore investigated whether cultured adipocytes also respond to oxygen deprivation, either with an impaired or excessive secretion of EVs.

SGBS cells were differentiated according to standard protocols and incubated 48 h under normoxic (20% O_2) or hypoxic conditions (3% O_2) for EV release. eWAT adipocytes from lean mice were isolated using collagen digestion, separated from the SVF and incubated 2 h applying the same normoxic or hypoxic conditions. EVs were isolated from the conditioned media and quantified by BCA analysis. In both types of adipocytes, oxygen deprivation did not significantly alter the amount of released EVs (Figure 15 A and B).

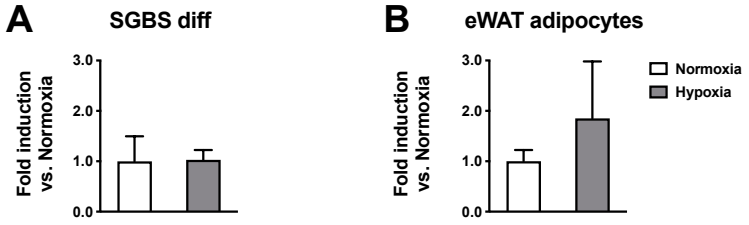

Figure 15: Hypoxia does not affect EV secretion of SGBS cells and eWAT adipocytes*. EV secretion of (**A**) differentiated SGBS cells (n=4) and (**B**) lean eWAT adipocytes (n=3) under hypoxic conditions. Data are expressed as fold induction compared to normoxia and shown as mean ± SD.*

3.1.5 Adipocyte EVs have no effect on adipocyte differentiation and browning

Prompted by findings of the proteome and miRNA analysis showing that adipocyte EVs carry various proteins and miRNAs involved in adipocyte biology (Table S 1 and Table 8), the next aim was to investigate paracrine effects of adipocyte EVs regarding adipocyte differentiation and browning.

In vitro-differentiated primary iWAT adipocytes were treated with EVs isolated from iWAT of lean and obese mice and after 24 h of incubation gene expression of *Ucp1* and *Ppargc1α* was analysed. Both genes are highly expressed in BAT and are increased in brite/beige adipocytes in WAT (226,227). However, neither treatment with lean nor obese iWAT EVs resulted in an altered expression of *Ucp1. Ppargc1α* was significantly downregulated with lean iWAT EVs compared to vehicle treated cells, while EVs from DIO mice had no effect (Figure 16A). Stimulation of browning with isoproterenol 6 h after the EV treatment induced a general increase of *Ucp1* and *Ppargc1α* expression in all groups (data not shown), treatment with lean or obese iWAT EVs, however, had no additional effect (Figure 16B). Gene expression in relation to adipocyte differentiation was investigated using the human adipocyte strain SGBS, by treatment of undifferentiated cells with EVs isolated from differentiated SGBS adipocytes for 48 h. Expression of the adipogenesis marker genes *PPARG* and *FABP4* was not altered after treatment with 1 µg of SGBS EVs, increasing the EV dose to 5 µg also did not lead to a change in gene expression compared to vehicle treated cells (Figure 16C).

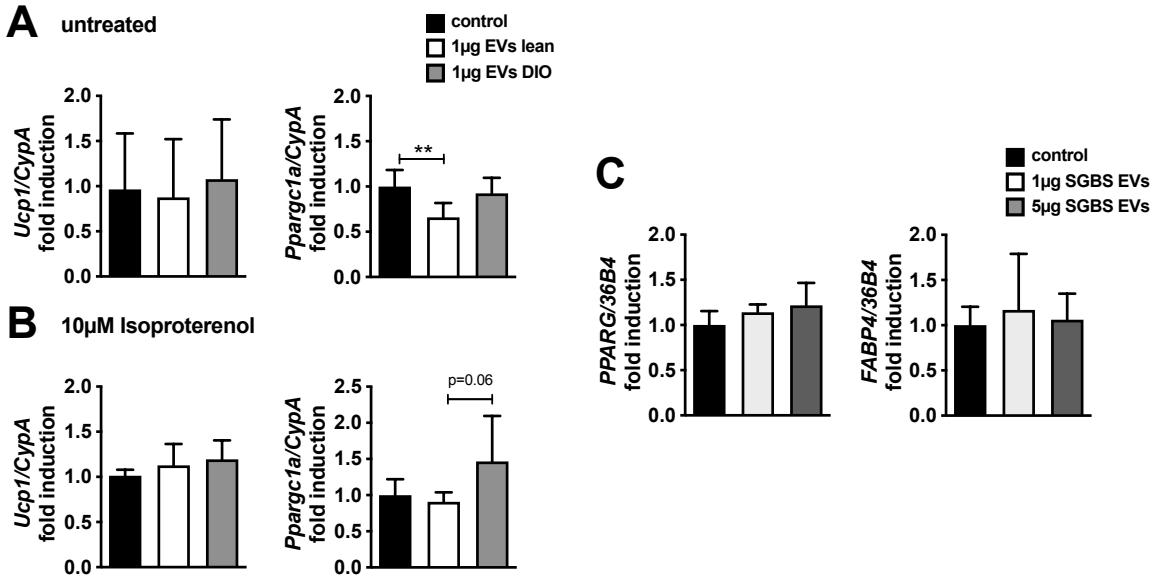

Figure 16: Adipocyte-derived EVs do not exert effects on characteristic gene expression involved in iWAT browning or adipocyte differentiation. *(**A**) mRNA expression of Ucp1 and Ppargc1α in primary inguinal adipocytes treated with control buffer or 1 µg of iWAT EVs isolated from lean or obese mice (n=3). (**B**) To induce browning, cells were treated for 6 h with 10 µM isoproterenol subsequent to the EV treatment of 24 h (n=3). (**C**) mRNA expression of PPARG and FABP4 in undifferentiated SGBS cells after 48 h treatment with 1 or 5 µg of EVs from differentiated SGBS cells (n=2). Gene expression was assayed in duplicates and normalized to house-keeping genes. All data were normalized to the respective buffer controls. Data are shown as mean ± SD. Statistical significance was analysed by One-Way ANOVA and Sidak's multiple comparisons test, ** p<0.01*

3.1.6 Macrophage polarity and function is not modulated by adipocyte EVs

In recent years, macrophages residing in AT have gained more and more attention as important contributors to AT function (186). Being also present in lean AT, macrophage numbers increase dramatically during obesity and concomitant inflammatory activation leads to metabolic complications such as insulin resistance (228,229). These previous investigations together with the detected proinflammatory miRNA signature in isolated eWAT EVs led to the hypothesis that adipocyte EVs contribute to the rising AT inflammation observed in the state of obesity by the activation and polarization of co-localized macrophages.

Therefore, BMDMs were treated with increasing concentrations of lean and obese eWAT-derived EVs for 24 h. Except for a vehicle-treated control group, macrophages were stimulated with either IFNγ or IL-4 to induce polarization towards a pro-inflammatory M1 or anti-inflammatory M2 phenotype, respectively. Expression of the M2 marker genes *Arg1*, *Clec10a* and *Fizz1* did not change with any EV treatment (Figure 17A). IFNγ-induced M1 polarization measured by *Nos2* gene expression was also not affected by lean or obese eWAT EVs (Figure 17B). Macrophage functionality assessed as phagocytotic uptake of

fluorescently labelled E.coli particles after 1.5 h of co-incubation following the EV exposure was also not altered upon the treatment with eWAT EVs from lean or DIO mice (Figure 17C).

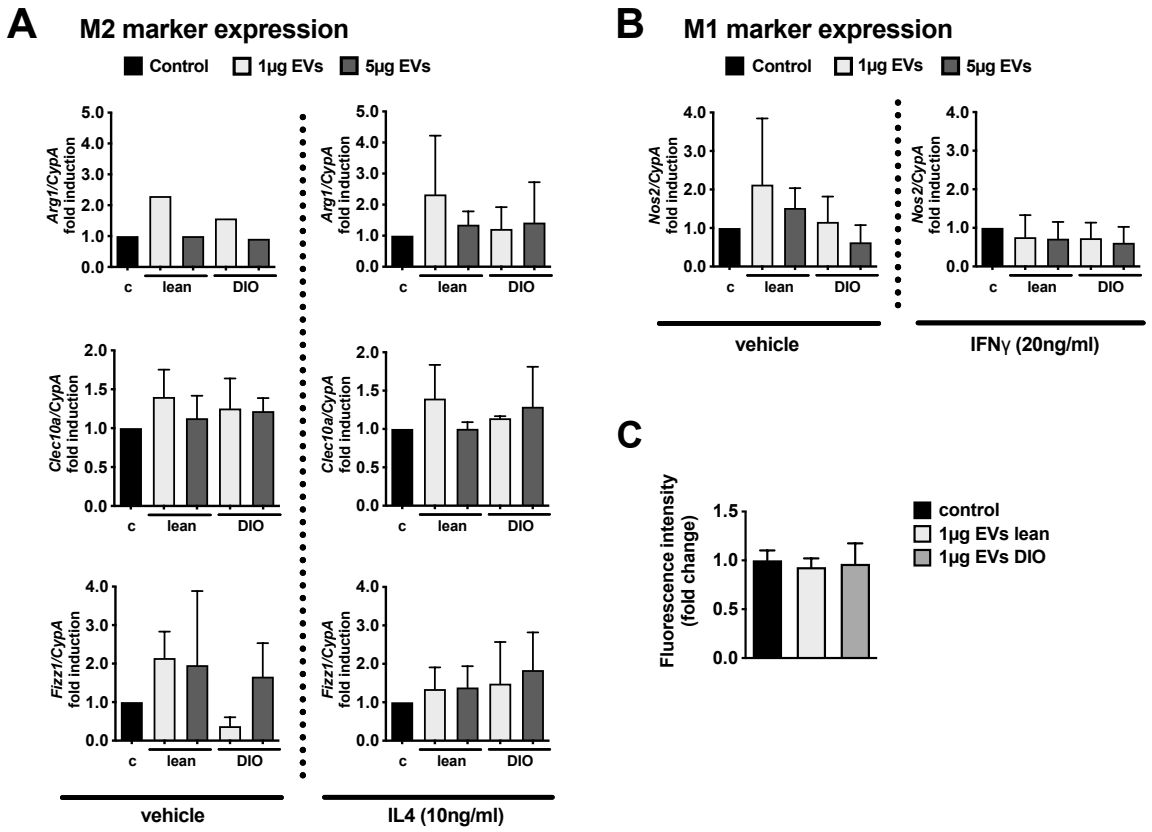

Figure 17: Macrophage polarization and functionality is not influenced by eWAT EVs. *(**A**) M2 marker gene expression of BMDMs treated with 1 µg or 5 µg EVs isolated from eWAT of lean or diet-induced obese (DIO) mice or with buffer control (c). Cells were treated with vehicle (left panels) or IL-4 (10 ng/ml) to promote M2 polarization (right panels). (**B**) M1 marker gene expression of BMDMs treated with 1 µg or 5 µg eWAT EVs from lean or diet-induced obese (DIO) mice or with buffer control (c). To induce M1 polarization, cells were treated with IFNγ (20 ng/ml, right panel), vehicle treated cells served as control (left panel). (**C**) Phagocytotic uptake of fluorescently labelled E.coli particles after 1.5 h of co-exposure following a 24 h treatment with eWAT EVs of lean and obese mice. (**A**-**C**): n=3. Gene expression was assayed in duplicates and normalized to house-keeping genes. All data were normalized to the respective buffer controls (control set to fold induction 1). The upper left panel only shows single values due to low gene expression. Data are shown as mean ± SD.*

3.1.7 EVs of obese but not of lean eWAT increase insulin release from pancreatic islets

The identification of a targeted delivery of eWAT EVs to metabolically active target organs such as liver, pancreas and eWAT in the DiR-experiments as well as the detection of several miRNAs in eWAT EVs with possible involvement in insulin expression and regulation directed me towards assessing a potential role of adipocyte EVs in glucoregulation. More specifically, based on early accumulation of eWAT EVs in the pancreas, I wanted to investigate the influence of eWAT EVs on insulin secretion from pancreatic β-cells. Therefore, primary pancreatic islets were incubated with increasing concentrations of EVs derived from eWAT of lean and DIO mice and glucose stimulated insulin secretion was assayed using a static incubation. Under low glucose (2.8 mM) conditions, treatment of murine pancreatic islets with eWAT EVs from chow or HFD-fed mice had no effect on insulin release (Figure 18A, left section). Switching the islets from low to high glucose (16.7 mM) resulted in an expected overall glucose-stimulated increase of insulin secretion in all treatment conditions (Figure 18A, right section). When comparing all experimental groups, however, no significant effect of eWAT EV treatment could be detected. Focusing only on the highest dosage with 10 µg revealed a statistically increased insulin secretion upon treatment with obese eWAT EVs compared to both, control and lean eWAT EVs (Figure 18B). In contrast, EVs originating from lean eWAT did not show any influence. The total cellular insulin content was not altered by EV treatment (Figure 18C), excluding this factor as a source of variation.

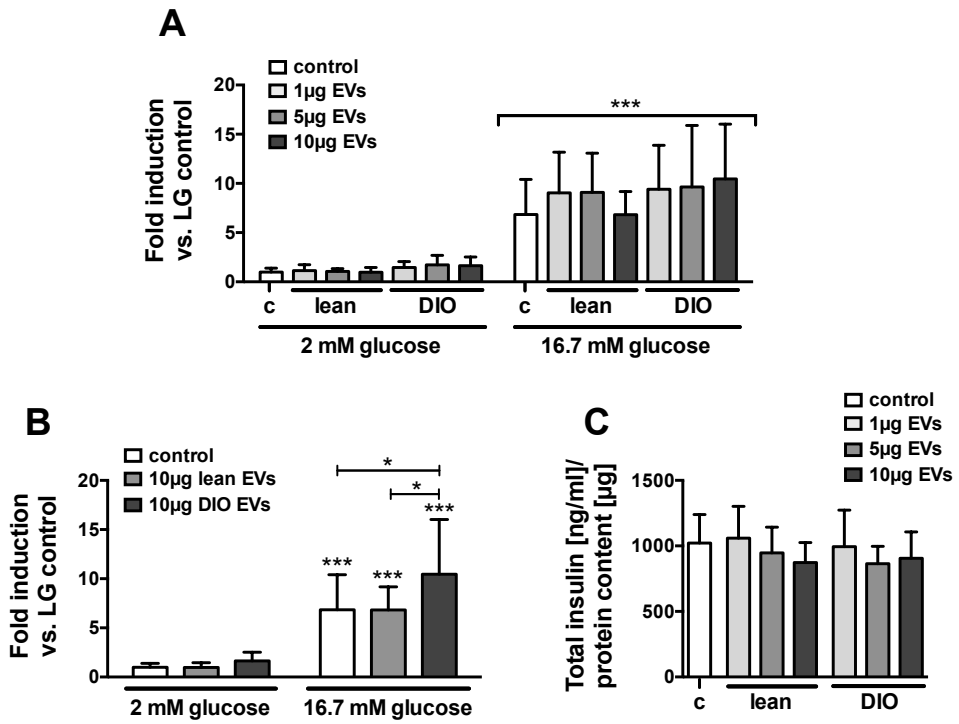

Figure 18: eWAT EVs of obese but not of lean mice increase insulin secretion from pancreatic β-cells. *(**A**-**B**) Glucose stimulated insulin secretion (GSIS) in cultured primary mouse islets exposed to eWAT EVs from lean or DIO mice. Insulin secretion was assessed in the same islets in presence of low (LG; 2.8 mM) followed by high glucose (16.7 mM). (**A**) shows all investigated conditions, (**B**) only depicts the effective treatment groups with 10 µg EVs. (**C**) Total insulin contents in islets treated with vehicle or EVs isolated from eWAT of lean or DIO mice. Data are pooled from 3 individual experiments where islets were incubated in separate wells. Samples showing less than 3-fold induction upon high glucose stimulation were excluded from the analysis, assuming insufficient islet quality (n=11-13 independent wells in total). Data are shown as mean ± SD. Statistical significance was analysed by One-Way ANOVA and Sidak's multiple comparisons test. * p<0.05, *** p<0.001.*

3.1.8 Modulation of glucose tolerance by eWAT EVs

The next aim was to investigate if eWAT EVs are capable of influencing glucoregulation not only in an *in vitro* setting but also in the more complex *in vivo* situation. Therefore, HFD-fed mice were fasted and injected *ip.* with a bolus of 10 µg freshly isolated eWAT EVs from lean mice. Four hours later, an ipGTT to investigate glucose clearance from the bloodstream was performed.

Subjecting DIO mice to an ipGTT after pre-injection with EVs isolated from lean eWAT revealed no significant differences in glucose excursion (Figure 19).

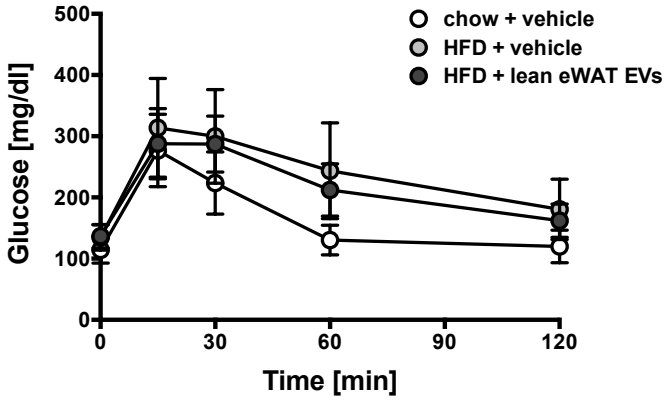

Figure 19: Treatment of DIO mice with EVs originating from lean eWAT adipocytes has no effect on glucose tolerance in vivo. *Glucose excursions in HFD-fed mice after pre-treatment with vehicle or 10 µg of adipocyte EVs isolated from eWAT of lean mice (cross-over study, n=12). Chow-fed mice injected with vehicle served as additional control group. 4 h after EV administration the ipGTT was performed with a glucose bolus injection of 1.7 mg glucose per g body weight. Data are shown as mean ± SD. Two-Way ANOVA revealed no significant differences between the three groups.*

Interestingly, follow-up experiments in my group have shown that, in line with the effect observed in pancreatic islets *in vitro*, injection of eWAT EVs from DIO mice into lean mice resulted in a significantly increased insulin secretion and subsequent decrease of glucose excursion. However, an additional increase of EV dosage from 10 µg to 50 µg was necessary to achieve this effect (data not shown, manuscript currently in revision).

3.1.9 Pharmacological inhibition of exosome biogenesis with GW4869 *in vivo*

In vivo, secreting organs constantly release EVs, resulting in a persistent exposure of target cells. To mimic this situation in experiments studying the potential influence of adipocyte EVs, chronic EV administration would be necessary. However, comparable low yields of EVs obtained from AT explant cultures turn this concept to a challenging obstacle. One option to overcome this difficulty is the use of systemic inhibitors of EV secretion in mice. Here, a non-competitive inhibitor of nSMase2 was used which has been published in multiple *in vivo* and *in vitro* studies aiming at blocking EV release (172,174,175,173). Work with this inhibitor was conducted in collaboration with David Sailer, a master student in my group which was co-supervised by me. Accordingly, the data of this experiment are partially included in David Sailer's Master's thesis. By blocking the ESCRT-independent pathways GW4869 inhibits exosome biogenesis and release (169). In order to ensure that AT is generally susceptible for GW4869-mediated inhibition, gene expression of nSMase1

and nSMase2 (encoded by the genes *Smpd2* and *Smpd3*, respectively) was analysed. Both forms were found to be present in AT, with higher expression levels in eWAT compared to iWAT followed by BAT (Table 9). RNA of stomach and cerebral cortex was used as positive control.

Table 9: Gene expression levels of nSMase1 (Smpd2), nSMase2 (Smpd3) and the housekeeper Ppib in mouse tissue. *mRNA expression was assayed in duplicates, n=3.*

Tissue	mean CT value *Smpd2*	mean CT value *Smpd3*	mean CT value *Ppib*
eWAT	27,669	29,200	24,125
iWAT	29,285	32,565	26,757
BAT	30,769	36,025	28,029
cerebral cortex	27,460	26,337	24,672
stomach	27,792	32,218	26,871

To study the effect of GW4869 administration on metabolic parameters, lean and DIO mice with a significantly different body weight were injected daily *ip.* with 1 mg/kg of the small molecule inhibitor for 16 days and were metabolically phenotyped. During the study, body weights did not differ significantly between vehicle and inhibitor treated groups (Figure 20A and B). Body composition was not altered upon GW4869 injections, except a significant decrease in fat mass in inhibitor treated HFD-fed mice at day 16 compared to day -3 (Figure 20C-F).

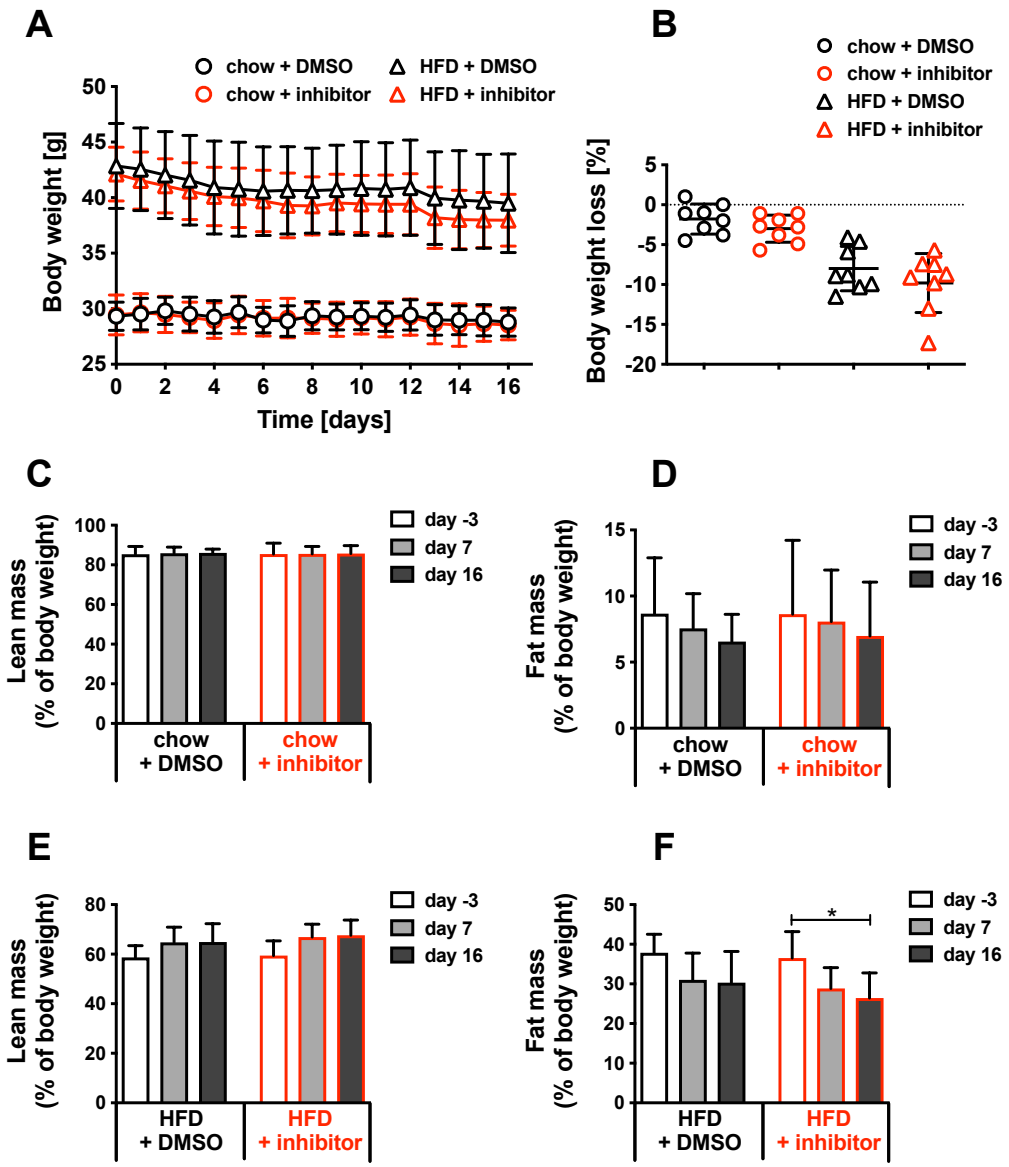

Figure 20: Development of body weight and body composition of lean and DIO mice during the GW4869 study. *Chow and HFD-fed mice received daily ip. injections either with vehicle or 1 mg/kg GW4869 (inhibitor) for 16 days (n=8). (**A**) Body weight and (**B**) percental body weight loss over the study period. Determination of (**C** and **E**) lean mass and (**D** and **F**) fat mass of chow or HFD-fed mice 3 days before study onset, at day 7 and at day 16. Left sections show vehicle injected animals, right sections GW4869 treated mice. Data are shown as mean ± SD. Statistical significance was analysed by One-Way ANOVA and Sidak's multiple comparisons test. * p<0.05.*

Food intake was not influenced by GW4869 treatment in both diet groups, neither measured in total amounts (Figure 21A and B) nor in caloric quantities (Figure 21C). Locomotor activity showed the expected patterning characteristic for nocturnal animals with a higher activity in the dark phase but was also not affected by GW4869 injections (Figure 21D and E).

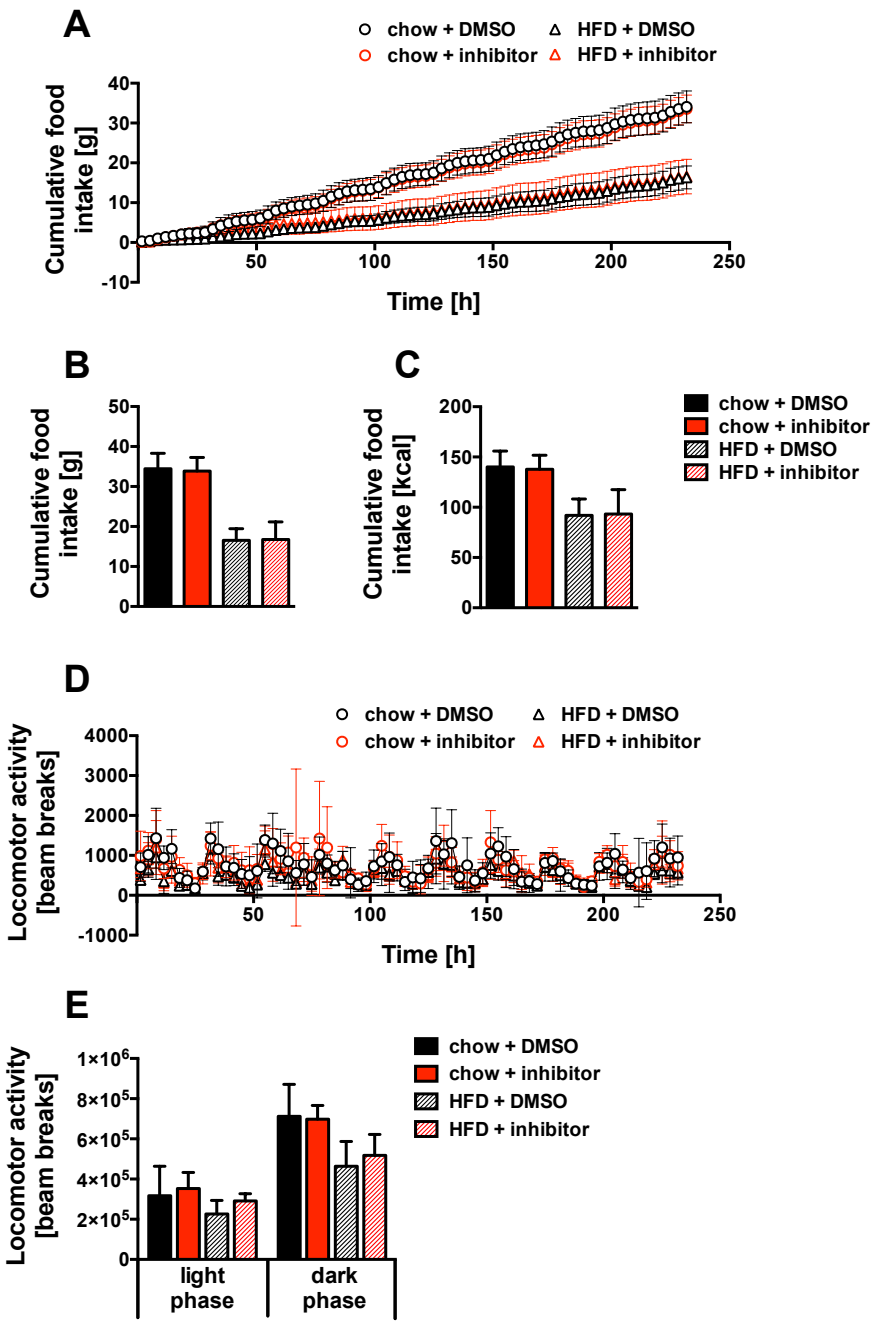

Figure 21: Food intake and locomotor activity is unaffected by GW4869 administration in lean and DIO mice. *Cumulative food intake over the study period (**A**) and summarized in gram (**B**) or kcal (**C**) of lean and obese mice treated with vehicle or the inhibitor GW4869. Locomotor activity over the period of metabolic phenotyping (**D**) and cumulated, differentiated between light and dark phase (**E**) in chow and HFD fed mice injected with vehicle or inhibitor (n=8). Data are shown as mean ± SD.*

Similar to food intake and locomotion, energy expenditure was affected only by the environmental factors diet and light-dark cycle in an expected way but was not influenced by GW4869 treatment (Figure 22A and B). Determining energy utilization of carbohydrates vs. fat expressed by the respiratory quotient (RQ) showed as well that high-fat diet feeding but not inhibitor treatment led to an expected decrease in RQ (Figure 22C).

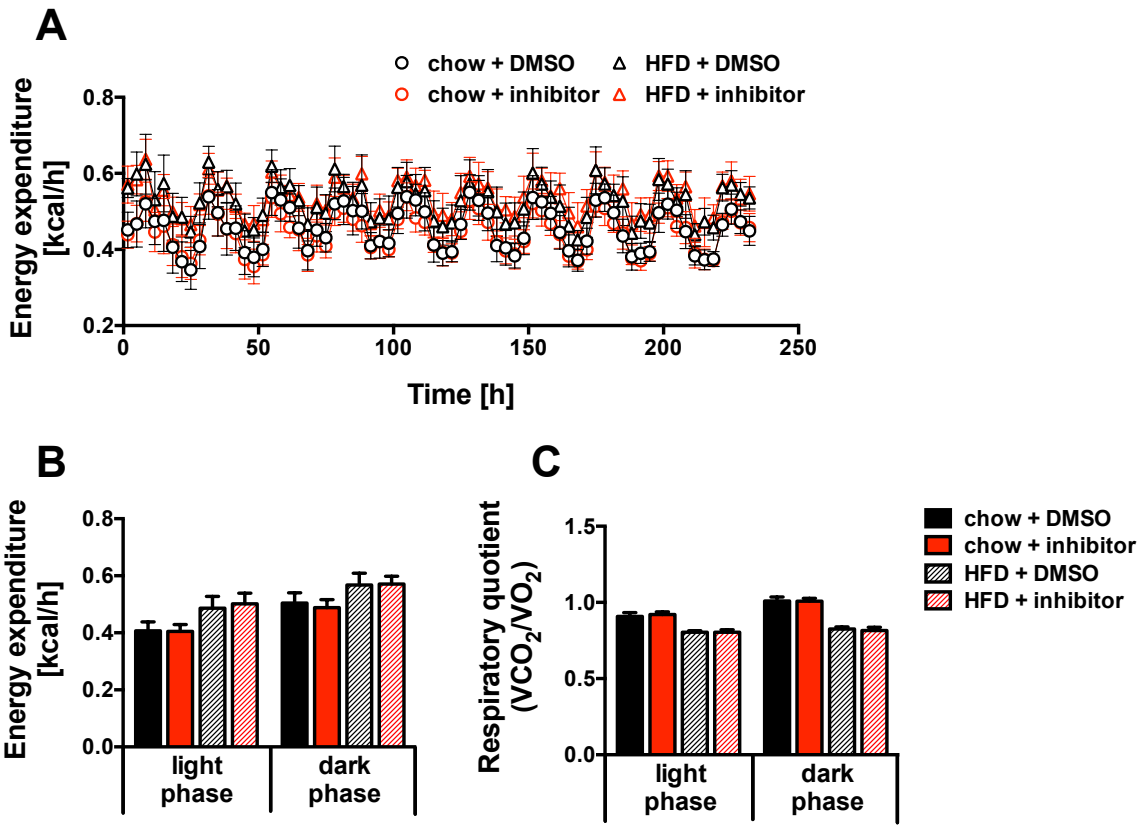

Figure 22: GW4869 treatment does not influence energy metabolism in chow or HFD-fed mice. *Energy expenditure over the period of metabolic phenotyping (**A**) and cumulated, differentiated between light and dark phase (**B**) in chow and HFD fed mice injected with DMSO or the inhibitor GW4869. (**C**) Respiratory quotient in lean or DIO mice with vehicle or inhibitor treatment, subdivided into light and dark phase. (n=8). Data are shown as mean ± SD.*

To assess chronic effects of EV secretion on glucoregulation, chow or HFD-fed mice were treated with GW4869 or vehicle and subjected to an ipGTT at day 16. After 6 h of fasting, mice received a glucose bolus injection of 2 mg glucose per g body weight and blood glucose levels were measured 15, 30, 60 and 120 min after glucose stimulation. GW4869 treatment impaired glucose tolerance in chow-fed mice, as demonstrated by higher glucose excursions 30 min after glucose injection (Figure 23A) and a significantly increased area under the curve (AUC) (Figure 23B). In contrast, similar glucose tolerance

was observed in HFD-fed mice treated with vehicle or GW4869 (Figure 23C). To assess insulin resistance and the development over the study period, homeostasis model assessment of insulin resistance (HOMA-IR) was determined before study start (day -6) and at day 13, revealing a generally decreased insulin resistance in HFD-fed mice after 13 days of study. GW4869 treatment, however, had no effect in both diet groups (Figure 23D).

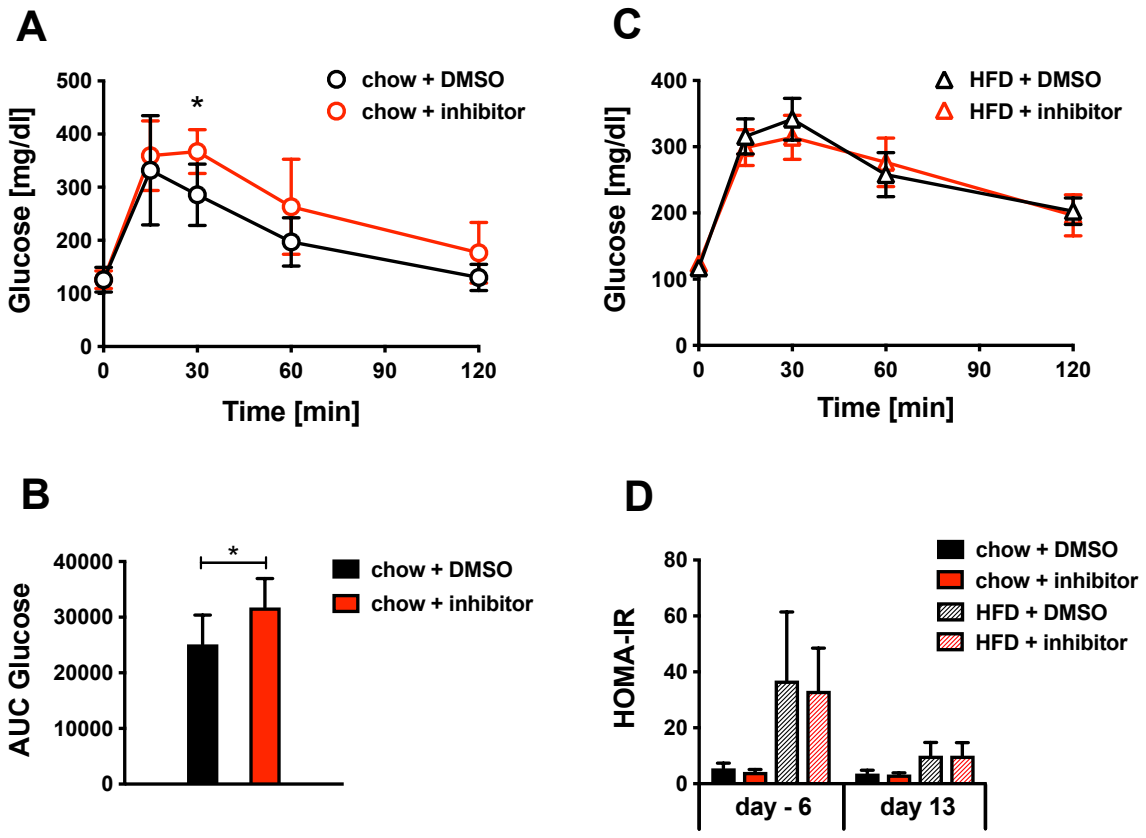

Figure 23: Glucose tolerance is impaired in lean but not in obese mice treated with GW4869. *(**A**) Glucose excursion and corresponding area under the curve (AUC) values (**B**) of DMSO or GW4869 inhibitor-treated chow mice or (**C**) HFD-fed mice subjected to an ipGTT after 6 h of fasting with a glucose bolus injection of 2 mg glucose per g body weight at day 16. (**D**) Insulin resistance measured by HOMA-IR 6 days before study onset and after 13 days of treatment in chow or HFD fed mice receiving vehicle or inhibitor GW4869 injections. Data are shown as mean ± SD. Significant differences were analysed by Two-Way ANOVA and Tukey's multiple comparison test (A) or two-tailed Student's t-test (B). * p<0.05.*

Ultimately, I wanted to investigate if chronic inhibition of exosome secretion by GW4869 administration had an impact on EV secretion of AT explant samples and on the amount of circulating EVs. Therefore, EVs were isolated from eWAT adipocytes and serum of chow and HFD-fed mice after 16 days of treatment with DMSO or GW4869. Data obtained from adipocyte EVs were normalized to eWAT mass used for isolation, for isolation of serum EVs the same volume was used across all samples. Analysing EVs derived from

eWAT, protein yield (Figure 24A) as well as particle concentration (Figure 24B) and mean particle peak diameter (Figure 24C) determined by NTA did not show any differences between diet and treatment groups. Similar results were obtained analysing serum EVs, with no effect of GW4869 on EV protein yield (Figure 24D), particle concentration (Figure 24E) and mean particle diameter (Figure 24F).

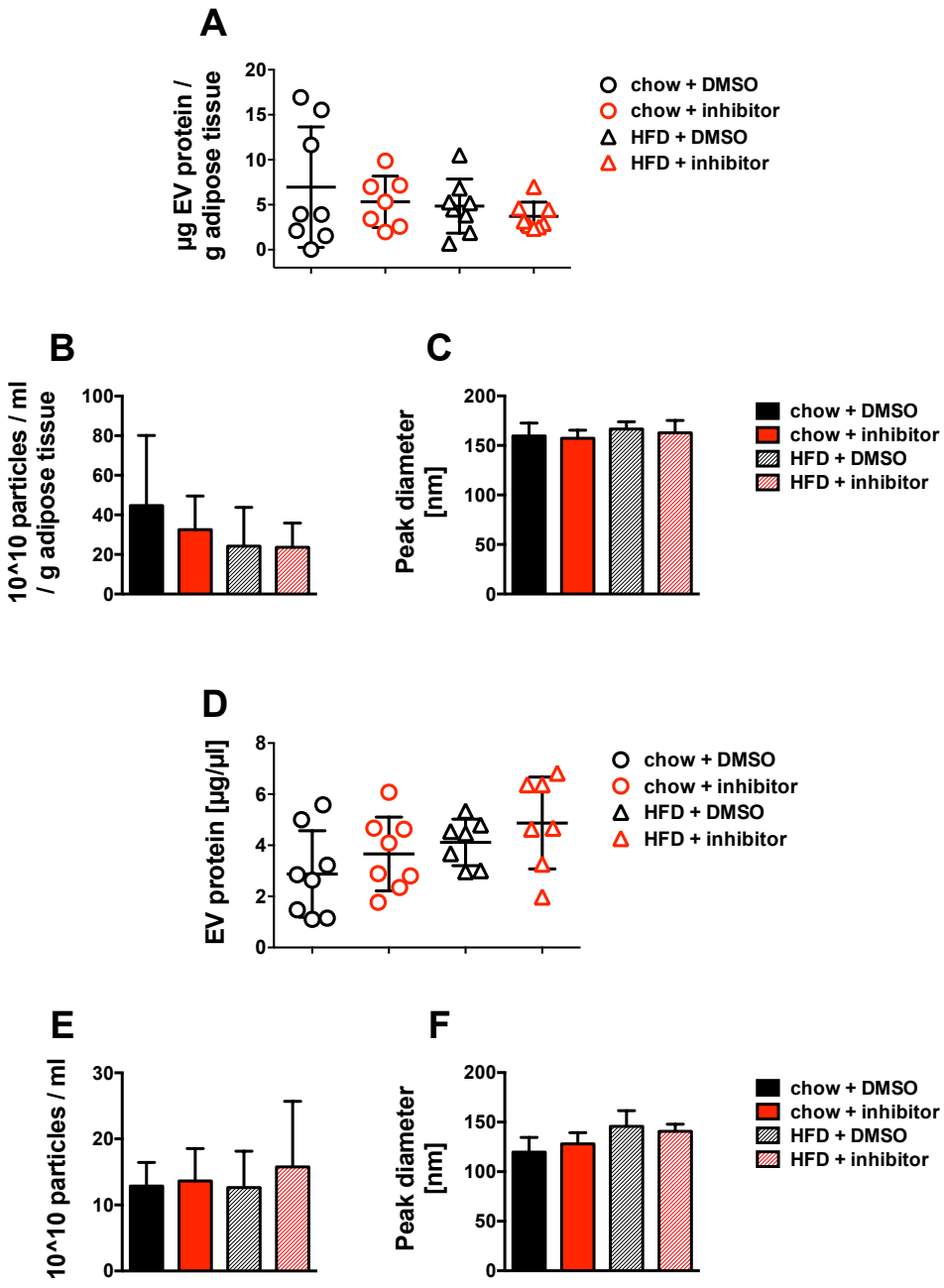

Figure 24: Systemic application of GW4869 does not affect EV secretion from eWAT and serum EV amounts. *Yield of isolated EV protein, particle concentration as well as particle peak diameter of EVs derived from eWAT (**A**-**C**) and serum (**D**-**F**) of chow and HFD-fed mice treated with vehicle or GW4869. Adipocyte EVs were normalized to adipose tissue mass used for isolation. n=8, except serum EVs chow mice GW4869 treated n=7. Data are shown as mean ± SD.*

3.2 Human adipocyte EVs as biomarkers for AT health

Based on their complex cargo, circulating EVs provide a rich source for molecular diagnostic analyses and thus represent a rapidly evolving frontier in clinical research. Especially in the field of cancer research, EVs have been shown to be a valuable biomarker for early diagnosis, prognosis and treatment response (85,86). A selective extraction and analysis of tissue specific EVs from the bloodstream could moreover propagate that diagnostic power of EVs. “Liquid biopsies” could in fact provide an unprecedented non-invasive way to monitor single organs during disease progression and pharmacological interventions. For instance, EV-based liquid adipocyte biopsies could help stratifying different disease stages colloquially classified as ”healthy” vs. “unhealthy” obesity that are characterized by differential WAT morphologies. Ultimately, such liquid biopsies could facilitate a personalized precision diagnosis and tailored therapeutic intervention. However, at present, technologies are lacking that allow discriminating between EVs of different tissue origin.

The second part of my thesis aimed to develop a novel technique for the antibody-based isolation of adipocyte derived-EVs from human blood samples. As the human AT specimen were obtained from subjects that underwent liposuction instead of taking whole tissue samples, the murine EV isolation protocol had to be adjusted (details are given in the material and methods part) to allow for sufficient yields and quality of the resulting EV fraction. Human adipocyte-derived EV characteristics isolated with the final protocol are shown below.

3.2.1 Vesicles with EV-like properties are secreted by human adipocytes

Isolated vesicles from human adipocytes were characterized by a cup-shaped morphology imaged by TEM (Figure 25A). The particle size determined by DLS showed an EV-like size distribution with a characteristic particle diameter of 101.5 nm (Figure 25B). As already observed in murine adipocyte EVs, the measured size range suggests a mixed population containing both small and large EVs also in the human adipocyte total EVs. Representative dot blots of EVs isolated from adipocytes, SVF and serum of three different subjects revealed a distinct staining for the EV markers GM1, CD63 and CD9 (Figure 25C). Further characterization by mass spectrometry showed that classical EV markers like flotillin 1 (FLOT1), annexin A6, RAB11B, as well as the tetraspanins CD9, CD63 and CD81 were present in the human adipocyte-derived vesicles (Figure 25D). Additional detection of the adipocyte markers leptin, FABP4 and adiponectin in the EV proteome further indicates that human adipocyte EVs actually reflect their tissue of origin.

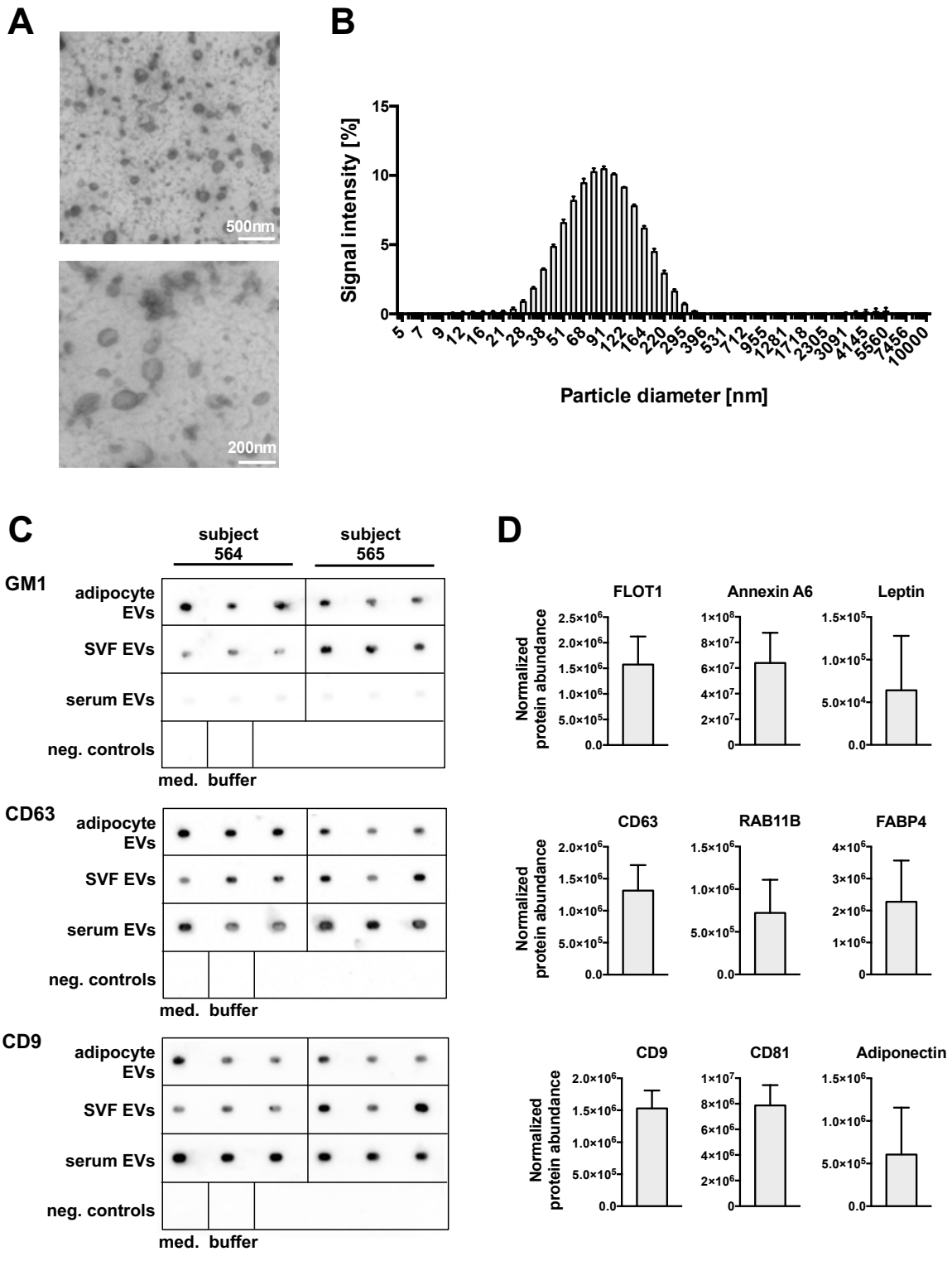

Figure 25: Human adipocytes secrete vesicles with characteristic EV features. *(**A**) Representative transmission electron microscopy of EVs isolated from human adipocytes (scale bar: 200 and 500 nm). (**B**) Size distribution of human adipocyte EVs, determined by dynamic light scattering (n=3). (**C**) Dot blots of EVs derived from human adipocytes, SVF and serum isolated from two subjects with staining for GM1 (upper panel), CD63 (middle panel) and CD9 (lower panel). Medium subjected to the same isolation protocol or EV buffer were used as negative controls. (**D**) Relative protein abundance of the EV marker proteins FLOT1, annexin A6, CD63, RAB11B, CD9 and CD81 (left and middle panels), as well as the adipocyte specific proteins leptin, fatty acid binding protein 4 (FABP4) and adiponectin (right panels), determined by mass spectrometry (normalized to all proteins, n=11). Data are shown as mean ± SD.*

3.2.2 Proteomic profiling of human EVs proposes a potential role as biomarker

Next, I aimed to uncover the biomarker potential of the adipocyte EV cargo. During my thesis, I received human AT and serum samples of 12 subjects undergoing liposuction. All patients were informed and gave their written consent for the use of the tissue for scientific purposes. One and the same patient underwent two liposuction procedures (P582 and P583), therefore the second sample from this patient (P583) was excluded from the following analyses. The study group included 10 female and one male person, aged from 24 to 47 with a mean age ± SD of 37 ± 7.5 years. Patient characteristics are shown in Table 10. The subjects were divided into two groups according to their body mass index (BMI): normal (BMI<23, n=6) and overweight (BMI>26, n=5) (Figure 26A). From each patient, EVs were isolated from the adipocyte and the SVF fraction of the AT as well as from serum samples. EV samples, as well as remaining whole AT samples were frozen and kept for LC-MS/MS analysis.

Table 10: Characteristics of subjects undergoing liposuctions used for EV isolations.

subject no.	gender	age [years]	height [cm]	body weight [kg]	BMI [kg/m^2]
566	male	30	175	68	22,2
568	female	29	172	80	27,0
574	female	38	162	75	28,6
575	female	37	175	60	19,6
576	female	34	175	85	27,8
577	female	45	172	82	27,7
578	female	47	162	69	26,3
579	female	35	164	52	19,3
581	female	47	160	54	21,1
582	female	40	174	65	21,5
583	female	40	174	65	21,5
587	female	24	169	65	22,8

To reveal possible BMI-related differences in adipocyte and serum EV signature, the proteomic profile of the EVs was analysed together with whole AT lysate. The investigation of a potential impact of BMI on the proteomic profiles studied by principal component analysis of the proteome could not detect an BMI-driven effect in the signatures neither of EVs originating from human adipocytes, serum and SVF nor of AT lysate (Figure 26B). The finding is likely based on the limited number of patient samples together with a generally high variability in human specimen. Accordingly, I abandoned

further analyses and focused on the development of an antibody to generate liquid AT biopsies.

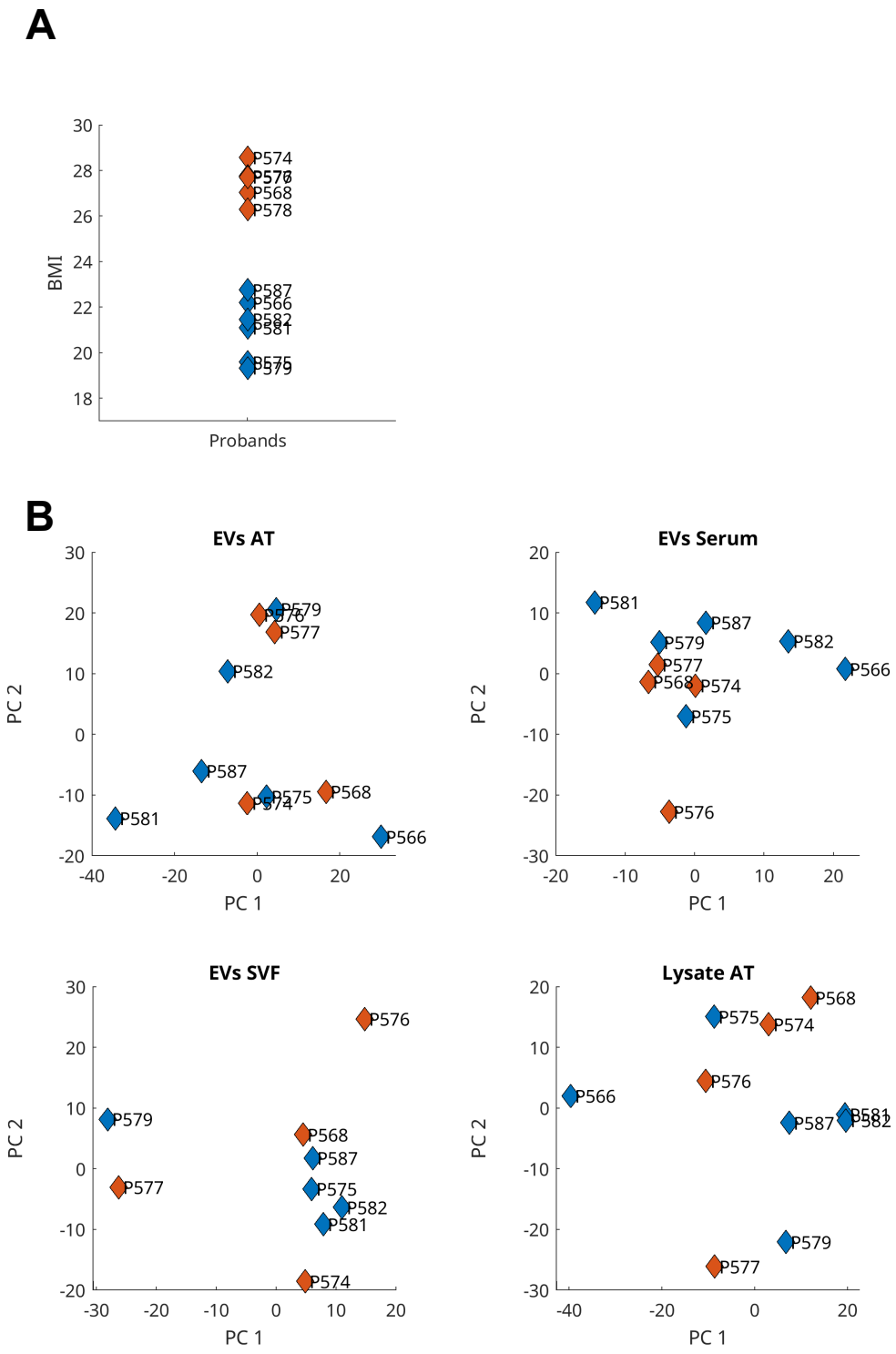

Figure 26: Proteomic profiling of human adipose tissue and EVs originating from adipocytes, SVF and serum elucidates a BMI-independent correlation. *(**A**) Classification of subjects according to BMI. Subjects were divided into two groups, normal (BMI<23, blue symbols) and overweight (BMI>26, red symbols). (**B**) Principal component analysis of the proteome of EVs originating from human adipocytes, serum EVs, SVF EVs or adipose tissue lysate. n=11.*

3.2.3 The human adipocyte cell strain SGBS releases EVs

To generate antibodies against circulating human adipocyte-derived EVs for liquid biopsy applications, I used the mouse hybridoma technique described by Köhler and Milstein (177). This method uses antibody-producing B lymphocytes from mice after immunizing the animals with specific antigens. The cells are subsequently fused with immortal myeloma cell lines to form antibody producing hybridoma cell lines. The antibody development was performed in collaboration with the Monoclonal Antibody Core Facility (Helmholtz Zentrum München, MAB), with Dr. Regina Feederle, Andrew Flatley and Dr. Elisabeth Kremmer. As antigen EVs isolated from the human pre-adipocyte strain SGBS were used. This cell strain can be differentiated in mature adipocytes *in vitro* with a function and behaviour like primary human adipocytes (142). Differentiated SGBS cells secrete EVs with typical morphology (Figure 27A) and particle size distribution with a mean particle diameter of 101.1 nm (Figure 27B). SGBS cell EVs were also positive for the classical EV-markers TSG101 and Alix as well as the tetraspanins CD9, CD63 and CD81 (Figure 27C). The absence of the negative control marker calnexin (9) suggested a clean isolation procedure with an absence of contaminating ER.

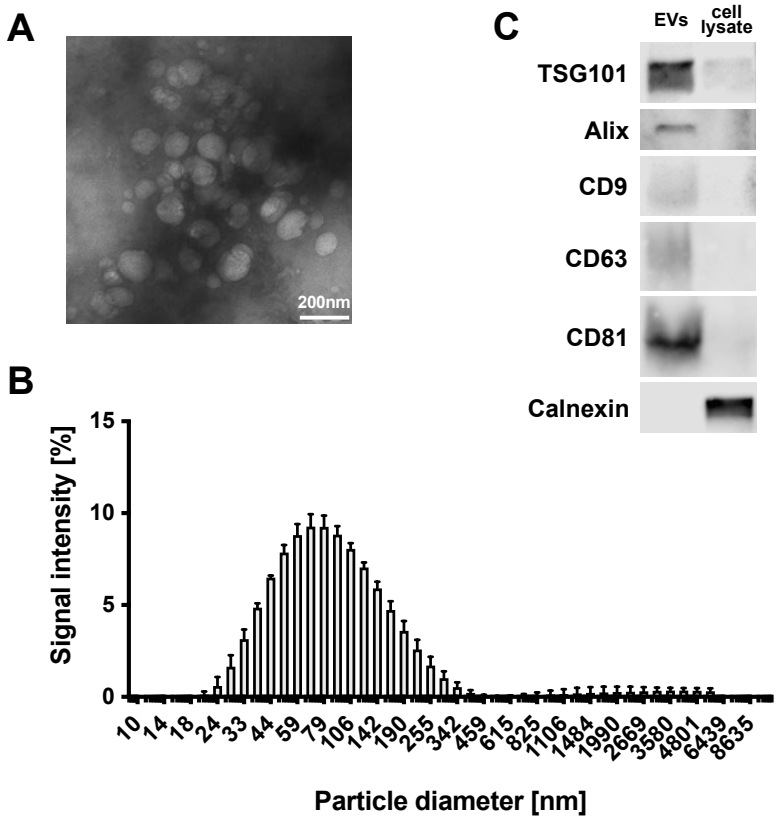

Figure 27: Vesicles isolated from differentiated SGBS cells show classical EV characteristics. *(**A**) Representative transmission electron microscopy of EVs isolated from differentiated SGBS cells (scale bar: 200 nm). (**B**) Size distribution of EVs isolated from differentiated SGBS cells, determined by dynamic light scattering (n=3). (**C**) Western blot of EVs and cell lysate derived from differentiated SGBS cells with staining for the EV markers TSG101, Alix, CD9, CD63 and CD81 and the negative marker Calnexin. Data are shown as mean ± SD.*

3.2.4 Selection of adipocyte EV-specific antibodies

One mouse and two rats were immunized with EVs isolated from differentiated SGBS cells, and more than 2 000 hybridoma clones were generated. In order to identify the hybridoma clones, which produce antibodies that specifically bind to EVs from adipocytes, I established a multistep screening protocol. A summary of this screening protocol is shown in Figure 28 and details to each step are given in the sections below.

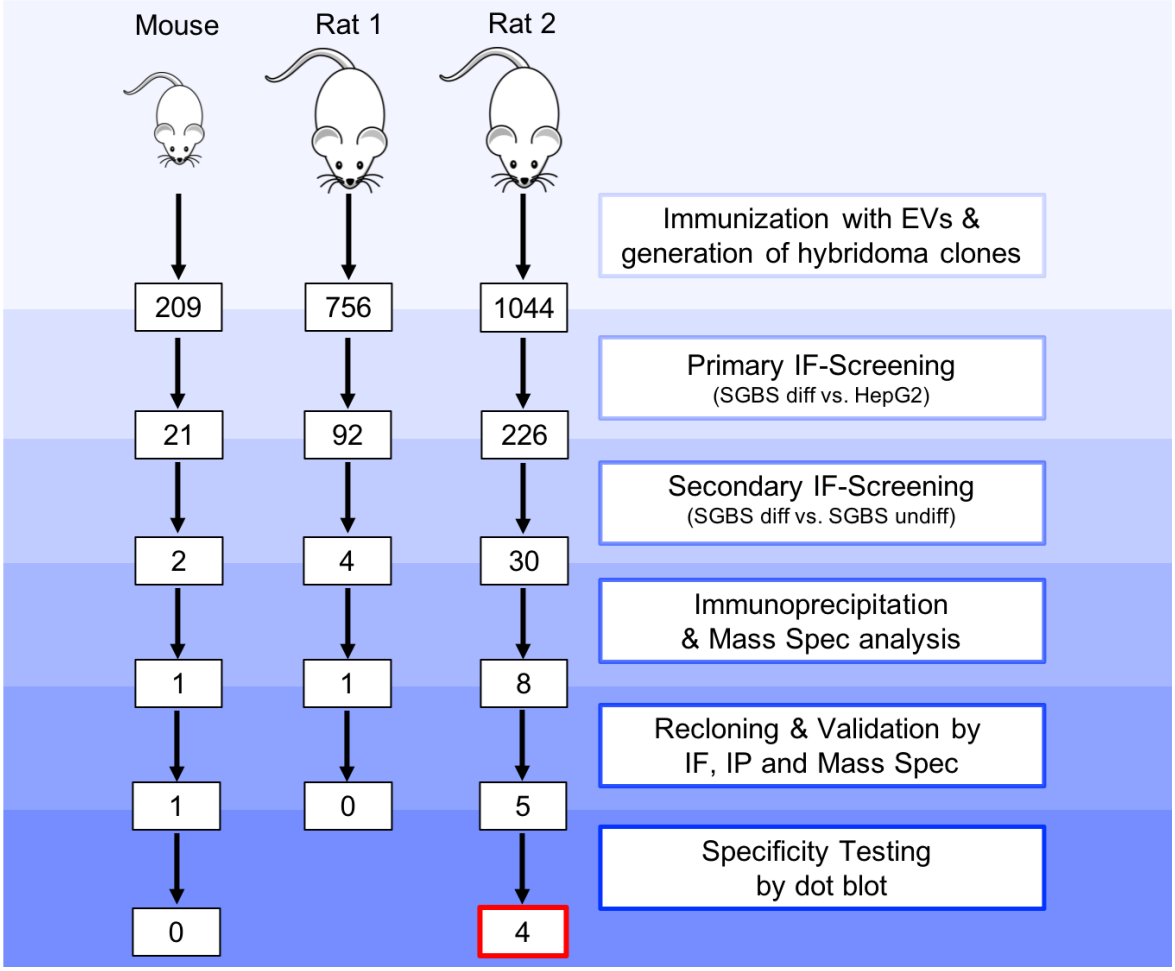

Figure 28: Overview of the experimental procedures to identify specific antibody clones together with the number of selected clones. *One mouse and two rats were immunized with EVs derived from differentiated SGBS cells followed by generation of antibody-secreting hybridoma clones. Specific antibodies were selected in a multi-stage screening approach including immunofluorescence (IF), immunoprecipitation (IP), mass spectrometry and dot blot assays.*

The first screening step was based on the assumption that EVs should carry parts of the adipocyte cellular membrane (see introduction, chapter 1.3). Therefore, the binding of the antibody-containing hybridoma cell supernatants was tested on differentiated SGBS cells for positive selection and on liver-derived HEPG2 cells for negative selection. The readout

of the assay was the immunofluorescent signal, generated by binding of a fluorophore-labelled antibody to a subclass-specific antibody which was attached to the first hybridoma-derived antibody (for exemplary imaging of selected clones, positive and negative controls as well as a not-selected clone see Figure 29). The secondary screening of 339 clones was based on detecting immunofluorescence on differentiated vs. undifferentiated SGBS cells and narrowed down the number of single positive clones to 36. Subsequent target identification by immunoprecipitation and mass spectrometry revealed ten clones of interest (see chapter 3.2.5). To stabilize the selected clones, they were re-cloned as single clones, followed by additional validation with immunofluorescence as well as confirmation of the antibody target by immunoprecipitation and mass spectrometry. The last selection step aimed to test the binding of the selected antibodies to adipocyte-derived EVs. Therefore, EVs were generated from a panel of different non-adipocyte-derived cell lines for negative selection (see chapter 3.2.6).

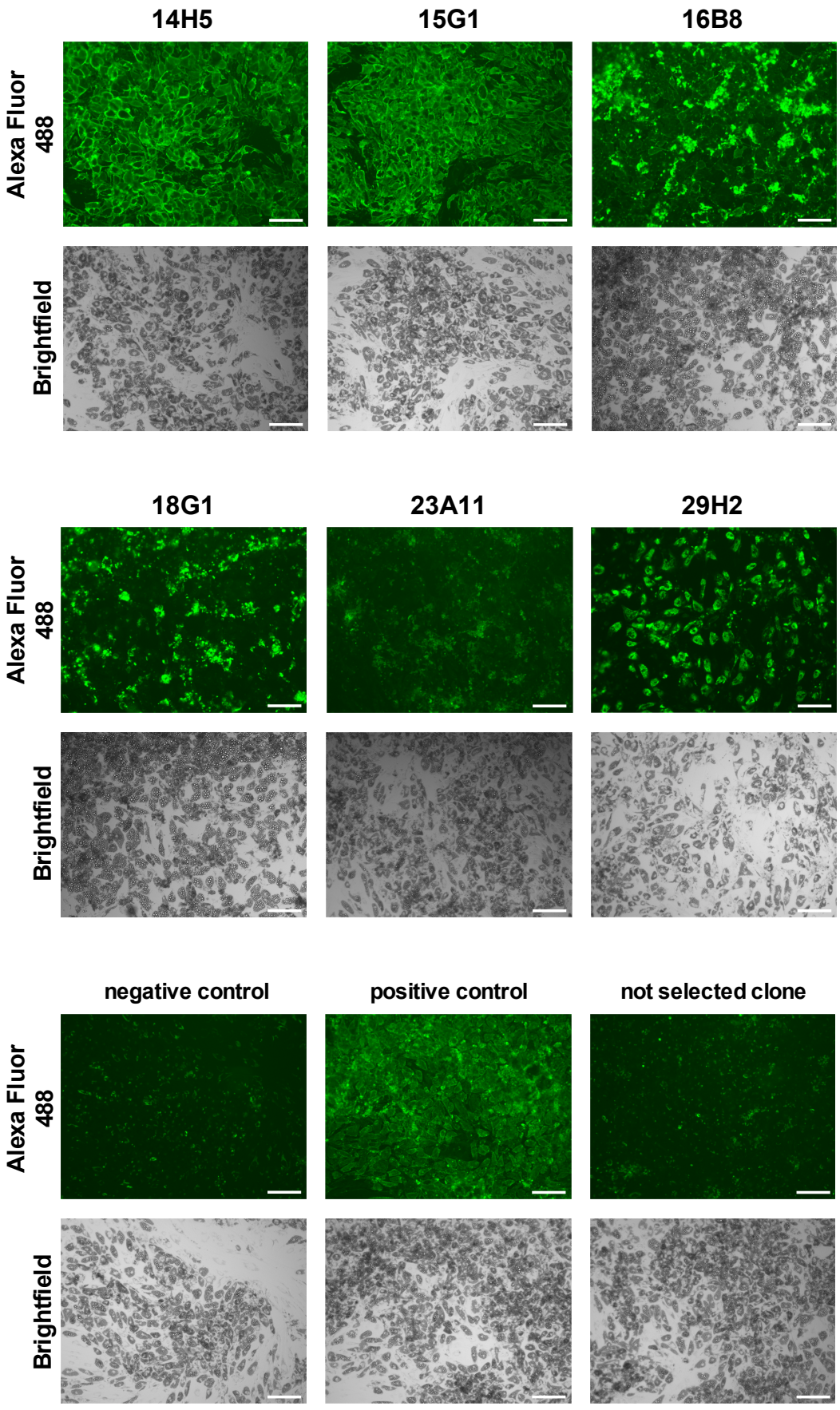

Figure 29: Microscopic evaluation of selected clones, negative and positive control as well as exemplary one not selected clone in the immunoprecipitation assay. *Alexa Fluor-imaging (upper panels) and corresponding bright field images (lower panels). Scale bar represents 100 µm.*

3.2.5 Target identification by immunoprecipitation and mass spectrometry

After narrowing down the number of potential clones in the first two screening steps to 36, the antibody targets were determined. Therefore, target epitopes were bound to the immobilized antibodies in an immunoprecipitation assay, eluted and analysed by mass spectrometry. Out of the 36 clones tested, 20 clones displayed a high confidence score for their detected targets. Interestingly, eight of these clones showed a specificity for the same target, namely the amine oxidase, copper containing 3 (AOC3), also known as vascular adhesion protein (VAP-1). From the 20 clones, ten clones with good scores and promising targets were selected for re-cloning, followed by subsequent validation with immunofluorescence as well as target identification by immunoprecipitation and mass spectrometry. Four clones could not be subcloned and were lost during the re-cloning procedure, reducing the number of positive clones for further investigation to six. Characteristics and identified targets of these six clones are summarized in Table 11.

Table 11: Identified targets of six selected antibody clones

clone	origin	IgG subclass	antibody target
14H5	Rat 2	IgG2b	AOC3
15G1	Rat 2	IgG2a	AOC3
16B8	Rat 2	IgG2a	CD63
18G1	Rat 2	IgG2a	LAMP2
23A11	Rat 2	IgG2a	COL6A
29H2	Mouse	IgG2a	MYH9/VIM

3.2.6 Evaluation of tissue specificity by dot blots

To further investigate the antibody specificity the six most promising clones were selected and tested in a dot blot. As positive controls SGBS EVs, SGBS lysate, human AT (hAT) EVs and human serum EVs were loaded on the membrane. EVs and cell lysate of the cell lines HepG2, Caco2, Panc1, Saos2 and MCF-7, reflecting liver, colon, pancreas, bone and breast tissue, respectively, served as potential negative controls. Three clones, namely 14H5, 15G1 and 23A11, showed a clear specificity for adipocyte-derived EVs and lysate without staining of EVs and lysates of the negative controls (Figure 30). Clone 16B8 exhibited a staining pattern specific for EVs only, strengthening the result of a target generally present on EVs. The clones 18G1 and 29H2 were positive in adipocyte and serum EVs, but also showed a staining in EVs and lysates of all negative controls. Therefore finally, out of more than 2000 clones in the beginning, the four clones 14H5, 15G1, 16B8 and 23A11 were selected for further studies.

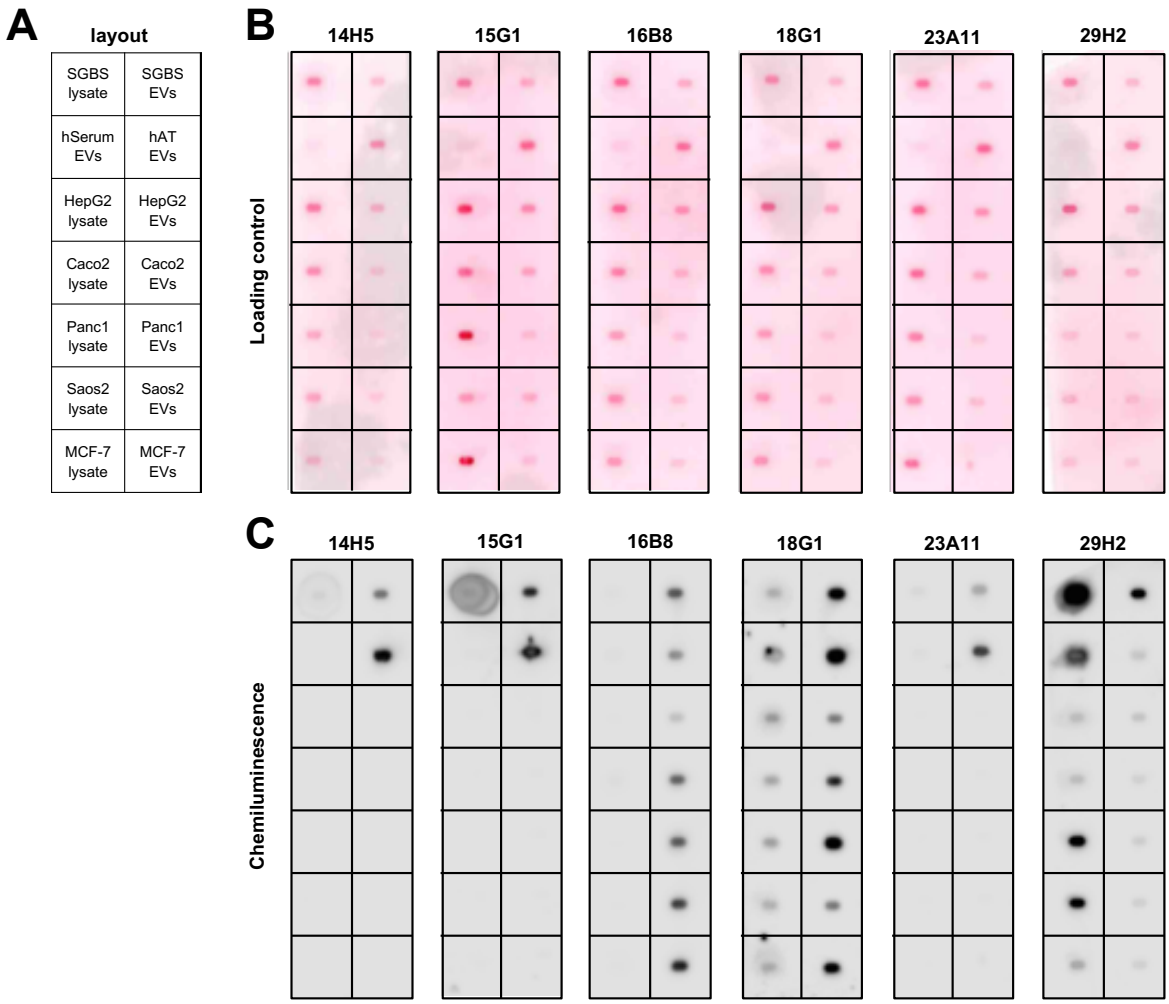

Figure 30: Specificity testing of six selected antibody clones by dot blot. *(**A**) layout of all tested dot blots including EVs and cell lysate of positive and negative controls, (**B**) loading control by ponceau S staining and (**C**) staining with the selected antibody clones. Different amounts of protein were loaded on the PVDF membrane: 2 µg of human adipose tissue (hAT) EVs and EVs derived from cell lines, 10 µg of serum EVs and 10 µg of cell lysates.*

3.2.7 Sequencing of the antigen binding sites

Immunoglobulins are Y-shapes proteins formed by four chains, two heavy and two light chains. The antigen binding site, reflecting the most important part of the antibody, is determined by the variable domains of the heavy and light chains. Three specific hypervariable regions each, also referred to as complementarity-determining regions (CDR) are responsible for interaction with the antigen. Together with four framework regions (FR) separating the CDRs from each other, they form the variable region of an immunoglobulin (230).

Finally, and to fully characterize the selected antibodies, the DNA sequences of the variable regions of heavy and light chain were analysed. The protein sequences were

determined and aligned according to the numbering scheme defined by Chothia et al. (231) with signal peptide, FR and CDRs 1-3 (Figure 31).

The antibodies, which were selected during this thesis, are major claims of a patent issued 2017 (232).

Figure 31: Identified protein sequences of the antigen binding sights of light and heavy chains of four selected antibody clones according to Chothia. *Sequences of light and heavy chains can be subdivided into signal peptide (green), framework regions (FR, yellow) and the hypervariable complementarity-determining regions (CDR) 1–3 (blue).*

4 Discussion

In my thesis, I demonstrate that adipocytes from both eWAT and iWAT secrete vesicles with EV-like properties. Depending on the tissue type and the state of nutrition, these vesicles differ in their protein and miRNA cargo. My thesis provides evidence that adipocyte-derived EVs are delivered to distinct metabolic target organs and can serve as novel route of communication. In detail, EVs arising from the adipocyte fraction of the eWAT were shown to regulate pancreatic insulin secretion and glucose tolerance. In the second part of my thesis, I show the development of an antibody specific for EVs originating from adipocytes, to be used for the antibody-based isolation of adipocyte-derived EVs from the blood stream and subsequent molecular analyses of the EV cargo.

Part 1: The functional role of adipocyte-derived EVs

Morphological and molecular characterisation of the EV cargo under different metabolic conditions

At the beginning of my thesis the knowledge about adipocyte-derived EVs was scarce and limited to EVs isolated from cultured and *in vitro* differentiated cell lines (233). Accordingly, the first aim of my thesis was the establishment of a robust protocol for the isolation of adipocyte-derived EVs from AT explants of lean and obese mice as well as liposuction samples from human individuals. The here established methods differ from other published protocols in two important aspects: First, the here developed protocol was designed to isolate EVs only from the adipocyte fraction instead of whole AT explants and therefore avoids the co-isolation of EVs from other AT-residing cell types like mesenchymal stem cells, endothelial cells, fibroblasts and a variety of immune cells (184,185). This allowed me to specifically address the signalling function of adipocyte-derived EVs. Second, the protocol avoids the application of a number of stimulating agents like palmitate, insulin or hydrogen peroxide, which have been shown to enhance EV secretion from adipocyte cell lines due to a stress response (109,234,235). These stressors were omitted to avoid confounders and to assess the intrinsic signature of adipocyte-derived EVs in their basal state. Secreted EVs were finally isolated from the supernatants of explanted adipocytes by differential ultracentrifugation, the mostly applied technique for vesicle preparations so far (53,56,236).

Using this protocol, the isolated EVs from the adipose depots eWAT and iWAT showed classical EV features like an EV-typical size, morphology and the presence of characteristic EV markers such as CD9, CD63 and CD81 (9,12). TEM images of the isolated EV fractions further demonstrate the typical EV-like morphology and absence of

visible cellular debris. Importantly, size measurements of the EV preparations also showed an absence of apoptotic bodies which are characterized by sizes between 1000 and 6000 nm. Consequently, the isolated adipocyte EVs meet the required quality standards as defined by the MISEV guideline (9) and are therefore suitable for follow-up characterization studies and functional assays.

EVs isolated with the here established protocol represent a mixed vesicle population including exosomes and MVs, also referred to small and large EVs (9,11,14,237). Increasing knowledge about distinct EV marker combinations allows to subcategorize EVs in up to six different vesicle populations (238) according to their size in small and large EVs (sEVs and lEVs, respectively), further subdivided according to their density into low and high density sEVs and lEVs. These vesicle subclasses differ in their quantitative composition, which is likely explained by the secreting cell type with its individual maturation and homeostatic state, and by differences in the cellular machinery involved in the ESCRT-dependent ILV and exosome biogenesis (10). Similarly, the physiological and pathophysiological state of a cell may determine EV composition and secretion. Furthermore, recent evidence suggests the presence of other subsets of EVs, such as oncosomes (239), exomeres (240) and mitovesicles (26), which adds further complexity to the EV field.

In the past more and more evidence has emerged that different EV subpopulations also bear distinct functional properties. For example, specific protein signatures and miRNA profiles have been shown for EVs originating from cancer cells (56), dendritic cells (33) and also adipocytes (36). Thereby, the EVs isolated from cultured 3T3-L1 and primary murine adipocytes could be separated into classes of small and large EVs, bearing a specific proteomic as well as lipidomic profile. However, since the yields of the individual vesicle subfractions are usually very low, functional *in vitro* and *in vivo* studies are limited. My thesis focused on total EV fractions from adipocytes.

Next to the establishment of the EV isolation protocol, I used mass spectrometry to study how the complex obesity related remodelling of the iWAT and eWAT adipocytes (101,121,122) translates into changes of the adipocyte EV protein cargo. I could confirm the presence of classical EV markers such as CD63 and CD81 (9) in all EV isolates. Detection of a panel of proteins involved in vesicle trafficking and secretion like flotillins and RAB proteins further confirmed significant amounts of small EVs in the studied isolations.

An in-depth comparison of the EV proteome signature from the AT depots eWAT and iWAT revealed a broad overlap of detected proteins, indicating a large similarity between

the EVs from both AT depots. However, especially upon the dietary challenge of HFD feeding, significant differences in the protein cargo of eWAT and iWAT EVs were found, with an enrichment of pathways involved in lipid metabolism, fat digestion and absorption, biosynthesis of fatty acids, PPAR signalling and steroid biosynthesis in eWAT EVs. The adipocyte-derived EVs therefore represent the functional differences of the visceral and the subcutaneous fat depots, with eWAT adipocytes being more metabolically active and having greater lipolytic activity compared to iWAT adipocytes (241).

Interestingly, EVs secreted by the adipocyte fraction of eWAT and iWAT also included the AT-specific hormones adiponectin and leptin, suggesting an alternative way of hormone secretion. Leptin, being an important adipokine in the regulation of energy balance and AT mass (242,243) was more abundant in EVs from obese eWAT and iWAT, reflecting the *in vivo* situation of overall increased adiposity upon HFD-feeding. The adipokine adiponectin has been described as a protective, insulin-sensitizing adipokine, being downregulated and thus contributing to decreased insulin sensitivity in an obese state (244,245). This downregulation was also observed in the isolated eWAT EVs but not in iWAT EVs. I moreover detected the AT specific protein FABP4 in iWAT EVs and, with higher abundance, also in eWAT EVs. Earlier reports showed that FABP4 levels are increased upon HFD feeding in eWAT of diabetic mice and are upregulated in visceral AT of obese humans (246). Interestingly, FABP4 has also been linked to glucose metabolism by stimulating insulin secretion under obesogenic conditions (247).

Overall, my data indicates that EVs from eWAT vs. iWAT differ in their morphology and content, indicating that they might play differential functional roles in whole body metabolism. Secreted adipocyte-derived EVs may elicit such para- or endocrine functions by transferring protein content to distinct cells and tissues. Next to the protein cargo, adipocyte EVs also carry miRNAs, which could further add to the EV-mediated para- and endocrine signalling. Specifically, the detailed analysis of miRNAs present in adipocyte-derived EVs revealed significant differences in a large panel of miRNAs with an already described role in metabolism and most strikingly, in glucose-stimulated insulin secretion and insulin resistance. In AT, the downregulation of miR-141-3p under HFD-feeding has for instance been linked to an inhibition of hepatocyte glucose uptake resulting in increased insulin resistance (248). Adipocyte-derived miR-27a, which was also expressed in the samples investigated in this thesis, has been shown to induce insulin resistance in skeletal muscle by repression of PPARγ (116). Additionally, in the samples of this study miR-34a was detected, which was reported to actively suppress macrophage polarization towards an anti-inflammatory M2 state (249). In my studies, miR141-3p, miR-27a and miR34a levels remained unchanged when mice were challenged with HFD-feeding.

Apart from proteins and miRNAs transported lipids could contribute to the transferred signal (250). Especially EVs originating from adipocytes as lipid storage entities have been proposed to specifically transfer triglycerides and fatty acids (8). However, only studies applying ultrafiltration or size exclusion chromatography as EV isolation techniques are suitable to investigate this contribution, as lipid-containing vesicles may float during the most commonly used ultracentrifugation procedure. Accordingly, I did not further consider the transfer of lipids in my study.

In summary, broad differences in the adipocyte EV miRNA and protein cargo suggest a potential role of adipocyte-derived EVs in autocrine, paracrine or endocrine signalling. Such functions may include direct effects on adipocytes or a transfer of signaling entities toward distant cells and organs to control macrophage polarization and glucose homeostasis. My studies were designed to reveal these putative roles of adipocyte-derived EV as novel paracrine and endocrine regulators of specific metabolic functions, as discussed below.

Paracrine effects of eWAT-derived EVs on adipocyte browning and differentiation

Proteome analyses of eWAT and iWAT EVs revealed a panel of proteins involved in PPAR signalling. PPARs are transcription factors that regulate AT development and function as well as the conversion of white into brown/ beige adipocytes (227). I thus aimed to test the hypothesis that an EV mediated transfer of proteins involved in PPAR signalling could be involved in a paracrine regulation of adipocyte differentiation and browning. I moreover wanted to assess whether miRNAs detected in my eWAT EV cargo that are associated with AT browning and differentiation can enhance that effect.

To investigate the potential role of adipocyte-derived EVs in adipocyte browning, murine primary subcutaneous adipocytes were treated with EVs isolated from iWAT of lean and obese mice followed by an expression analysis of browning related target genes including *Ucp1* or *Pgc1α* (226,227,251). However, despite the promising evidence of the proteome and miRNA, I was not able to detect substantial changes on gene expression levels, except for a mild induction of *Pgc1*α upon treatment with lean adipocyte EVs. Also for adipocyte differentiation, I was unable to find changes in adipocyte gene expression markers *FABP4* and *PPARG* in SGBS preadipocytes after 48 h of treatment with EVs isolated from fully differentiated SGBS adipocytes. An increased differentiation of preadipocytes had been reported for the treatment with adipocyte EVs (105,109,252). This discrepancy may result from the different outcome measures used for adipocyte differentiation. The published studies focused on lipid droplet formation as measure for adipocyte differentiation. An effect on lipid accumulation has already been investigated

earlier, showing that large rat adipocytes can release EVs which stimulate lipid accumulation and increase cell size in small adipocytes in an endocrine fashion (134), potentially in order to synchronize the surrounding adipocytes and spread the burden of lipid storage between cells. This suggests a more lipogenic than a differentiation effect on preadipocytes. In later studies, an increase in adipogenic gene expression levels after EV treatment has been confirmed for human mesenchymal stem cells or human adipose-derived stem cells, indicating that not preadipocytes but cell populations already in an earlier stage of lineage differentiation might be the target of adipocyte EVs (110,111).

Paracrine effects of eWAT-derived EVs on AT inflammation

To test my hypothesis that lean and DIO-derived eWAT EVs have differential effects on macrophage polarization, I stimulated primary BMDMs with lean or obese adipocyte EVs. However, I found no evidence for an impact on macrophage polarization and changes toward a pro-inflammatory phenotype, even in the presence of additional stimulants for macrophage polarization. My data are thus in contrast to a considerable body of *in vitro* and *in vivo* evidence indicating that adipocyte EVs are capable to influence monocyte and macrophage differentiation to a more pro-inflammatory phenotype (103–106,133,253). These studies either investigated the effects of adipocyte-derived EVs on primary ATMs or naïve unstimulated BMDMs and RAW264.7 macrophages, not in M1 or M2-stimulated BMDMs. Some studies also used whole AT explants as EV source, including the SVF EVs. Collectively, these studies suggest that the EV-mediated signalling between adipocytes and macrophages occurs in a reciprocal manner, potentially in a vicious cycle. In a state of diet-induced obesity, inflamed AT macrophages may drive insulin resistance in adipocytes, which in turn exacerbate inflammation and macrophage polarity, ultimately contributing to the pathology of obesity and related disorders (41,133,254,255).

Tissue distribution kinetics of adipocyte-derived EVs

To investigate a potential endocrine role of adipocyte EVs, I analysed the biodistribution of circulating eWAT EVs and their accumulation in potential target organs *in vivo* in mice. My work was hereby the first to combine fluorophore-labelled EVs and whole mouse cryo-imaging. Most strikingly, I observed an organotrophic uptake of *ip.* and *iv.* injected adipocyte EVs into metabolically active target with highest signals in pancreas and liver, indicating a potential involvement in the regulation of metabolism and metabolic diseases. My study adds to a number of other studies investigating the biodistribution of labelled EVs of other cellular origins. Together these studies observed distinct EV accumulation patterns dependent on the EV origin (60,61,256–258). The organotropism of EVs likely depends on specific integrin patterns present on different EVs, as already shown for

tumour exosomes inducing either lung or liver metastasis by different integrin expression (68). The proteome analysis of the adipocyte EVs in this thesis also identified a cluster of integrins (α1, 5, 6, 7, v, and β1, 2, 5), but an involvement in organ-specific EV distribution requires further study. These targeting characteristics may also be influenced by the EV subtype, as small EVs seem to have a different biodistribution profile compared to large EVs, likely resulting from their different size, composition and cargo and consequent differences in barrier crossing abilities (56,259). Here, the distinct biodistribution pattern of my eWAT EVs, which differs to that of EVs from other tissues as reported by others, suggests specific adipocyte EV organ targeting characteristics and high specificity of the applied method. Nevertheless, the use of lipophilic dyes for EV labelling may have limitations. Specifically, the results could be confounded by the modification with the label per se (9,60) or by vesicles other than EVs, such as lipoproteins (260) or EV-mimicking dye nanoparticles that are almost undistinguishable from EVs (9,82). While I could not fully exclude minor contaminations with other vesicular particles, I controlled for the presence of confounding dye aggregates by injecting mice with dye only, subjected to the same staining protocol as the investigated EVs. Additionally, the route of application may also have an impact on the observed biodistribution patterning (258). In the state of obesity which is also characterized by an increase of visceral AT, the route of *ip.* injection may reflect the paracrine effect of the secreted EVs on surrounding organs in the peritoneal cavity. As the accumulation of abdominal fat is strongly associated with the development of comorbidities like insulin resistance and T2D (261,262), studying *ip.* injected adipocyte EV-distribution is of importance and relevance. But besides acting in a paracrine manner, EVs are also distributed via the bloodstream. This results in a broad mixture of EVs from numerous different sources present in plasma, therefore most of the biodistribution studies focus on *i.v.* injected vesicles (61). Interestingly, Thomou et al. proposed AT to be one of the most prominent sources of EV-derived miRNAs found in the circulation (40) whereas Flaherty et al. stated the opposite (106). To date, that discrepancy remains unresolved, and studies to specifically quantify that relative contribution of adipocyte EVs to the total EV pool in health and disease are warranted.

One more fundamental question in EV transport remains unresolved: to enter and exit the blood stream and to reach the target organs, EVs have to cross several barriers like the endothelium of blood vessels or the blood-brain-barrier without losing their specific properties and cargo. There is evidence and consensus that EVs are functionally distributed via the circulation to distinct target organs including the brain (263,264), but the mechanistic process of transmembrane trafficking still remains elusive (265,266). Studies proposed that transcytosis represents the primary mechanism, but also macropinocytosis and clathrin-dependent endocytosis have been suggested to be involved (64,71,267).

However, the ongoing development of novel high resolution live imaging and tracing techniques will help to unravel also these mechanistic processes. In order to obtain a higher resolution of EV biodistribution current innovations include bioluminescent reporters where luciferase or GFP fused to transmembrane proteins or classical EV markers are used to track EV distribution (11,268). A more sophisticated labelling technique is the application of the Cre-LoxP system (269). Implanted tumour cells carrying the Cre-recombinase secrete Cre-mRNA-containing EVs, which are taken up from reporter-expressing cells and induce a colour switch upon EV uptake. This elegant system could also be applied in AT transplant studies, giving the great opportunity to investigate EV biodistribution *in vivo* on a detailed cellular level.

Adipocyte-derived EVs target the pancreas and act as insulin secretagogues

The predominant enrichment of eWAT EVs in the pancreas after *i.p.* administration, in combination with the results from the EV proteome and miRNA profiling suggesting a role of eWAT EVs in insulin secretion, prompted me to further investigate a possible functional involvement of adipocyte EVs in glucose metabolism and insulin secretion. Indeed, *in vitro* treatment of primary murine islets with EVs isolated from eWAT of lean or DIO mice revealed an increase of glucose stimulated insulin secretion only in islets treated with eWAT EVs from obese mice, whereas lean AT EVs or EV concentrations lower than 10 µg did not cause an effect. Translated to the physiologic situation *in vivo*, the observed enhanced insulin secretion rates *in vitro* should result in an acute increase of glucose uptake into liver and muscle and therefore lead to lower glucose excursions in an ipGTT. To additionally examine a possible protective effect of EVs from lean eWAT, DIO mice were treated with a bolus injection of lean eWAT EVs prior to the performance of an ipGTT. In this setting, no alterations of glucose metabolism were detected but follow-up studies to this thesis showed - in line with the findings obtained with primary islets - lower glucose excursions in chow-fed mice after injection of DIO eWAT EVs (manuscript in revision). However, an increase of dosage from 10 µg to 50 µg was necessary to achieve this effect. In contrast to these findings, Deng et al demonstrated that injection of EVs isolated from the AT of genetically modified obese *ob/ob* mice but not from WT mice resulted in significant deterioration of glucose tolerance in an ipGTT (103). However, a number of differences in the study design may contribute to these discrepant results: 1) the EV isolation procedure not excluding the SVF which also has been shown to release EVs with strong signalling effects, especially in obesity related inflammation (8); 2) the prolonged treatment regimen (30 µg EVs per mouse every 3 days for 21 days vs. single injection of 50 µg EVs per mouse in the studies of this thesis), or 3) the use of a mouse model with a different genetic background (*ob/ob* mice instead of HFD-fed WT

mice). A recent publication confirmed the proposed regulation showing that EVs isolated from inflamed murine 3T3-L1 cells and human EVs from obese AT aggravate ß-cell survival and function (270). Likewise, this study also used whole AT samples for EV isolation without removing the SVF and examined longer treatment intervals (24 h for cell lines or 72 h for primary islets) in contrast to the more acute treatment of 4 h used in the experiments of this thesis. Additionally, the EV isolation procedure included a 0,22 µm filtration step which diminishes larger EV fractions. If and how different EV subpopulations contribute to the contradictory results also in a time-dependent manner warrants further study.

Therefore, besides the acute stimulation assays, this thesis additionally aimed to investigate the impact of EVs on a more chronic level as well as in the complex *in vivo* environment. Yet, as the isolation of sufficient quantities of primary adipocyte-derived EVs would have required the excessive sacrifice of many donor mice, chronic treatment studies with recurrent EV administration were hardly feasible and ethically not justifiable for my thesis. A possible option to circumvent this difficulty was the use of systemic inhibitors of EV secretion. To investigate whole body EV release *in vivo*, chow and HFD-fed mice were thus treated with the EV secretion inhibitor GW4869 (16,170), which was shown to reduce exosome secretion from several cell lines and diminish exosome release in mice (173–175). In my studies, pharmacological inhibition of EV secretion had no impact on body composition, energy expenditure or food intake in lean or DIO mice. Notably, GW4869 treatment had no significant effect on the secretion of adipocyte-derived EVs or serum EV levels, but lead to a mild impairment of glucose tolerance in chow fed mice. However, it has to be noted that by inhibiting nSMase-2-mediated ceramide formation, GW4869 is only able to block one route of EV biogenesis, whereas other routes like the ESCRT-dependent pathway or MV budding are unaffected. This suggests ceramide independent secreted EVs as possible effectors in this setting. In fact, other studies also detected only partial reduction of EV release (271) or even a compensatory upregulation of the secretion of larger EVs under treatment with GW4869 (272,273). Moreover, there also exists discrepancy on how the high *in vivo* dosages reported in the literature could be achieved given the limited solubility of GW4869 in DMSO and the maximum amount of DMSO approved for injections in mice (174). In primary cells, inhibitor treatment has additionally been reported to cause cell death, or in lower concentration increase EV secretion of all size subclasses (274). Furthermore, the normal and healthy phenotype of a nSMase knockout mouse model (275) questions the overall impact of the ceramide-dependent EV secretion route and implicates robust alternative pathways for EV biogenesis. Other models are necessary to further approach this issue of blocking whole body EV secretion. Most importantly, knocking out components of the EV

secretion machinery will impair numerous other crucial cellular membrane trafficking processes, leading to severe side effects or even lethal phenotypes as seen in different RAB-protein family knockout models (276).

Together, the findings of my thesis provide clear evidence that eWAT EVs affect insulin secretion and glucose metabolism. The aim of my study was to generate clean and pure fractions of eWAT EVs excluding major contamination by membrane debris or other vesicle types. This was, however, at the expense of the achievable EV yields and accordingly the number of studies I could run, especially in absence of appropriate genetic models with gain or loss of function modifications. Accordingly, my studies do not provide insight into the complex dynamics of EV secretion from AT *in vivo*. This thesis provides first evidence that EV secretion rates may correlate with the amount of AT mass, while the impact of other possible suggested stimulants of EV secretion like pro-inflammatory cytokines, fatty acids or hypoxia on EV release *in vivo* remain to be determined. This prompted me to develop a tool for the isolation and quantification of eWAT-derived EVs from the blood stream which also offers the opportunity of detailed downstream molecular characterization of adipocyte EVs in different metabolic stages.

Current limitations of functional *in vivo* studies

Studies investigating cultured adipocytes have shown that obesity-associated stress stimuli like pro-inflammatory cytokines, fatty acids or hypoxia enhance EV release (36,109,253). Higher secretion rates together with increased AT mass in DIO mice therefore should translate to an overall higher eWAT EV secretion and elevated circulating AT EVs under obese conditions. Deng et al. detected an increased EV secretion of obese murine AT explant cultures, accompanied by a significant increase in circulating EVs (103). Increased EV levels in the circulation were also measured in rodents as well as human obese subjects (123) and correlated significantly with decreased glucose sensitivity, elevated triglyceride levels and increased insulin resistance (277). In a similar eWAT explant study, I observed a mild increase of EV secretion from obese compared to lean AT when normalized to the same amount of tissue. However, in my studies, EV protein levels measured in serum were not influenced by HFD-feeding. The latter is in line with a study by Mleczko, which also could not detect an elevated level of serum EVs in obesity (112).

In summary, even in obese individuals the levels of total serum EVs may not solely depend on the secretion from AT. However, it is at current nearly impossible to distinguish the exact tissue or cell-type of origin of circulating EVs. Although adipocyte EVs may provide an important fraction of the circulating EVs, the exact proportion is still up for

debate. To address this open gap in our understanding of circulating EVs, tissue specific EV isolation techniques are required to quantify, isolate and characterize adipocyte-derived EVs from overweight and obese subjects and to better assess their phenotypic risk for comorbid sequelae. This open gap together with the diagnostic potential of circulating EVs guided me to generate an antibody specific against adipocyte-derived EVs, as discussed in the second part of this section.

Part 2: Generation of an antibody-based method for the isolation of circulating adipocyte EVs

To investigate the contribution of adipocyte EVs to the entirety of EVs present in the bloodstream and to analyse the dynamics of EV composition upon metabolic changes, methods to specifically isolate adipocyte-derived EVs from the circulation are essential. However, up to date no particular tools are available to separate adipocyte EVs from a mixed EV population of different cellular origin. Therefore, the second part of this thesis was dedicated to the development of an antibody specific for adipocyte EVs which can serve as a technical tool as well as a diagnostic marker to specifically isolate adipocyte-derived EVs followed by detailed molecular characterization.

First, I aimed to establish that human adipocytes indeed secrete EVs. Human AT samples were obtained from patients undergoing liposuction or abdominoplasty and the protocol already established for murine adipocytes was slightly modified to take account of the differing primary material. This protocol also separates the SVF before the EV isolation and is therefore specifically isolating adipocyte-derived EVs. I could show that also human adipocytes release vesicles bearing typical EV characteristics like rounded shape, with sizes of approximately 100 nm and classical EV marker proteins like CD63 or CD9. The next question was whether the isolated adipocyte EVs were suitable as predictors for AT status and can be used as biomarkers. The usage of EVs as tissue biomarkers has several advantages compared to whole tissue biopsies: First, EVs are easily accessible in biological fluids like blood or urine and can be obtained in a minimal or even non-invasive way. Second, due to their structure, the EVs' cargo is protected from environmental impacts like degradation and third, isolation of EVs allows the concentration and analysis of specific molecules of interest in easy to obtain particles. And finally, after isolation, EVs are relatively stable and can be stored for longer periods at -80°C (278). However, there are also limitations in this study: the investigated human AT samples obtained from liposuctions of abdominoplasty represent only subcutaneous AT which, in contrast to visceral AT, is of minor relevance in the context of metabolic diseases (279). The donating

patients were mostly females, and the BMI ranged within a mildly overweight rather than morbidly obese state. Additionally, liposuction or abdominoplasty are often performed in (formerly) obese individuals that already lost weight, which could influence and/or reprogram adipocyte metabolism towards a more healthy state (280) or lead to a differing EV composition. Collecting additional patient characteristics like waist to hip ratio, weight changes over the last years or the presence of metabolic comorbidities other than diabetes would have helped to draw a more detailed picture of the metabolic state of the EV releasing adipocytes. As the availability of human AT is limited and wouldn't have met the required amounts and the frequency necessary for the whole process of antibody generation and screening, an alternative source for human adipocyte-derived EVs had to be found to conduct the experimental procedures. The well-established and widely used human cell strain SGBS can be differentiated *in vitro* to mature adipocytes that are functionally comparable to primary human adipocytes (142). I could demonstrate that differentiated SGBS cells also release vesicles with EV-like characteristics such as shape, size and marker expression and therefore used these cells and vesicles for the antibody generation process. To generate a monoclonal antibody specific for human adipocyte EVs a well-established experimental procedure was executed, which additionally was published in a patent (232). The initial step was the immunization of two rats and one mouse with isolated EVs from differentiated SGBS cells. The approach to immunize with mature vesicles and not with isolated proteins or fragments carries the advantage that the generated antibody may not only be directed against distinct proteins but also could target bigger and more complex structures like secondary protein modifications. Interestingly, EVs have recently been shown to transport, additional to their intrinsic proteome, on their outer surface a functional corona of proteins that could have an impact on EV signalling and biodistribution properties (281–283). Specific proteome analyses of the so-called "surfaceome" also suggests the importance of EV surface proteins for intercellular trafficking and signalling (284). Following immunization and an additional boosting injection after six weeks, antibody producing hybridoma clones were generated by the fusion of spleen cells with a myeloma cell line. The specificity of the antibody clones was tested in a multi-step screening approach, starting with an initial screening comparing differentiated SGBS cells as positive and HepG2 cells as negative control. In the second step, differentiated vs. undifferentiated SGBS cells were tested, followed by identification of the antibody targets with immunoprecipitation and mass spectrometry. The selected antibody producing clones were then subcloned in order to obtain stable clones and the screening approach with immunofluorescence, immunoprecipitation and target verification by mass spectrometry was repeated to validate the results. The tissue specificity of the generated antibodies to human adipocyte EVs was further investigated by a dot blot with

several negative controls like liver, pancreas, colon or bone cell models, finally revealing four antibody clones out of more than 2 000 clones in the beginning for follow-up studies. To fully characterize the generated monoclonal antibodies, the DNA sequence of the variable regions of heavy and light chain was determined. Of special interest are the identified targets of the selected antibodies: Two antibody clones target the protein AOC3 (Amine oxidase, copper containing 3), an enzyme catalysing the oxidation of amines, also known as vascular adhesion protein 1 (VAP-1). The expression of AOC3 has already been reported in EVs originating from rat primary adipocytes (285) and from mouse embryonic fibroblasts (precursor cells for adipocytes) (286), as well as in human AT (287), supporting the adipocyte-EV specificity of the generated antibodies. However, AOC3 expression was also reported in smooth muscle, alveolar cells and the adrenal gland but to a much lesser extent compared to the high levels found in AT (288). Proposed functions of AOC3 in adipocytes include the regulation of glucose uptake via GLUT4 or control of cellular metabolism by the selection of metabolic fuels (289,290). Intriguingly, AOC3 has also already been linked to diabetes and related comorbidities being explored as drug target to inhibit beta cell damage and diabetic complications like retinopathy (291,292). Two of the generated antibody clones showed a specificity against CD63 or LAMP2, representing two general markers for EVs as these proteins are both involved in the process of EV formation (293,294). This also supports that the EV-immunization and screening approach was successful. The dot blot with the antibody against LAMP2, however, shows a more general staining also in the tested cell lysates which can be explained by the fact that LAMP2 is a highly abundant lysosomal membrane glycoprotein (295). Another identified antibody target is COL6A (Collagen Type VI Alpha), an extracellular matrix protein that is the primary component of the white AT extracellular matrix (296). COL6A is highly expressed in adipocytes (297), which is reflected by the specific positive staining of adipocyte EVs and lysates in the dot blot analysis. COL6A expression is increased in murine and human obesity and contributes to adipocyte inflammation and insulin resistance (298,299). COL6A was also found in adipocyte EVs (109,285) as well as in the secretome of human AT with a significantly higher release from visceral compared to subcutaneous AT (300), further supporting the link between COL6A and metabolic diseases. The last identified antibody target is vimentin, a cytoskeletal protein which is secreted and transported in EVs from different cell lines, including adipocyte progenitor cells (301–303). These findings are confirmed by the dot blot analysis which shows a staining also in the cell lysates due to their cytoskeletal components. To what extent the finally selected antibody clones are suitable for the future goal to specifically isolate adipocyte EVs from blood samples remains to be determined. Adipocyte EVs are present in the circulation (40,304) and have been suggested as novel

circulating biomarkers for metabolic stress in mice and humans (123,277). These studies used the marker protein Perilipin A (also known as Perilipin 1) to identify adipocyte EVs in the bloodstream. Perilipin A could also be detected in this thesis in the proteomic profile of adipocyte EVs from murine and human AT as well as human serum EVs. Intriguingly, in a preliminary experiment (data not shown) using the clone 23A11 in an IP assay with human serum EVs, the presence of Perilipin A was confirmed in the antibody bound EVs, which corroborates the adipocyte EV specificity of the generated antibody clone. However, some concerns were raised as Perilipin A also localizes with lipid droplets, suggesting it to be a potentially co-isolated artefact from plasma samples (233). To avoid this, proper EV purification methodology is of importance, not the least due to a recent report that some adipocyte marker proteins also exist as soluble forms which would result in a false positive detection without a proper EV isolation protocol (304). An additional challenge for an EV-based biomarker approach is the complexity of serum as the sample matrix. Especially the high albumin content may influence EV isolation and disturb distinct assays (53). The elimination or at least reduction of possible confounding co-isolates in serum is highly challenging, as for example shown for lipoproteins that mimic EV characteristics during purification (305,306). However, other approaches like immunoaffinity-based methods using CD63 or CD81 may also be limited to isolate non-specific populations carrying these partially generic marker proteins (233). Furthermore, also blood cells could contribute to confounding effects, as for example platelet EVs were proposed to be a major source of EVs present in the circulation (307). Besides the complex sample matrix, other factors influencing circulating EVs have been discussed in the literature: metabolic aspects like the time of the day at sample collection (308) and physical activity prior to sample withdrawal (309) or technical issues like the type of tube used for blood collection and handling conditions as blood cells may continue to secrete vesicles after sample collection *in vitro* (310). Therefore, there is a high need to standardize not only the protocols of sample collection, isolation and storage, but also minimize the influence of other confounding factors when a liquid biopsy-based approach is transferred to a clinical setting (85). A cell-specific, antibody-based enrichment of EVs from plasma has already been published for EVs of neuronal origin (63), which are currently investigated as biomarkers for cognitive decline in Alzheimer's disease (311,312). The main future goal for the antibody developed in this thesis will be an application as tool for biomarker isolation in the context of obesity and metabolic diseases, for example to characterize more in detail the differences between healthy obese subjects from unhealthy obese subjects with established comorbidities. Ultimately, such an approach could help predicting the individual risk and current metabolic status before the onset of associated diseases like T2DM or cardiovascular complications. The link between obesity and EV

composition is also already investigated in clinical trials: 2 clinical studies investigate the underlying mechanisms of healthy or unhealthy obese combined with the impact of dietary interventions in adults and analyse EVs from serum as well as from AT (125,126). Another clinical trial in overweight children with high risk of developing T2DM, the PREDIKID study, investigated the effect of a multidisciplinary intervention program on the miRNA profile of circulating exosomes (313). Currently, other useful approaches are emerging in the field of biomarker discovery, like the effort to create a common database by proteomic profiling of serum EVs from healthy donors which could be used as a reference catalogue in biomarker development (314).

Apart from that, in addition to protein-based markers also computational approaches for the characterization of circulating EVs have been introduced recently. The so called EV-origin technique uses RNA-seq data to estimate the tissue-cellular source of circulating EVs and the functional state of their cellular origin (315).

Besides studying the evolving accumulation of AT in the development of obesity, also the opposite, an excessive loss of AT mass as seen in cancer patients, could represent a possible application of an adipocyte-EV specific biomarker: Cancer cachexia, a metabolic disorder which is characterized by rapid and substantial loss of AT and skeletal muscle weight in a futile cycle that is not reversable by conventional nutritional support (316). Cachexia is a multi-organ energy wasting syndrome involving mostly skeletal muscle and AT, but also bone, liver, the neural system and gut, and is associated with poor prognosis and increased mortality (317). A key factor defining cancer cachexia is a constant AT remodelling resulting in dysfunctional AT and it has been reported that these changes in AT occur even before an involvement of skeletal muscle (318). Therefore, an adipocyte EV-specific biomarker could be of advantage in early diagnosis of cachexia to improve quality of life and life expectancy. Additionally, investigating a potential genetic predisposition for the development of cachexia based on an adipocyte EV-biomarker would be favourable for cancer patients.

4.1 Conclusion and Perspective

The first aim of this thesis was to elucidate if EVs could serve as novel endocrine signalling entity between adipocytes and different metabolic target organs. Therefore, a robust protocol to isolate EVs from the adipocyte fraction of murine and human AT was established. This protocol considered the presence of other AT resident cells which represent an additional source of EVs from whole AT and avoided this confounding factor by only isolating adipocyte-derived EVs. Morphological and surface marker

characterization confirmed the isolated vesicles as EVs. The detailed investigation of the proteome cargo of adipocyte EVs isolated from two fat pads, eWAT and iWAT, from lean and obese mice revealed substantial differences depending on the tissue of origin and the dietary intervention. Comparison of the proteome of eWAT EVs with whole tissue lysate showed firstly that the EVs closely reflect the tissue of origin and secondly that EVs can even serve as a superior predictor for the metabolic state of the secreting adipocytes compared to the analysis of whole AT. Besides proteins, miRNAs have also been recognized as important signal mediators of EVs (319). In line with the proteome analyses of this study, miRNA profiling of eWAT EVs from lean and obese murine AT revealed a distinct patterning upon dietary intervention. Detailed pathway analysis of the proteome and miRNA profile suggested a potential impact of eWAT EVs on fatty acid metabolism, PPAR and PI3K-Akt signalling, adipogenesis, adipocyte browning, inflammation and macrophage polarization as well as insulin signalling. Biodistribution studies showed an organ-specific delivery pattern especially to metabolically active target organs such as liver, pancreas and eWAT. Led by these findings several functional assays were performed investigating hypoxia, the impact of EVs on adipocyte differentiation or browning. Unexpectedly after the promising omics results and in contrast to other studies no effects of eWAT EV treatment were observed. Additionally, EVs did not influence macrophage polarization, which represents an important hallmark of AT inflammation in the development of obesity and related comorbidities (4). On the other hand, an impact of eWAT EVs on insulin secretion was observed, as shown by an increased GSIS of pancreatic islets after treatment with eWAT EVs originating from HFD-fed mice. Furthermore, the systemic influence of exosome secretion was investigated by *in vivo* administration of the exosome secretion inhibitor GW4869 in chow and HFD-fed mice. Metabolic phenotyping showed no general influence of secretion blockage, but also here a mild effect on glucoregulation was observed, indicated by a decreased glucose tolerance in lean inhibitor treated animals. Upon inhibitor treatment, however, no overall reduction of EV secretion from AT or levels in serum could be detected. This finding may be caused by the selective inhibition of only one route of EV secretion by GW4869, whereas unaffected alternative mechanisms could be upregulated in a compensatory way. Taken together, this thesis showed that adipocyte-derived EVs originating from obese eWAT, being considered the more relevant AT depot in the context of metabolic diseases, serve as regulators of insulin secretion.

My thesis strongly supports more in-depth experiments on the glucoregulatory role of eWAT EVs. For instance, the specific targeting of pancreatic beta cells by eWAT EVs should be confirmed and analysed in more detail by high resolution imaging techniques. Subsequent investigation of beta cells changes after EV uptake could give novel insights

into the cellular mechanisms targeted by eWAT EVs. Indeed, ongoing *in vivo* studies conducted after this thesis confirm the beneficial effect of DIO eWAT EVs on glucose tolerance. Prompted by my thesis and corroborated in these ongoing studies, my data suggest a model whereby EVs act as insulin stimulants to prime the organism for a higher insulin demand in a state of obesity and insulin resistance. More detailed investigation of the EV subpopulations should now reveal if a specific subset of EVs with distinct properties and cargo is responsible for mediating this effect, as suggested by the results of my GW4869 *in vivo* study suggesting the coexistence of alternative pathways of EV secretion. However, novel imaging and intracellular trafficking techniques are needed for this purpose, which are currently being developed (273). The influence on insulin secretion also suggests a therapeutic potential of EVs in the context of insulin resistance and metabolic diseases which should be explored in future studies. The detailed characterization of the underlying mechanisms for this beneficial effect could provide further insights into the regulation of insulin secretion and reveal potential future targets for therapeutic approaches. Finally, for a proof-of-principle, the creation of an adipocyte-specific EV-secretion knock out mouse model would allow to study paracrine and systemic effects of adipocyte EVs in a complex *in vivo* setting, especially in the context of obesity and related comorbidities.

The second part of this thesis aimed to investigate the potential role of AT-derived EVs as biomarkers for metabolic diseases. To initially address this question, a monoclonal antibody specific for adipocyte-derived EVs was generated, serving as technical tool as well as a possible source for the detection of biomarkers of AT health. In a multistep screening approach, the number of potential antibody clones was narrowed down from more than 2000 to four promising candidates by the end of this thesis. Follow up studies should first aim to characterize and prove the specific and direct binding of adipocyte EVs in more detail, for example by immunogold-labelling followed by electron microscopy. Secondly, by methods like FACS-sorting the binding characteristics of the generated antibody should be further explored using EVs of different origin. The ultimate future goal of this project is the investigation of human blood samples as liquid biopsies for an assessment of adipocyte health and pathogenesis. The specific isolation of adipocyte EVs from serum of patients with different metabolic conditions like lean and healthy, morbidly obese with metabolic complications, or obese but healthy, would allow to investigate differences in EV cargo and composition which could be applied in following studies as biomarkers for adipocyte health. Additionally, biomarkers for other disorders closely linked to adipocyte function could be investigated with the generated antibody, for example the excessive loss of AT seen in cancer cachexia. Next to the focus on adipocytes, this antibody-based approach could also be implemented for other target organs. For example,

in diagnosis and monitoring of chronic liver diseases a liquid biopsy by analysing hepatocyte EVs directly from the bloodstream could replace current invasive biopsy approaches and thereby increase treatment success and quality of life of affected patients.

Last, one of the key challenges in the field of EV research is finding a consensus about minimal requirements for isolation and characterization procedures. This became even more important given that interest in EV research has rapidly increased over the last decade creating an immense and constantly growing number of publications. Overall, these reports support the conclusion that EVs represent a heterogenous population with distinct properties and particular functions. Whether that EV heterogeneity is the result of differing methodologies or a true biological effect remains a matter of debate. Accordingly, at current the reported variance in EV populations often hampers a clear interpretation and proper comparison of different results. Finding a realistic and reasonable compromise between necessary and scientifically valid demands on the one hand and feasible methodologies in a practical way on the other hand seems to be the major challenge, especially in a technical as well as knowledge-wise rapidly developing research field.

5 References

1. Engin A. The Definition and Prevalence of Obesity and Metabolic Syndrome. In: Engin AB, Engin A, editors. Obesity and Lipotoxicity. Cham: Springer International Publishing; 2017. p. 1–17. (Advances in Experimental Medicine and Biology; vol. 960).

2. WHO fact sheet. Obesity and overweight [Internet]. 2021 [cited 2022 Aug 29]. Available from: https://www.who.int/news-room/fact-sheets/detail/obesity-and-overweight

3. WHO. Obesity [Internet]. 2021 [cited 2022 Oct 30]. Available from: https://www.who.int/news-room/facts-in-pictures/detail/6-facts-on-obesity

4. Chait A, den Hartigh LJ. Adipose Tissue Distribution, Inflammation and Its Metabolic Consequences, Including Diabetes and Cardiovascular Disease. Front Cardiovasc Med. 2020;7.

5. Balistreri CR, Caruso C, Candore G. The Role of Adipose Tissue and Adipokines in Obesity-Related Inflammatory Diseases. Mediators Inflamm. 2010 Jul 1;2010:e802078.

6. Zatterale F, Longo M, Naderi J, Raciti GA, Desiderio A, Miele C, et al. Chronic Adipose Tissue Inflammation Linking Obesity to Insulin Resistance and Type 2 Diabetes. Front Physiol. 2019;10:1607.

7. Rana MN, Neeland IJ. Adipose Tissue Inflammation and Cardiovascular Disease: An Update. Curr Diab Rep. 2022 Jan 1;22(1):27–37.

8. Crewe C, Scherer PE. Intercellular and interorgan crosstalk through adipocyte extracellular vesicles. Rev Endocr Metab Disord. 2022 Feb 1;23(1):61–9.

9. Théry C, Witwer KW, Aikawa E, Alcaraz MJ, Anderson JD, Andriantsitohaina R, et al. Minimal information for studies of extracellular vesicles 2018 (MISEV2018): a position statement of the International Society for Extracellular Vesicles and update of the MISEV2014 guidelines. J Extracell Vesicles. 2018 Dec 1;7(1):1535750.

10. van Niel G, D'Angelo G, Raposo G. Shedding light on the cell biology of extracellular vesicles. Nat Rev Mol Cell Biol. 2018 Apr;19(4):213–28.

11. Zaborowski MP, Balaj L, Breakefield XO, Lai CP. Extracellular Vesicles: Composition, Biological Relevance, and Methods of Study. BioScience. 2015 Aug 1;65(8):783–97.

12. Raposo G, Stoorvogel W. Extracellular vesicles: Exosomes, microvesicles, and friends. J Cell Biol. 2013 Feb 18;200(4):373–83.

13. György B, Szabó TG, Pásztói M, Pál Z, Misják P, Aradi B, et al. Membrane vesicles, current state-of-the-art: emerging role of extracellular vesicles. Cell Mol Life Sci. 2011

Aug;68(16):2667–88.

14. Yáñez-Mó M, Siljander PRM, Andreu Z, Bedina Zavec A, Borràs FE, Buzas EI, et al. Biological properties of extracellular vesicles and their physiological functions. J Extracell Vesicles. 2015 Jan 1;4(1):27066.

15. Lawson C, Vicencio JM, Yellon DM, Davidson SM. Microvesicles and exosomes: new players in metabolic and cardiovascular disease. J Endocrinol. 2016 Feb;228(2):R57-71.

16. Catalano M, O'Driscoll L. Inhibiting extracellular vesicles formation and release: a review of EV inhibitors. J Extracell Vesicles. 2020 Sep;9(1):1703244.

17. Février B, Raposo G. Exosomes: endosomal-derived vesicles shipping extracellular messages. Curr Opin Cell Biol. 2004 Aug;16(4):415–21.

18. Bobrie A, Colombo M, Raposo G, Théry C. Exosome Secretion: Molecular Mechanisms and Roles in Immune Responses. Traffic. 2011 Dec;12(12):1659–68.

19. Robbins PD, Morelli AE. Regulation of immune responses by extracellular vesicles. Nat Rev Immunol. 2014 Mar;14(3):195–208.

20. Hessvik NP, Llorente A. Current knowledge on exosome biogenesis and release. Cell Mol Life Sci. 2018 Jan;75(2):193–208.

21. Trajkovic K, Hsu C, Chiantia S, Rajendran L, Wenzel D, Wieland F, et al. Ceramide triggers budding of exosome vesicles into multivesicular endosomes. Science. 2008 Feb 29;319(5867):1244–7.

22. Ostrowski M, Carmo NB, Krumeich S, Fanget I, Raposo G, Savina A, et al. Rab27a and Rab27b control different steps of the exosome secretion pathway. Nat Cell Biol. 2010 Jan;12(1):19–30.

23. Atkin-Smith GK, Tixeira R, Paone S, Mathivanan S, Collins C, Liem M, et al. A novel mechanism of generating extracellular vesicles during apoptosis via a beads-on-a-string membrane structure. Nat Commun. 2015 Jun 15;6(1):7439.

24. Santavanond JP, Rutter SF, Atkin-Smith GK, Poon IKH. Apoptotic Bodies: Mechanism of Formation, Isolation and Functional Relevance. In: Mathivanan S, Fonseka P, Nedeva C, Atukorala I, editors. New Frontiers: Extracellular Vesicles. Cham: Springer International Publishing; 2021. p. 61–88. (Subcellular Biochemistry).

25. Battistelli M, Falcieri E. Apoptotic Bodies: Particular Extracellular Vesicles Involved in Intercellular Communication. Biology. 2020 Jan;9(1):21.

26. D'Acunzo P, Pérez-González R, Kim Y, Hargash T, Miller C, Alldred MJ, et al.

Mitovesicles are a novel population of extracellular vesicles of mitochondrial origin altered in Down syndrome. Sci Adv. 2021 Feb 12;7(7):eabe5085.

27. Jeppesen DK, Fenix AM, Franklin JL, Higginbotham JN, Zhang Q, Zimmerman LJ, et al. Reassessment of Exosome Composition. Cell. 2019 Apr 4;177(2):428-445.e18.

28. Meehan B, Rak J, Di Vizio D. Oncosomes – large and small: what are they, where they came from? J Extracell Vesicles. 2016 Jan 1;5(1):33109.

29. Gurung S, Perocheau D, Touramanidou L, Baruteau J. The exosome journey: from biogenesis to uptake and intracellular signalling. Cell Commun Signal. 2021 Apr 23;19(1):47.

30. Théry C, Boussac M, Véron P, Ricciardi-Castagnoli P, Raposo G, Garin J, et al. Proteomic Analysis of Dendritic Cell-Derived Exosomes: A Secreted Subcellular Compartment Distinct from Apoptotic Vesicles. J Immunol. 2001 Jun 15;166(12):7309–18.

31. Wubbolts R, Leckie RS, Veenhuizen PTM, Schwarzmann G, Möbius W, Hoernschemeyer J, et al. Proteomic and Biochemical Analyses of Human B Cell-derived Exosomes. J Biol Chem. 2003 Mar;278(13):10963–72.

32. Menck K, Scharf C, Bleckmann A, Dyck L, Rost U, Wenzel D, et al. Tumor-derived microvesicles mediate human breast cancer invasion through differentially glycosylated EMMPRIN. J Mol Cell Biol. 2015 Apr;7(2):143–53.

33. Kowal J, Arras G, Colombo M, Jouve M, Morath JP, Primdal-Bengtson B, et al. Proteomic comparison defines novel markers to characterize heterogeneous populations of extracellular vesicle subtypes. Proc Natl Acad Sci. 2016 Feb 23;113(8):E968–77.

34. Pezzicoli G, Tucci M, Lovero D, Silvestris F, Porta C, Mannavola F. Large Extracellular Vesicles—A New Frontier of Liquid Biopsy in Oncology. Int J Mol Sci. 2020 Jan;21(18):6543.

35. Yoshioka Y, Konishi Y, Kosaka N, Katsuda T, Kato T, Ochiya T. Comparative marker analysis of extracellular vesicles in different human cancer types. J Extracell Vesicles. 2013 Jan 1;2(1):20424.

36. Durcin M, Fleury A, Taillebois E, Hilairet G, Krupova Z, Henry C, et al. Characterisation of adipocyte-derived extracellular vesicle subtypes identifies distinct protein and lipid signatures for large and small extracellular vesicles. J Extracell Vesicles. 2017 Dec 1;6(1):1305677.

37. Phillips W, Willms E, Hill AF. Understanding extracellular vesicle and nanoparticle heterogeneity: Novel methods and considerations. PROTEOMICS. 2021;21(13–14):2000118.

38. Valadi H, Ekström K, Bossios A, Sjöstrand M, Lee JJ, Lötvall JO. Exosome-mediated transfer of mRNAs and microRNAs is a novel mechanism of genetic exchange between cells.

Nat Cell Biol. 2007 Jun;9(6):654–9.

39. Théry C. Exosomes: secreted vesicles and intercellular communications. F1000 Biol Rep. 2011 Jul 1;3(15):Epub.

40. Thomou T, Mori MA, Dreyfuss JM, Konishi M, Sakaguchi M, Wolfrum C, et al. Adipose-derived circulating miRNAs regulate gene expression in other tissues. Nature. 2017 Feb;542(7642):450–5.

41. Ying W, Riopel M, Bandyopadhyay G, Dong Y, Birmingham A, Seo JB, et al. Adipose Tissue Macrophage-Derived Exosomal miRNAs Can Modulate In Vivo and In Vitro Insulin Sensitivity. Cell. 2017 Oct;171(2):372-384.e12.

42. Zhou Y, Tan C. miRNAs in Adipocyte-Derived Extracellular Vesicles: Multiple Roles in Development of Obesity-Associated Disease. Front Mol Biosci. 2020;7:171.

43. Yang P, Peng Y, Feng Y, Xu Z, Feng P, Cao J, et al. Immune Cell-Derived Extracellular Vesicles – New Strategies in Cancer Immunotherapy. Front Immunol. 2021;12.

44. Hurwitz SN, Rider MA, Bundy JL, Liu X, Singh RK, Meckes DG. Proteomic profiling of NCI-60 extracellular vesicles uncovers common protein cargo and cancer type-specific biomarkers. Oncotarget. 2016 Nov 24;7(52):86999–7015.

45. Ekström K, Crescitelli R, Pétursson HI, Johansson J, Lässer C, Olofsson Bagge R. Characterization of surface markers on extracellular vesicles isolated from lymphatic exudate from patients with breast cancer. BMC Cancer. 2022 Jan 10;22(1):50.

46. L Ramos T, Sánchez-Abarca LI, Muntión S, Preciado S, Puig N, López-Ruano G, et al. MSC surface markers (CD44, CD73, and CD90) can identify human MSC-derived extracellular vesicles by conventional flow cytometry. Cell Commun Signal CCS. 2016 Jan 12;14:2.

47. You Y, Muraoka S, Jedrychowski MP, Hu J, McQuade AK, Young-Pearse T, et al. Human neural cell type-specific extracellular vesicle proteome defines disease-related molecules associated with activated astrocytes in Alzheimer's disease brain. J Extracell Vesicles. 2022 Jan;11(1):e12183.

48. ExoCarta: Home - Exosome database [Internet]. [cited 2022 Sep 14]. Available from: http://www.exocarta.org

49. Vesiclepedia: Home - Extracellular vesicles database [Internet]. [cited 2022 Sep 14]. Available from: http://www.microvesicles.org/

50. Subra C, Laulagnier K, Perret B, Record M. Exosome lipidomics unravels lipid sorting at the level of multivesicular bodies. Biochimie. 2007 Feb;89(2):205–12.

51. Zhang Y, Liu Y, Liu H, Tang WH. Exosomes: biogenesis, biologic function and clinical potential. Cell Biosci. 2019 Dec;9(1):19.

52. Donoso-Quezada J, Ayala-Mar S, González-Valdez J. The role of lipids in exosome biology and intercellular communication: Function, analytics and applications. Traffic. 2021;22(7):204–20.

53. Konoshenko MY, Lekchnov EA, Vlassov AV, Laktionov PP. Isolation of Extracellular Vesicles: General Methodologies and Latest Trends. BioMed Res Int. 2018 Jan 30;2018:e8545347.

54. Carnino JM, Lee H, Jin Y. Isolation and characterization of extracellular vesicles from Broncho-alveolar lavage fluid: a review and comparison of different methods. Respir Res. 2019 Oct 30;20(1):240.

55. Davidson SM, Boulanger CM, Aikawa E, Badimon L, Barile L, Binder CJ, et al. Methods for the identification and characterization of extracellular vesicles in cardiovascular studies: from exosomes to microvesicles. Cardiovasc Res. 2022 Mar 24;cvac031.

56. Willms E, Johansson HJ, Mäger I, Lee Y, Blomberg KEM, Sadik M, et al. Cells release subpopulations of exosomes with distinct molecular and biological properties. Sci Rep. 2016 Apr;6(1):22519.

57. Van Deun J, Mestdagh P, Agostinis P, Akay Ö, Anand S, Anckaert J, et al. EV-TRACK: transparent reporting and centralizing knowledge in extracellular vesicle research. Nat Methods. 2017 Mar;14(3):228–32.

58. Mathivanan S, Fahner CJ, Reid GE, Simpson RJ. ExoCarta 2012: database of exosomal proteins, RNA and lipids. Nucleic Acids Res. 2012 Jan 1;40(D1):D1241–4.

59. Alberro A, Iparraguirre L, Fernandes A, Otaegui D. Extracellular Vesicles in Blood: Sources, Effects, and Applications. Int J Mol Sci. 2021 Jan;22(15):8163.

60. Murphy DE, de Jong OG, Brouwer M, Wood MJ, Lavieu G, Schiffelers RM, et al. Extracellular vesicle-based therapeutics: natural versus engineered targeting and trafficking. Exp Mol Med. 2019 Mar;51(3):1–12.

61. Kang M, Jordan V, Blenkiron C, Chamley LW. Biodistribution of extracellular vesicles following administration into animals: A systematic review. J Extracell Vesicles. 2021;10(8):e12085.

62. Alvarez-Erviti L, Seow Y, Yin H, Betts C, Lakhal S, Wood MJA. Delivery of siRNA to the mouse brain by systemic injection of targeted exosomes. Nat Biotechnol. 2011 Apr;29(4):341–5.

63. Mustapic M, Eitan E, Werner JK, Berkowitz ST, Lazaropoulos MP, Tran J, et al. Plasma Extracellular Vesicles Enriched for Neuronal Origin: A Potential Window into Brain Pathologic Processes. Front Neurosci. 2017;11.

64. Morad G, Carman CV, Hagedorn EJ, Perlin JR, Zon LI, Mustafaoglu N, et al. Tumor-Derived Extracellular Vesicles Breach the Intact Blood–Brain Barrier via Transcytosis. ACS Nano. 2019 Dec 24;13(12):13853–65.

65. Nguyen SL, Ahn SH, Greenberg JW, Collaer BW, Agnew DW, Arora R, et al. Integrins mediate placental extracellular vesicle trafficking to lung and liver in vivo. Sci Rep. 2021 Feb 18;11(1):4217.

66. Milbank E, Dragano NRV, González-García I, Garcia MR, Rivas-Limeres V, Perdomo L, et al. Small extracellular vesicle-mediated targeting of hypothalamic AMPKα1 corrects obesity through BAT activation. Nat Metab. 2021 Oct;3(10):1415–31.

67. Zhang H, Freitas D, Kim HS, Fabijanic K, Li Z, Chen H, et al. Identification of distinct nanoparticles and subsets of extracellular vesicles by asymmetric flow field-flow fractionation. Nat Cell Biol. 2018 Mar;20(3):332–43.

68. Hoshino A, Costa-Silva B, Shen TL, Rodrigues G, Hashimoto A, Tesic Mark M, et al. Tumour exosome integrins determine organotropic metastasis. Nature. 2015 Nov;527(7578):329–35.

69. Laulagnier K, Javalet C, Hemming FJ, Chivet M, Lachenal G, Blot B, et al. Amyloid precursor protein products concentrate in a subset of exosomes specifically endocytosed by neurons. Cell Mol Life Sci. 2018 Feb 1;75(4):757–73.

70. Rana S, Yue S, Stadel D, Zöller M. Toward tailored exosomes: The exosomal tetraspanin web contributes to target cell selection. Int J Biochem Cell Biol. 2012 Sep 1;44(9):1574–84.

71. Matsumoto J, Stewart T, Sheng L, Li N, Bullock K, Song N, et al. Transmission of α-synuclein-containing erythrocyte-derived extracellular vesicles across the blood-brain barrier via adsorptive mediated transcytosis: another mechanism for initiation and progression of Parkinson's disease? Acta Neuropathol Commun. 2017 Sep 13;5(1):71.

72. Shimoda A, Tahara Y, Sawada S ichi, Sasaki Y, Akiyoshi K. Glycan profiling analysis using evanescent-field fluorescence-assisted lectin array: Importance of sugar recognition for cellular uptake of exosomes from mesenchymal stem cells. Biochem Biophys Res Commun. 2017 Sep 23;491(3):701–7.

73. Mulcahy LA, Pink RC, Carter DRF. Routes and mechanisms of extracellular vesicle uptake. J Extracell Vesicles. 2014 Jan 1;3(1):24641.

74. Tkach M, Kowal J, Zucchetti AE, Enserink L, Jouve M, Lankar D, et al. Qualitative differences in T-cell activation by dendritic cell-derived extracellular vesicle subtypes. EMBO J. 2017 Oct 16;36(20):3012–28.

75. Munich S, Sobo-Vujanovic A, Buchser WJ, Beer-Stolz D, Vujanovic NL. Dendritic cell exosomes directly kill tumor cells and activate natural killer cells via TNF superfamily ligands. OncoImmunology. 2012 Oct 1;1(7):1074–83.

76. Jahn R, Südhof TC. Membrane Fusion and Exocytosis. Annu Rev Biochem. 1999 Jun;68(1):863–911.

77. Grant BD, Donaldson JG. Pathways and mechanisms of endocytic recycling. Nat Rev Mol Cell Biol. 2009 Sep;10(9):597–608.

78. Lakhal S, Wood MJA. Exosome nanotechnology: An emerging paradigm shift in drug delivery. BioEssays. 2011;33(10):737–41.

79. Izquierdo-Useros N, Naranjo-Gómez M, Archer J, Hatch SC, Erkizia I, Blanco J, et al. Capture and transfer of HIV-1 particles by mature dendritic cells converges with the exosome-dissemination pathway. Blood. 2009 Mar 19;113(12):2732–41.

80. Heusermann W, Hean J, Trojer D, Steib E, von Bueren S, Graff-Meyer A, et al. Exosomes surf on filopodia to enter cells at endocytic hot spots, traffic within endosomes, and are targeted to the ER. J Cell Biol. 2016 Apr 25;213(2):173–84.

81. Santos MF, Rappa G, Karbanová J, Kurth T, Corbeil D, Lorico A. VAMP-associated protein-A and oxysterol-binding protein–related protein 3 promote the entry of late endosomes into the nucleoplasmic reticulum. J Biol Chem. 2018 Sep 1;293(36):13834–48.

82. Pužar Dominkuš P, Stenovec M, Sitar S, Lasič E, Zorec R, Plemenitaš A, et al. PKH26 labeling of extracellular vesicles: Characterization and cellular internalization of contaminating PKH26 nanoparticles. Biochim Biophys Acta BBA - Biomembr. 2018 Jun 1;1860(6):1350–61.

83. Biomarkers Definitions Working Group. Biomarkers and surrogate endpoints: Preferred definitions and conceptual framework. Clin Pharmacol Ther. 2001;69(3):89–95.

84. Ciferri MC, Quarto R, Tasso R. Extracellular Vesicles as Biomarkers and Therapeutic Tools: From Pre-Clinical to Clinical Applications. Biology. 2021 May;10(5):359.

85. Lane RE, Korbie D, Hill MM, Trau M. Extracellular vesicles as circulating cancer biomarkers: opportunities and challenges. Clin Transl Med. 2018 Dec;7(1):14.

86. Melo SA, Luecke LB, Kahlert C, Fernandez AF, Gammon ST, Kaye J, et al. Glypican-1 identifies cancer exosomes and detects early pancreatic cancer. Nature. 2015 Jul;523(7559):177–82.

87. Tutrone R, Donovan MJ, Torkler P, Tadigotla V, McLain T, Noerholm M, et al. Clinical utility of the exosome based ExoDx Prostate(IntelliScore) EPI test in men presenting for initial Biopsy with a PSA 2–10 ng/mL. Prostate Cancer Prostatic Dis. 2020 Dec;23(4):607–14.

88. Zhou H, Pisitkun T, Aponte A, Yuen PST, Hoffert JD, Yasuda H, et al. Exosomal Fetuin-A identified by proteomics: A novel urinary biomarker for detecting acute kidney injury. Kidney Int. 2006 Nov 2;70(10):1847–57.

89. Alvarez S, Suazo C, Boltansky A, Ursu M, Carvajal D, Innocenti G, et al. Urinary Exosomes as a Source of Kidney Dysfunction Biomarker in Renal Transplantation. Transplant Proc. 2013 Dec 1;45(10):3719–23.

90. Liang Y, Lehrich BM, Zheng S, Lu M. Emerging methods in biomarker identification for extracellular vesicle-based liquid biopsy. J Extracell Vesicles. 2021;10(7):e12090.

91. Liu S, Wu X, Chandra S, Lyon C, Ning B, jiang L, et al. Extracellular vesicles: Emerging tools as therapeutic agent carriers. Acta Pharm Sin B. 2022 Oct 1;12(10):3822–42.

92. Oskouie MN, Aghili Moghaddam NS, Butler AE, Zamani P, Sahebkar A. Therapeutic use of curcumin-encapsulated and curcumin-primed exosomes. J Cell Physiol. 2019;234(6):8182–91.

93. Song H, Liu B, Dong B, Xu J, Zhou H, Na S, et al. Exosome-Based Delivery of Natural Products in Cancer Therapy. Front Cell Dev Biol. 2021;9.

94. Naseri M, Bozorgmehr M, Zöller M, Ranaei Pirmardan E, Madjd Z. Tumor-derived exosomes: the next generation of promising cell-free vaccines in cancer immunotherapy. OncoImmunology. 2020 Jan 1;9(1):1779991.

95. Nikfarjam S, Rezaie J, Kashanchi F, Jafari R. Dexosomes as a cell-free vaccine for cancer immunotherapy. J Exp Clin Cancer Res. 2020 Nov 23;39(1):258.

96. Fan J, Lee CS, Kim S, Chen C, Aghaloo T, Lee M. Generation of Small RNA-Modulated Exosome Mimetics for Bone Regeneration. ACS Nano. 2020 Sep 22;14(9):11973–84.

97. Hade MD, Suire CN, Suo Z. Mesenchymal Stem Cell-Derived Exosomes: Applications in Regenerative Medicine. Cells. 2021 Aug;10(8):1959.

98. Metabolic syndrome [Internet]. nhs.uk. 2017 [cited 2022 Nov 1]. Available from: https://www.nhs.uk/conditions/metabolic-syndrome/

99. Després J. Is visceral obesity the cause of the metabolic syndrome? Ann Med. 2006 Jan 1;38(1):52–63.

100. Després JP, Lemieux I. Abdominal obesity and metabolic syndrome. Nature. 2006 Dec;444(7121):881–7.

101. Kawai T, Autieri MV, Scalia R. Adipose tissue inflammation and metabolic dysfunction in obesity. Am J Physiol-Cell Physiol. 2021 Mar;320(3):C375–91.

102. Orliaguet L, Ejlalmanesh T, Alzaid F. Metabolic and Molecular Mechanisms of Macrophage Polarisation and Adipose Tissue Insulin Resistance. Int J Mol Sci. 2020 Jan;21(16):5731.

103. Deng Z b., Poliakov A, Hardy RW, Clements R, Liu C, Liu Y, et al. Adipose Tissue Exosome-Like Vesicles Mediate Activation of Macrophage-Induced Insulin Resistance. Diabetes. 2009 Nov 1;58(11):2498–505.

104. Zhang Y, Mei H, Chang X, Chen F, Zhu Y, Han X. Adipocyte-derived microvesicles from obese mice induce M1 macrophage phenotype through secreted miR-155. J Mol Cell Biol. 2016 Dec 1;8(6):505–17.

105. Camino T, Lago-Baameiro N, Bravo SB, Sueiro A, Couto I, Santos F, et al. Vesicles Shed by Pathological Murine Adipocytes Spread Pathology: Characterization and Functional Role of Insulin Resistant/Hypertrophied Adiposomes. Int J Mol Sci. 2020 Jan;21(6):2252.

106. Flaherty SE, Grijalva A, Xu X, Ables E, Nomani A, Ferrante A. A lipase-independent pathway of lipid release and immune modulation by adipocytes. Science. 2019 Mar 1;363(6430):989–93.

107. Brestoff JR, Wilen CB, Moley JR, Li Y, Zou W, Malvin NP, et al. Intercellular Mitochondria Transfer to Macrophages Regulates White Adipose Tissue Homeostasis and Is Impaired in Obesity. Cell Metab. 2021 Feb 2;33(2):270-282.e8.

108. Crewe C, Funcke JB, Li S, Joffin N, Gliniak CM, Ghaben AL, et al. Extracellular vesicle-based interorgan transport of mitochondria from energetically stressed adipocytes. Cell Metab. 2021 Sep 7;33(9):1853-1868.e11.

109. Sano S, Izumi Y, Yamaguchi T, Yamazaki T, Tanaka M, Shiota M, et al. Lipid synthesis is promoted by hypoxic adipocyte-derived exosomes in 3T3-L1 cells. Biochem Biophys Res Commun. 2014 Mar;445(2):327–33.

110. Narayanan K, Kumar S, Padmanabhan P, Gulyas B, Wan ACA, Rajendran VM. Lineage-specific exosomes could override extracellular matrix mediated human mesenchymal stem cell differentiation. Biomaterials. 2018 Nov 1;182:312–22.

111. Jung YJ, Kim HK, Cho Y, Choi JS, Woo CH, Lee KS, et al. Cell reprogramming using extracellular vesicles from differentiating stem cells into white/beige adipocytes. Sci Adv. 2020

Mar 25;6(13):eaay6721.

112. Mleczko J, Ortega FJ, Falcon-Perez JM, Wabitsch M, Fernandez-Real JM, Mora S. Extracellular Vesicles from Hypoxic Adipocytes and Obese Subjects Reduce Insulin-Stimulated Glucose Uptake. Mol Nutr Food Res. 2018;62(5):1700917.

113. Müller G, Schneider M, Biemer-Daub G, Wied S. Microvesicles released from rat adipocytes and harboring glycosylphosphatidylinositol-anchored proteins transfer RNA stimulating lipid synthesis. Cell Signal. 2011 Jul;23(7):1207–23.

114. Wang F, Chen F fang, Shang Y yuan, Li Y, Wang Z hao, Han L, et al. Insulin resistance adipocyte-derived exosomes aggravate atherosclerosis by increasing vasa vasorum angiogenesis in diabetic ApoE−/− mice. Int J Cardiol. 2018 Aug 15;265:181–7.

115. Kranendonk MEG, Visseren FLJ, van Herwaarden JA, Nolte-'t Hoen ENM, de Jager W, Wauben MHM, et al. Effect of extracellular vesicles of human adipose tissue on insulin signaling in liver and muscle cells: Adipose Tissue Vesicles and Insulin Signaling. Obesity. 2014 Oct;22(10):2216–23.

116. Yu Y, Du H, Wei S, Feng L, Li J, Yao F, et al. Adipocyte-Derived Exosomal MiR-27a Induces Insulin Resistance in Skeletal Muscle Through Repression of PPARγ. Theranostics. 2018 Mar 8;8(8):2171–88.

117. Koeck ES, Iordanskaia T, Sevilla S, Ferrante SC, Hubal MJ, Freishtat RJ, et al. Adipocyte exosomes induce transforming growth factor beta pathway dysregulation in hepatocytes: a novel paradigm for obesity-related liver disease. J Surg Res. 2014 Dec 1;192(2):268–75.

118. Gan L, Xie D, Liu J, Bond Lau W, Christopher TA, Lopez B, et al. Small Extracellular Microvesicles Mediated Pathological Communications Between Dysfunctional Adipocytes and Cardiomyocytes as a Novel Mechanism Exacerbating Ischemia/Reperfusion Injury in Diabetic Mice. Circulation. 2020 Mar 24;141(12):968–83.

119. Gao J, Li X, Wang Y, Cao Y, Yao D, Sun L, et al. Adipocyte-derived extracellular vesicles modulate appetite and weight through mTOR signalling in the hypothalamus. Acta Physiol. 2020;228(2):e13339.

120. Le Lay S, Rome S, Loyer X, Nieto L. Adipocyte-derived extracellular vesicles in health and diseases: Nano-packages with vast biological properties. FASEB BioAdvances. 2021;3(6):407–19.

121. Goossens GH. The Metabolic Phenotype in Obesity: Fat Mass, Body Fat Distribution, and Adipose Tissue Function. Obes Facts. 2017;10(3):207–15.

122. Longo M, Zatterale F, Naderi J, Parrillo L, Formisano P, Raciti GA, et al. Adipose Tissue Dysfunction as Determinant of Obesity-Associated Metabolic Complications. Int J Mol Sci. 2019 Jan;20(9):2358.

123. Eguchi A, Lazic M, Armando AM, Phillips SA, Katebian R, Maraka S, et al. Circulating adipocyte-derived extracellular vesicles are novel markers of metabolic stress. J Mol Med. 2016 Nov 1;94(11):1241–53.

124. Hubal MJ, Nadler EP, Ferrante SC, Barberio MD, Suh JH, Wang J, et al. Circulating adipocyte-derived exosomal MicroRNAs associated with decreased insulin resistance after gastric bypass. Obesity. 2017;25(1):102–10.

125. Washington University School of Medicine. Complex Effects of Dietary Manipulation on Metabolic Function, Inflammation and Health [Internet]. clinicaltrials.gov; 2021 Nov [cited 2022 Oct 25]. Report No.: NCT02706262. Available from: https://clinicaltrials.gov/ct2/show/NCT02706262

126. Washington University School of Medicine. Precision Nutrition and Metabolic Function [Internet]. clinicaltrials.gov; 2021 Nov [cited 2022 Oct 25]. Report No.: NCT04131166. Available from: https://clinicaltrials.gov/ct2/show/NCT04131166

127. Akbar N, Azzimato V, Choudhury RP, Aouadi M. Extracellular vesicles in metabolic disease. Diabetologia. 2019 Dec 1;62(12):2179–87.

128. Zhang HG, Grizzle WE. Exosomes: a novel pathway of local and distant intercellular communication that facilitates the growth and metastasis of neoplastic lesions. Am J Pathol. 2014 Jan;184(1):28–41.

129. Peinado H, Alečković M, Lavotshkin S, Matei I, Costa-Silva B, Moreno-Bueno G, et al. Melanoma exosomes educate bone marrow progenitor cells toward a pro-metastatic phenotype through MET. Nat Med. 2012 Jun;18(6):883–91.

130. Rahman MJ, Regn D, Bashratyan R, Dai YD. Exosomes Released by Islet-Derived Mesenchymal Stem Cells Trigger Autoimmune Responses in NOD Mice. Diabetes. 2014 Mar 1;63(3):1008–20.

131. Coleman BM, Hill AF. Extracellular vesicles – Their role in the packaging and spread of misfolded proteins associated with neurodegenerative diseases. Semin Cell Dev Biol. 2015 Apr;40:89–96.

132. Jansen F, Li Q, Pfeifer A, Werner N. Endothelial- and Immune Cell-Derived Extracellular Vesicles in the Regulation of Cardiovascular Health and Disease. JACC Basic Transl Sci. 2017 Dec;2(6):790–807.

133. Kranendonk MEG, Visseren FLJ, van Balkom BWM, Nolte-'t Hoen ENM, van Herwaarden JA, de Jager W, et al. Human adipocyte extracellular vesicles in reciprocal signaling between adipocytes and macrophages: Human Adipocyte EVs and Macrophages. Obesity. 2014 May;22(5):1296–308.

134. Müller G, Schneider M, Biemer-Daub G, Wied S. Upregulation of Lipid Synthesis in Small Rat Adipocytes by Microvesicle-Associated CD73 From Large Adipocytes. Obesity. 2011 Aug;19(8):1531–44.

135. Cheng HL, Fu CY, Kuo WC, Chen YW, Chen YS, Lee YM, et al. Detecting miRNA biomarkers from extracellular vesicles for cardiovascular disease with a microfluidic system. Lab Chip. 2018 Sep 26;18(19):2917–25.

136. Yang J, Li C, Zhang L, Wang X. Extracellular Vesicles as Carriers of Non-coding RNAs in Liver Diseases. Front Pharmacol. 2018 Apr 24;9:415.

137. Thompson AG, Gray E, Heman-Ackah SM, Mäger I, Talbot K, Andaloussi SE, et al. Extracellular vesicles in neurodegenerative disease — pathogenesis to biomarkers. Nat Rev Neurol. 2016 Jun;12(6):346–57.

138. Ghai V, Wu X, Bheda-Malge A, Argyropoulos CP, Bernardo JF, Orchard T, et al. Genome-wide Profiling of Urinary Extracellular Vesicle microRNAs Associated With Diabetic Nephropathy in Type 1 Diabetes. Kidney Int Rep. 2018 May;3(3):555–72.

139. Yamamoto CM, Murakami T, Oakes ML, Mitsuhashi M, Kelly C, Henry RR, et al. Uromodulin mRNA from Urinary Extracellular Vesicles Correlate to Kidney Function Decline in Type 2 Diabetes Mellitus. Am J Nephrol. 2018;47(5):283–91.

140. Wabitsch M, Brenner RE, Melzner I, Braun M, Möller P, Heinze E, et al. Characterization of a human preadipocyte cell strain with high capacity for adipose differentiation. Int J Obes Relat Metab Disord J Int Assoc Study Obes. 2001 Jan;25(1):8–15.

141. DeBaun MR, Ess J, Saunders S. Simpson Golabi Behmel syndrome: progress toward understanding the molecular basis for overgrowth, malformation, and cancer predisposition. Mol Genet Metab. 2001 Apr;72(4):279–86.

142. Fischer-Posovszky P, Newell FS, Wabitsch M, Tornqvist HE. Human SGBS cells - a unique tool for studies of human fat cell biology. Obes Facts. 2008;1(4):184–9.

143. Aden DP, Fogel A, Plotkin S, Damjanov I, Knowles BB. Controlled synthesis of HBsAg in a differentiated human liver carcinoma-derived cell line. Nature. 1979 Dec 6;282(5739):615–6.

144. Knowles BB, Howe CC, Aden DP. Human hepatocellular carcinoma cell lines secrete

the major plasma proteins and hepatitis B surface antigen. Science. 1980 Jul 25;209(4455):497–9.

145. Gevaert E, Dollé L, Billiet T, Dubruel P, van Grunsven L, van Apeldoorn A, et al. High Throughput Micro-Well Generation of Hepatocyte Micro-Aggregates for Tissue Engineering. Matsusaki M, editor. PLoS ONE. 2014 Aug 18;9(8):e105171.

146. Fogh J, Wright WC, Loveless JD. Absence of HeLa cell contamination in 169 cell lines derived from human tumors. J Natl Cancer Inst. 1977 Feb;58(2):209–14.

147. Fogh J, Fogh JM, Orfeo T. One Hundred and Twenty-Seven Cultured Human Tumor Cell Lines Producing Tumors in Nude Mice23. JNCI J Natl Cancer Inst. 1977 Jul;59(1):221–6.

148. Meunier V, Bourrié M, Berger Y, Fabre G. The human intestinal epithelial cell line Caco-2; pharmacological and pharmacokinetic applications. Cell Biol Toxicol. 1995 Aug;11(3–4):187–94.

149. Lieber M, Mazzetta J, Nelson-Rees W, Kaplan M, Todaro G. Establishment of a continuous tumor-cell line (PANC-1) from a human carcinoma of the exocrine pancreas. Int J Cancer. 1975 May 15;15(5):741–7.

150. Corbett TH, Roberts BJ, Leopold WR, Peckham JC, Wilkoff LJ, Griswold DP, et al. Induction and chemotherapeutic response of two transplantable ductal adenocarcinomas of the pancreas in C57BL/6 mice. Cancer Res. 1984 Feb;44(2):717–26.

151. Soule HD, Vazquez J, Long A, Albert S, Brennan M. A Human Cell Line From a Pleural Effusion Derived From a Breast Carcinoma 2. JNCI J Natl Cancer Inst. 1973 Nov;51(5):1409–16.

152. Lee AV, Oesterreich S, Davidson NE. MCF-7 Cells--Changing the Course of Breast Cancer Research and Care for 45 Years. JNCI J Natl Cancer Inst. 2015 Mar 31;107(7):djv073.

153. Goodwin AM. In vitro assays of angiogenesis for assessment of angiogenic and anti-angiogenic agents. Microvasc Res. 2007 Sep;74(2–3):172–83.

154. Weischenfeldt J, Porse B. Bone Marrow-Derived Macrophages (BMM): Isolation and Applications. Cold Spring Harb Protoc. 2008 Dec 1;2008(12):5080.

155. Davis BK. Evaluation of Classical, Alternative, and Regulatory Functions of Bone Marrow-Derived Macrophages. In: Allen IC, editor. Mouse Models of Allergic Disease. Totowa, NJ: Humana Press; 2013. p. 79–89.

156. Hanson MS, Stephenson AH, Bowles EA, Sridharan M, Adderley S, Sprague RS. Phosphodiesterase 3 is present in rabbit and human erythrocytes and its inhibition potentiates iloprost-induced increases in cAMP. Am J Physiol-Heart Circ Physiol. 2008 Aug;295(2):H786–

93.

157. Miltenyi Biotech GmbH. Isolation of mononuclear cells from human peripheral blood by density gradient centrifugation [Internet]. 2008 [cited 2017 Feb 28]. Available from: https://www.miltenyibiotec.com/~/media/Files/Navigation/Research/Stem%20Cell/SP_MC_PB_density_gradient.ashx

158. de Gassart A. Lipid raft-associated protein sorting in exosomes. Blood. 2003 Dec 15;102(13):4336–44.

159. Lötvall J, Hill AF, Hochberg F, Buzás EI, Di Vizio D, Gardiner C, et al. Minimal experimental requirements for definition of extracellular vesicles and their functions: a position statement from the International Society for Extracellular Vesicles. J Extracell Vesicles. 2014 Jan;3(1):26913.

160. QIAGEN GmbH. RNeasy® Lipid Tissue Handbook [Internet]. 2009 [cited 2018 Feb 13]. Available from: https://www.qiagen.com/us/resources/resourcedetail?id=bcff828a-b4f0-4de0-9cc5-36331a5dc95f&lang=en

161. Pfaffl MW. A new mathematical model for relative quantification in real-time RT-PCR. Nucleic Acids Res. 2001 May 1;29(9):e45.

162. EL Andaloussi S, Mäger I, Breakefield XO, Wood MJA. Extracellular vesicles: biology and emerging therapeutic opportunities. Nat Rev Drug Discov. 2013 May;12(5):347–57.

163. Wiśniewski JR, Zougman A, Nagaraj N, Mann M. Universal sample preparation method for proteome analysis. Nat Methods. 2009 May;6(5):359–62.

164. Grosche A, Hauser A, Lepper MF, Mayo R, von Toerne C, Merl-Pham J, et al. The Proteome of Native Adult Müller Glial Cells From Murine Retina. Mol Cell Proteomics. 2016 Feb;15(2):462–80.

165. Hauck SM, Dietter J, Kramer RL, Hofmaier F, Zipplies JK, Amann B, et al. Deciphering Membrane-Associated Molecular Processes in Target Tissue of Autoimmune Uveitis by Label-Free Quantitative Mass Spectrometry. Mol Cell Proteomics. 2010 Oct;9(10):2292–305.

166. Merl J, Ueffing M, Hauck SM, von Toerne C. Direct comparison of MS-based label-free and SILAC quantitative proteome profiling strategies in primary retinal Müller cells. PROTEOMICS. 2012 Jun;12(12):1902–11.

167. Andersen CL, Jensen JL, Ørntoft TF. Normalization of Real-Time Quantitative Reverse Transcription-PCR Data: A Model-Based Variance Estimation Approach to Identify Genes Suited for Normalization, Applied to Bladder and Colon Cancer Data Sets. Cancer Res. 2004 Aug 1;64(15):5245–50.

168. Barapatre N, Symvoulidis P, Möller W, Prade F, Deliolanis NC, Hertel S, et al. Quantitative detection of drug dose and spatial distribution in the lung revealed by Cryoslicing Imaging. J Pharm Biomed Anal. 2015 Jan;102:129–36.

169. Luberto C, Hassler DF, Signorelli P, Okamoto Y, Sawai H, Boros E, et al. Inhibition of Tumor Necrosis Factor-induced Cell Death in MCF7 by a Novel Inhibitor of Neutral Sphingomyelinase. J Biol Chem. 2002 Oct 25;277(43):41128–39.

170. Shamseddine AA, Airola MV, Hannun YA. Roles and regulation of neutral sphingomyelinase-2 in cellular and pathological processes. Adv Biol Regul. 2015 Jan;57:24–41.

171. Hannun YA, Obeid LM. Many Ceramides. J Biol Chem. 2011 Aug 12;286(32):27855–62.

172. Kosaka N, Iguchi H, Yoshioka Y, Takeshita F, Matsuki Y, Ochiya T. Secretory Mechanisms and Intercellular Transfer of MicroRNAs in Living Cells. J Biol Chem. 2010 Jun 4;285(23):17442–52.

173. Tabatadze N, Savonenko A, Song H, Bandaru VVR, Chu M, Haughey NJ. Inhibition of neutral sphingomyelinase-2 perturbs brain sphingolipid balance and spatial memory in mice. J Neurosci Res. 2010 Jul 13;88(13):2940–51.

174. Dinkins MB, Dasgupta S, Wang G, Zhu G, Bieberich E. Exosome reduction in vivo is associated with lower amyloid plaque load in the 5XFAD mouse model of Alzheimer's disease. Neurobiol Aging. 2014 Aug;35(8):1792–800.

175. Essandoh K, Yang L, Wang X, Huang W, Qin D, Hao J, et al. Blockade of exosome generation with GW4869 dampens the sepsis-induced inflammation and cardiac dysfunction. Biochim Biophys Acta BBA - Mol Basis Dis. 2015 Nov;1852(11):2362–71.

176. Burns C, Morris T, Jones B, Koch W, Borer M, Riber U, et al. Proposal to initiate a project to evaluate a candidate International Standard for Human Recombinant Insulin - WHO/BS/10.2143 - Working document QAS/10.381 [Internet]. 2010 [cited 2018 Feb 6]. Available from: http://www.who.int/biologicals/expert_committee/BS_2143_Human_Recombinant_Insulin_final.pdf

177. Köhler G, Milstein C. Continuous cultures of fused cells secreting antibody of predefined specificity. Nature. 1975 Aug;256(5517):495–7.

178. Schlepckow K, Monroe KM, Kleinberger G, Cantuti-Castelvetri L, Parhizkar S, Xia D, et al. Enhancing protective microglial activities with a dual function TREM2 antibody to the stalk region. EMBO Mol Med. 2020 Apr 7;12(4):e11227.

179. Dean CB, Nielsen JD. Generalized linear mixed models: a review and some extensions. Lifetime Data Anal. 2007 Dec;13(4):497–512.

180. Rainer J, Sanchez-Cabo F, Stocker G, Sturn A, Trajanoski Z. CARMAweb: comprehensive R- and bioconductor-based web service for microarray data analysis. Nucleic Acids Res. 2006 Jul 1;34(Web Server):W498–503.

181. Greening DW, Xu R, Ji H, Tauro BJ, Simpson RJ. A Protocol for Exosome Isolation and Characterization: Evaluation of Ultracentrifugation, Density-Gradient Separation, and Immunoaffinity Capture Methods. In: Posch A, editor. Proteomic Profiling. New York, NY: Springer New York; 2015. p. 179–209. (Methods in Molecular Biology; vol. 1295).

182. Lobb RJ, Becker M, Wen Wen S, Wong CSF, Wiegmans AP, Leimgruber A, et al. Optimized exosome isolation protocol for cell culture supernatant and human plasma. J Extracell Vesicles. 2015 Jan 1;4(1):27031.

183. Connolly KD, Guschina IA, Yeung V, Clayton A, Draman MS, Von Ruhland C, et al. Characterisation of adipocyte-derived extracellular vesicles released pre- and post-adipogenesis. J Extracell Vesicles. 2015 Jan 1;4(1):29159.

184. Bourin P, Bunnell BA, Casteilla L, Dominici M, Katz AJ, March KL, et al. Stromal cells from the adipose tissue-derived stromal vascular fraction and culture expanded adipose tissue-derived stromal/stem cells: a joint statement of the International Federation for Adipose Therapeutics and Science (IFATS) and the International Society for Cellular Therapy (ISCT). Cytotherapy. 2013 Jun;15(6):641–8.

185. Senesi L, De Francesco F, Farinelli L, Manzotti S, Gagliardi G, Papalia GF, et al. Mechanical and Enzymatic Procedures to Isolate the Stromal Vascular Fraction From Adipose Tissue: Preliminary Results. Front Cell Dev Biol. 2019 Jun 7;7:88.

186. Boutens L, Stienstra R. Adipose tissue macrophages: going off track during obesity. Diabetologia. 2016 May;59(5):879–94.

187. Ratajczak J, Wysoczynski M, Hayek F, Janowska-Wieczorek A, Ratajczak MZ. Membrane-derived microvesicles: important and underappreciated mediators of cell-to-cell communication. Leukemia. 2006 Sep;20(9):1487–95.

188. Zhang J, Li S, Li L, Li M, Guo C, Yao J, et al. Exosome and Exosomal MicroRNA: Trafficking, Sorting, and Function. Genomics Proteomics Bioinformatics. 2015 Feb;13(1):17–24.

189. Vlachos IS, Zagganas K, Paraskevopoulou MD, Georgakilas G, Karagkouni D, Vergoulis T, et al. DIANA-miRPath v3.0: deciphering microRNA function with experimental support. Nucleic Acids Res. 2015 Jul 1;43(W1):W460–6.

190. Chen L, Hou J, Ye L, Chen Y, Cui J, Tian W, et al. MicroRNA-143 Regulates Adipogenesis by Modulating the MAP2K5–ERK5 Signaling. Sci Rep. 2015 May;4(1):3819.

191. Mi L, Chen Y, Zheng X, Li Y, Zhang Q, Mo D, et al. MicroRNA-139-5p Suppresses 3T3-L1 Preadipocyte Differentiation Through Notch and IRS1/PI3K/Akt Insulin Signaling Pathways. J Cell Biochem. 2015 Jul;116(7):1195–204.

192. Ouyang D, Xu L, Zhang L, Guo D, Tan X, Yu X, et al. MiR-181a-5p regulates 3T3-L1 cell adipogenesis by targeting Smad7 and Tcf7l2. Acta Biochim Biophys Sin. 2016 Nov;48(11):1034–41.

193. Wang L, Xu L, Xu M, Liu G, Xing J, Sun C, et al. Obesity-Associated MiR-342-3p Promotes Adipogenesis of Mesenchymal Stem Cells by Suppressing CtBP2 and Releasing C/EBPα from CtBP2 Binding. Cell Physiol Biochem. 2015;35(6):2285–98.

194. Chen FF, Xiong Y, Peng Y, Gao Y, Qin J, Chu GY, et al. miR-425-5p Inhibits Differentiation and Proliferation in Porcine Intramuscular Preadipocytes. Int J Mol Sci. 2017 Oct 6;18(10):2101.

195. Ahn J, Lee H, Jung CH, Jeon TI, Ha TY. MicroRNA-146b promotes adipogenesis by suppressing the SIRT1-FOXO1 cascade: microRNA146-b/SIRT1 regulates adipogenesis. EMBO Mol Med. 2013 Oct;5(10):1602–12.

196. Zhang XM, Wang LH, Su DJ, Zhu D, Li QM, Chi MH. MicroRNA-29b promotes the adipogenic differentiation of human adipose tissue-derived stromal cells: MiR-29b Regulates Adipogenesis by TNF-A via SP1. Obesity. 2016 May;24(5):1097–105.

197. Zhang Y, Yu M, Dai M, Chen C, Tang Q, Jing W, et al. miR-450a-5p within rat adipose tissue exosome-like vesicles promotes adipogenic differentiation by targeting WISP2. J Cell Sci. 2017 Feb 6;130:1158–68.

198. Du J, Cheng X, Shen L, Tan Z, Luo J, Wu X, et al. Methylation of miR-145a-5p promoter mediates adipocytes differentiation. Biochem Biophys Res Commun. 2016 Jun;475(1):140–8.

199. Dong P, Mai Y, Zhang Z, Mi L, Wu G, Chu G, et al. MiR-15a/b promote adipogenesis in porcine pre-adipocyte via repressing FoxO1. Acta Biochim Biophys Sin. 2014 Jul;46(7):565–71.

200. Fan F, Liu Y, Zhang Y, Zhang J, Li Q. miR-141 promotes differentiation of adipocyte and contributes to the obesity by targeting to FOXA2. Int J Clin Exp Med. 2007 Sep 30;10(9):13254–62.

201. Song G, Xu G, Ji C, Shi C, Shen Y, Chen L, et al. The role of microRNA-26b in human

adipocyte differentiation and proliferation. Gene. 2014 Jan;533(2):481–7.

202. Belarbi Y, Mejhert N, Lorente-Cebrián S, Dahlman I, Arner P, Rydén M, et al. MicroRNA-193b Controls Adiponectin Production in Human White Adipose Tissue. J Clin Endocrinol Metab. 2015 Aug;100(8):E1084–8.

203. Chou CF, Lin YY, Wang HK, Zhu X, Giovarelli M, Briata P, et al. KSRP Ablation Enhances Brown Fat Gene Program in White Adipose Tissue Through Reduced miR-150 Expression. Diabetes. 2014 Sep 1;63(9):2949–61.

204. Arias N, Aguirre L, Fernández-Quintela A, González M, Lasa A, Miranda J, et al. MicroRNAs involved in the browning process of adipocytes. J Physiol Biochem. 2016 Sep;72(3):509–21.

205. Zheng Z, Liu X, Zhao Q, Zhang L, Li C, Xue Y. Regulation of UCP1 in the Browning of Epididymal Adipose Tissue by β3-Adrenergic Agonist: A Role for MicroRNAs. Int J Endocrinol. 2014;2014:1–6.

206. Ortega FJ, Moreno M, Mercader JM, Moreno-Navarrete JM, Fuentes-Batllevell N, Sabater M, et al. Inflammation triggers specific microRNA profiles in human adipocytes and macrophages and in their supernatants. Clin Epigenetics. 2015 Dec;7(1):49.

207. Sonda N, Simonato F, Peranzoni E, Calì B, Bortoluzzi S, Bisognin A, et al. miR-142-3p Prevents Macrophage Differentiation during Cancer-Induced Myelopoiesis. Immunity. 2013 Jun;38(6):1236–49.

208. Zhang Q, Xiao X, Li M, Li W, Yu M, Zhang H, et al. Acarbose Reduces Blood Glucose by Activating miR-10a-5p and miR-664 in Diabetic Rats. Ahmad R, editor. PLoS ONE. 2013 Nov 18;8(11):e79697.

209. Wei Y, Nazari-Jahantigh M, Chan L, Zhu M, Heyll K, Corbalan-Campos J, et al. The microRNA-342-5p Fosters Inflammatory Macrophage Activation Through an Akt1- and microRNA-155-Dependent Pathway During Atherosclerosis. Circulation. 2013 Apr 16;127(15):1609–19.

210. Li W, Chang N, Tian L, Yang J, Ji X, Xie J, et al. miR-27b-3p, miR-181a-1-3p, and miR-326-5p are involved in the inhibition of macrophage activation in chronic liver injury. J Mol Med. 2017 Oct;95(10):1091–105.

211. Zhu S, Pan W, Song X, Liu Y, Shao X, Tang Y, et al. The microRNA miR-23b suppresses IL-17-associated autoimmune inflammation by targeting TAB2, TAB3 and IKK-α. Nat Med. 2012 Jul;18(7):1077–86.

212. Jaiswal A, Reddy SS, Maurya M, Maurya P, Barthwal MK. MicroRNA-99a mimics

inhibit M1 macrophage phenotype and adipose tissue inflammation by targeting TNFα. Cell Mol Immunol. 2019 May;16(5):495–507.

213. Xu Z, Xiao SB, Xu P, Xie Q, Cao L, Wang D, et al. miR-365, a Novel Negative Regulator of Interleukin-6 Gene Expression, Is Cooperatively Regulated by Sp1 and NF-κB. J Biol Chem. 2011 Jun 17;286(24):21401–12.

214. Lang H, Ai Z, You Z, Wan Y, Guo W, Xiao J, et al. Characterization of miR-218/322-Stxbp1 pathway in the process of insulin secretion. J Mol Endocrinol. 2015 Jan 21;54(1):65–73.

215. Esguerra JLS, Bolmeson C, Cilio CM, Eliasson L. Differential Glucose-Regulation of MicroRNAs in Pancreatic Islets of Non-Obese Type 2 Diabetes Model Goto-Kakizaki Rat. Maedler K, editor. PLoS ONE. 2011 Apr 7;6(4):e18613.

216. Agarwal P, Srivastava R, Srivastava AK, Ali S, Datta M. miR-135a targets IRS2 and regulates insulin signaling and glucose uptake in the diabetic gastrocnemius skeletal muscle. Biochim Biophys Acta BBA - Mol Basis Dis. 2013 Aug;1832(8):1294–303.

217. Bagge A, Dahmcke C, Dalgaard L. Syntaxin-1a is a Direct Target of miR-29a in Insulin-producing β-Cells. Horm Metab Res. 2013 Jan 11;45(06):463–6.

218. Melkman-Zehavi T, Oren R, Kredo-Russo S, Shapira T, Mandelbaum AD, Rivkin N, et al. miRNAs control insulin content in pancreatic β-cells via downregulation of transcriptional repressors: miRNA control insulin content in pancreatic β-cells. EMBO J. 2011 Mar 2;30(5):835–45.

219. Panda AC, Sahu I, Kulkarni SD, Martindale JL, Abdelmohsen K, Vindu A, et al. miR-196b-Mediated Translation Regulation of Mouse Insulin2 via the 5′UTR. Kim YK, editor. PLoS ONE. 2014 Jul 8;9(7):e101084.

220. Blüher M. Adipose tissue dysfunction contributes to obesity related metabolic diseases. Best Pract Res Clin Endocrinol Metab. 2013 Apr;27(2):163–77.

221. Trayhurn P. Hypoxia and Adipocyte Physiology: Implications for Adipose Tissue Dysfunction in Obesity. Annu Rev Nutr. 2014 Jul 17;34(1):207–36.

222. Crewe C, An YA, Scherer PE. The ominous triad of adipose tissue dysfunction: inflammation, fibrosis, and impaired angiogenesis. J Clin Invest. 2017 Jan 3;127(1):74–82.

223. Park JE, Tan HS, Datta A, Lai RC, Zhang H, Meng W, et al. Hypoxic Tumor Cell Modulates Its Microenvironment to Enhance Angiogenic and Metastatic Potential by Secretion of Proteins and Exosomes. Mol Cell Proteomics. 2010 Jun;9(6):1085–99.

224. King HW, Michael MZ, Gleadle JM. Hypoxic enhancement of exosome release by

breast cancer cells. BMC Cancer. 2012 Dec;12(1):421.

225. Shao C, Yang F, Miao S, Liu W, Wang C, Shu Y, et al. Role of hypoxia-induced exosomes in tumor biology. Mol Cancer. 2018 Aug 11;17(1):120.

226. Cannon B, Nedergaard J. Brown Adipose Tissue: Function and Physiological Significance. Physiol Rev. 2004 Jan;84(1):277–359.

227. Kroon T, Harms M, Maurer S, Bonnet L, Alexandersson I, Lindblom A, et al. PPARγ and PPARα synergize to induce robust browning of white fat in vivo. Mol Metab. 2020 Jun 1;36:100964.

228. Cinti S, Mitchell G, Barbatelli G, Murano I, Ceresi E, Faloia E, et al. Adipocyte death defines macrophage localization and function in adipose tissue of obese mice and humans. J Lipid Res. 2005 Nov;46(11):2347–55.

229. Lumeng CN, Bodzin JL, Saltiel AR. Obesity induces a phenotypic switch in adipose tissue macrophage polarization. J Clin Invest. 2007 Jan 2;117(1):175–84.

230. Padlan EA. Anatomy of the antibody molecule. Mol Immunol. 1994 Feb;31(3):169–217.

231. Al-Lazikani B, Lesk AM, Chothia C. Standard conformations for the canonical structures of immunoglobulins 1 1Edited by I. A. Wilson. J Mol Biol. 1997 Nov;273(4):927–48.

232. Stemmer K, Tschöp M, Bauer M, Zeidler R, Feederle R. Tissue-specific exosomes as biomarkers [Internet]. WO2017194499A1, 2017 [cited 2022 Oct 23]. Available from: https://patents.google.com/patent/WO2017194499A1/en?oq=WO2017%2f194499

233. Gómez-Serrano M, Ponath V, Preußer C, Pogge von Strandmann E. Beyond the Extracellular Vesicles: Technical Hurdles, Achieved Goals and Current Challenges When Working on Adipose Cells. Int J Mol Sci. 2021 Jan;22(7):3362.

234. Müller G, Jung C, Straub J, Wied S, Kramer W. Induced release of membrane vesicles from rat adipocytes containing glycosylphosphatidylinositol-anchored microdomain and lipid droplet signalling proteins. Cell Signal. 2009 Feb;21(2):324–38.

235. Müller G, Jung C, Wied S, Biemer-Daub G. Induced translocation of glycosylphosphatidylinositol-anchored proteins from lipid droplets to adiposomes in rat adipocytes. Br J Pharmacol. 2009 Oct;158(3):749–70.

236. Akbar N, Pinnick KE, Paget D, Choudhury RP. Isolation and Characterization of Human Adipocyte-Derived Extracellular Vesicles using Filtration and Ultracentrifugation. J Vis Exp. 2021 Apr 19;(170):61979.

237. Gould SJ, Raposo G. As we wait: coping with an imperfect nomenclature for

extracellular vesicles. J Extracell Vesicles. 2013;2.

238. Crescitelli R, Lässer C, Lötvall J. Isolation and characterization of extracellular vesicle subpopulations from tissues. Nat Protoc. 2021 Mar;16(3):1548–80.

239. Minciacchi VR, Freeman MR, Di Vizio D. Extracellular Vesicles in Cancer: Exosomes, Microvesicles and the Emerging Role of Large Oncosomes. Semin Cell Dev Biol. 2015 Apr 1;40:41–51.

240. Zhang Q, Higginbotham JN, Jeppesen DK, Yang YP, Li W, McKinley ET, et al. Transfer of Functional Cargo in Exomeres. Cell Rep. 2019 Apr 16;27(3):940-954.e6.

241. Arner P. Differences in Lipolysis between Human Subcutaneous and Omental Adipose Tissues. Ann Med. 1995 Jan 1;27(4):435–8.

242. Maffei M, Halaas J, Ravussin E, Pratley RE, Lee GH, Zhang Y, et al. Leptin levels in human and rodent: Measurement of plasma leptin and ob RNA in obese and weight-reduced subjects. Nat Med. 1995 Nov;1(11):1155–61.

243. Friedman J. 20 YEARS OF LEPTIN: Leptin at 20: an overview. J Endocrinol. 2014 Oct 1;223(1):T1–8.

244. Kadowaki T, Yamauchi T. Adiponectin and Adiponectin Receptors. Endocr Rev. 2005 May 1;26(3):439–51.

245. Yamauchi T, Kamon J, Waki H, Terauchi Y, Kubota N, Hara K, et al. The fat-derived hormone adiponectin reverses insulin resistance associated with both lipoatrophy and obesity. Nat Med. 2001 Aug;7(8):941–6.

246. Garin-Shkolnik T, Rudich A, Hotamisligil GS, Rubinstein M. FABP4 Attenuates PPARγ and Adipogenesis and Is Inversely Correlated With PPARγ in Adipose Tissues. Diabetes. 2014 Feb 13;63(3):900–11.

247. Wu LE, Samocha-Bonet D, Whitworth PT, Fazakerley DJ, Turner N, Biden TJ, et al. Identification of fatty acid binding protein 4 as an adipokine that regulates insulin secretion during obesity. Mol Metab. 2014 Jul 1;3(4):465–73.

248. Dang SY, Leng Y, Wang ZX, Xiao X, Zhang X, Wen T, et al. Exosomal transfer of obesity adipose tissue for decreased miR-141-3p mediate insulin resistance of hepatocytes. Int J Biol Sci. 2019 Jan 1;15(2):351–68.

249. Pan Y, Hui X, Hoo RLC, Ye D, Chan CYC, Feng T, et al. Adipocyte-secreted exosomal microRNA-34a inhibits M2 macrophage polarization to promote obesity-induced adipose inflammation. J Clin Invest. 2019 Feb 1;129(2):834–49.

250. Boilard E. Extracellular vesicles and their content in bioactive lipid mediators: more than a sack of microRNA. J Lipid Res. 2018 Nov;59(11):2037–46.

251. Bargut TCL, Souza-Mello V, Aguila MB, Mandarim-de-Lacerda CA. Browning of white adipose tissue: lessons from experimental models. Horm Mol Biol Clin Investig. 2017 Jul 1;31(1).

252. Kim MS, Muallem S, Kim SH, Kwon KB, Kim MS. Exosomal release through TRPML1-mediated lysosomal exocytosis is required for adipogenesis. Biochem Biophys Res Commun. 2019 Mar 12;510(3):409–15.

253. Eguchi A, Mulya A, Lazic M, Radhakrishnan D, Berk MP, Povero D, et al. Microparticles Release by Adipocytes Act as “Find-Me” Signals to Promote Macrophage Migration. PLOS ONE. 2015 Jul 4;10(4):e0123110.

254. Liu T, Sun YC, Cheng P, Shao HG. Adipose tissue macrophage-derived exosomal miR-29a regulates obesity-associated insulin resistance. Biochem Biophys Res Commun. 2019 Jul 23;515(2):352–8.

255. Zhang Y, Shi L, Mei H, Zhang J, Zhu Y, Han X, et al. Inflamed macrophage microvesicles induce insulin resistance in human adipocytes. Nutr Metab. 2015 Jun 6;12(1):21.

256. Haney MJ, Klyachko NL, Harrison EB, Zhao Y, Kabanov AV, Batrakova EV. TPP1 Delivery to Lysosomes with Extracellular Vesicles and their Enhanced Brain Distribution in the Animal Model of Batten Disease. Adv Healthc Mater. 2019;8(11):1801271.

257. Zhou X, Li Z, Sun W, Yang G, Xing C, Yuan L. Delivery Efficacy Differences of Intravenous and Intraperitoneal Injection of Exosomes: Perspectives from Tracking Dye Labeled and MiRNA Encapsulated Exosomes. Curr Drug Deliv. 2020 Apr 26;17(3):186–94.

258. Wiklander OPB, Nordin JZ, O’Loughlin A, Gustafsson Y, Corso G, Mäger I, et al. Extracellular vesicle in vivo biodistribution is determined by cell source, route of administration and targeting. J Extracell Vesicles. 2015 Jan 1;4(1):26316.

259. Ferguson SW, Nguyen J. Exosomes as therapeutics: The implications of molecular composition and exosomal heterogeneity. J Controlled Release. 2016 Apr 28;228:179–90.

260. Takov K, Yellon DM, Davidson SM. Confounding factors in vesicle uptake studies using fluorescent lipophilic membrane dyes. J Extracell Vesicles. 2017 Dec 1;6(1):1388731.

261. Kahn DE, Bergman BC. Keeping It Local in Metabolic Disease: Adipose Tissue Paracrine Signaling and Insulin Resistance. Diabetes. 2022 Mar 22;71(4):599–609.

262. Singh RG, Yoon HD, Wu LM, Lu J, Plank LD, Petrov MS. Ectopic fat accumulation in the pancreas and its clinical relevance: A systematic review, meta-analysis, and meta-

regression. Metabolism. 2017 Apr 1;69:1–13.

263. Saint-Pol J, Gosselet F, Duban-Deweer S, Pottiez G, Karamanos Y. Targeting and Crossing the Blood-Brain Barrier with Extracellular Vesicles. Cells. 2020 Apr;9(4):851.

264. Elsharkasy OM, Nordin JZ, Hagey DW, de Jong OG, Schiffelers RM, Andaloussi SE, et al. Extracellular vesicles as drug delivery systems: Why and how? Adv Drug Deliv Rev. 2020 Jan 1;159:332–43.

265. Banks WA, Sharma P, Bullock KM, Hansen KM, Ludwig N, Whiteside TL. Transport of Extracellular Vesicles across the Blood-Brain Barrier: Brain Pharmacokinetics and Effects of Inflammation. Int J Mol Sci. 2020 Jun 21;21(12):4407.

266. Ramos-Zaldívar HM, Polakovicova I, Salas-Huenuleo E, Corvalán AH, Kogan MJ, Yefi CP, et al. Extracellular vesicles through the blood–brain barrier: a review. Fluids Barriers CNS. 2022 Jul 25;19(1):60.

267. Chen CC, Liu L, Ma F, Wong CW, Guo XE, Chacko JV, et al. Elucidation of Exosome Migration Across the Blood–Brain Barrier Model In Vitro. Cell Mol Bioeng. 2016 Dec 1;9(4):509–29.

268. Gupta D, Liang X, Pavlova S, Wiklander OPB, Corso G, Zhao Y, et al. Quantification of extracellular vesicles in vitro and in vivo using sensitive bioluminescence imaging. J Extracell Vesicles. 2020 Jan 1;9(1):1800222.

269. Zomer A, Maynard C, Verweij FJ, Kamermans A, Schäfer R, Beerling E, et al. In Vivo Imaging Reveals Extracellular Vesicle-Mediated Phenocopying of Metastatic Behavior. Cell. 2015 May 21;161(5):1046–57.

270. Gesmundo I, Pardini B, Gargantini E, Gamba G, Birolo G, Fanciulli A, et al. Adipocyte-derived extracellular vesicles regulate survival and function of pancreatic β cells. JCI Insight. 2021 Mar 8;6(5):141962.

271. Nguyen MA, Karunakaran D, Geoffrion M, Cheng HS, Tandoc K, Perisic Matic L, et al. Extracellular Vesicles Secreted by Atherogenic Macrophages Transfer MicroRNA to Inhibit Cell Migration. Arterioscler Thromb Vasc Biol. 2018 Jan;38(1):49–63.

272. Menck K, Sönmezer C, Worst TS, Schulz M, Dihazi GH, Streit F, et al. Neutral sphingomyelinases control extracellular vesicles budding from the plasma membrane. J Extracell Vesicles. 2017 Dec 1;6(1):1378056.

273. Mathieu M, Névo N, Jouve M, Valenzuela JI, Maurin M, Verweij FJ, et al. Specificities of exosome versus small ectosome secretion revealed by live intracellular tracking of CD63 and CD9. Nat Commun. 2021 Jul 19;12(1):4389.

274. Colombo M, Raposo G, Théry C. Biogenesis, Secretion, and Intercellular Interactions of Exosomes and Other Extracellular Vesicles. Annu Rev Cell Dev Biol. 2014 Oct 11;30(1):255–89.

275. Zumbansen M, Stoffel W. Neutral Sphingomyelinase 1 Deficiency in the Mouse Causes No Lipid Storage Disease. Mol Cell Biol. 2002 Jun;22(11):3633–8.

276. Homma Y, Hiragi S, Fukuda M. Rab family of small GTPases: an updated view on their regulation and functions. FEBS J. 2021;288(1):36–55.

277. Kobayashi Y, Eguchi A, Tempaku M, Honda T, Togashi K, Iwasa M, et al. Circulating extracellular vesicles are associated with lipid and insulin metabolism. Am J Physiol Endocrinol Metab. 2018 Oct 1;315(4):E574–82.

278. Garcia-Contreras M, Brooks RW, Boccuzzi L, Robbins PD, Ricordi C. Exosomes as biomarkers and therapeutic tools for type 1 diabetes mellitus. Eur Rev Med Pharmacol Sci. 2017 Jun;21(12):2940–56.

279. Wajchenberg BL. Subcutaneous and Visceral Adipose Tissue: Their Relation to the Metabolic Syndrome. Endocr Rev. 2000 Dec 1;21(6):697–738.

280. Magkos F, Fraterrigo G, Yoshino J, Luecking C, Kirbach K, Kelly SC, et al. Effects of Moderate and Subsequent Progressive Weight Loss on Metabolic Function and Adipose Tissue Biology in Humans with Obesity. Cell Metab. 2016 Apr 12;23(4):591–601.

281. Tóth EÁ, Turiák L, Visnovitz T, Cserép C, Mázló A, Sódar BW, et al. Formation of a protein corona on the surface of extracellular vesicles in blood plasma. J Extracell Vesicles. 2021 Sep;10(11):e12140.

282. Wolf M, Poupardin RW, Ebner-Peking P, Andrade AC, Blöchl C, Obermayer A, et al. A functional corona around extracellular vesicles enhances angiogenesis, skin regeneration and immunomodulation. J Extracell Vesicles. 2022 Apr;11(4):e12207.

283. Gomes FG, Andrade AC, Wolf M, Hochmann S, Krisch L, Maeding N, et al. Synergy of Human Platelet-Derived Extracellular Vesicles with Secretome Proteins Promotes Regenerative Functions. Biomedicines. 2022 Jan 23;10(2):238.

284. Rai A, Fang H, Claridge B, Simpson RJ, Greening DW. Proteomic dissection of large extracellular vesicle surfaceome unravels interactive surface platform. J Extracell Vesicles. 2021;10(13):e12164.

285. Lee JE, Moon PG, Lee IK, Baek MC. Proteomic Analysis of Extracellular Vesicles Released by Adipocytes of Otsuka Long-Evans Tokushima Fatty (OLETF) Rats. Protein J. 2015 Jun 1;34(3):220–35.

286. Anand S, Foot N, Ang CS, Gembus KM, Keerthikumar S, Adda CG, et al. Arrestin-Domain Containing Protein 1 (Arrdc1) Regulates the Protein Cargo and Release of Extracellular Vesicles. PROTEOMICS. 2018;18(17):1800266.

287. Bour S, Daviaud D, Gres S, Lefort C, Prévot D, Zorzano A, et al. Adipogenesis-related increase of semicarbazide-sensitive amine oxidase and monoamine oxidase in human adipocytes. Biochimie. 2007 Aug 1;89(8):916–25.

288. Tissue expression of AOC3 - Summary - The Human Protein Atlas [Internet]. [cited 2022 Oct 29]. Available from: https://www.proteinatlas.org/ENSG00000131471-AOC3/tissue

289. Enrique-Tarancón G, Marti L, Morin N, Lizcano J, Unzeta M, Sevilla L, et al. Role of Semicarbazide-sensitive Amine Oxidase on Glucose Transport and GLUT4 Recruitment to the Cell Surface in Adipose Cells*. J Biol Chem. 1998 Apr 3;273(14):8025–32.

290. Yang H, Ralle M, Wolfgang MJ, Dhawan N, Burkhead JL, Rodriguez S, et al. Copper-dependent amino oxidase 3 governs selection of metabolic fuels in adipocytes. PLOS Biol. 2018 Oct 9;16(9):e2006519.

291. Tékus V, Horváth ÁI, Csekő K, Szabadfi K, Kovács-Valasek A, Dányádi B, et al. Protective effects of the novel amine-oxidase inhibitor multi-target drug SZV 1287 on streptozotocin-induced beta cell damage and diabetic complications in rats. Biomed Pharmacother. 2021 Feb 1;134:111105.

292. Boyer DS, Rippmann JF, Ehrlich MS, Bakker RA, Chong V, Nguyen QD. Amine oxidase copper-containing 3 (AOC3) inhibition: a potential novel target for the management of diabetic retinopathy. Int J Retina Vitr. 2021 Apr 12;7(1):30.

293. Andreu Z, Yáñez-Mó M. Tetraspanins in Extracellular Vesicle Formation and Function. Front Immunol. 2014;5.

294. Ferreira JV, da Rosa Soares A, Ramalho J, Máximo Carvalho C, Cardoso MH, Pintado P, et al. LAMP2A regulates the loading of proteins into exosomes. Sci Adv. 2022 Mar 25;8(12):eabm1140.

295. Eskelinen EL. Roles of LAMP-1 and LAMP-2 in lysosome biogenesis and autophagy. Mol Aspects Med. 2006 Oct 1;27(5):495–502.

296. Divoux A, Clément K. Architecture and the extracellular matrix: the still unappreciated components of the adipose tissue. Obes Rev. 2011;12(5):e494–503.

297. COL6A1 Gene - GeneCards | CO6A1 Protein | CO6A1 Antibody [Internet]. [cited 2022 Oct 23]. Available from: https://www.genecards.org/cgi-bin/carddisp.pl?gene=COL6A1

298. Khan T, Muise ES, Iyengar P, Wang ZV, Chandalia M, Abate N, et al. Metabolic

Dysregulation and Adipose Tissue Fibrosis: Role of Collagen VI. Mol Cell Biol. 2009 Mar 15;29(6):1575–91.

299. Pasarica M, Gowronska-Kozak B, Burk D, Remedios I, Hymel D, Gimble J, et al. Adipose Tissue Collagen VI in Obesity. J Clin Endocrinol Metab. 2009 Dec 1;94(12):5155–62.

300. Roca-Rivada A, Belen Bravo S, Pérez-Sotelo D, Alonso J, Isabel Castro A, Baamonde I, et al. CILAIR-Based Secretome Analysis of Obese Visceral and Subcutaneous Adipose Tissues Reveals Distinctive ECM Remodeling and Inflammation Mediators. Sci Rep. 2015 Jul 22;5(1):12214.

301. Sharma M, Liu W, Perincheri S, Gunasekaran M, Mohanakumar T. Exosomes expressing the self-antigens myosin and vimentin play an important role in syngeneic cardiac transplant rejection induced by antibodies to cardiac myosin. Am J Transplant. 2018;18(7):1626–35.

302. Adolf A, Rohrbeck A, Münster-Wandowski A, Johansson M, Kuhn HG, Kopp MA, et al. Release of astroglial vimentin by extracellular vesicles: Modulation of binding and internalization of C3 transferase in astrocytes and neurons. Glia. 2019;67(4):703–17.

303. Parvanian S, Zha H, Su D, Xi L, Jiu Y, Chen H, et al. Exosomal Vimentin from Adipocyte Progenitors Protects Fibroblasts against Osmotic Stress and Inhibits Apoptosis to Enhance Wound Healing. Int J Mol Sci. 2021 Jan;22(9):4678.

304. Connolly KD, Wadey RM, Mathew D, Johnson E, Rees DA, James PE. Evidence for Adipocyte-Derived Extracellular Vesicles in the Human Circulation. Endocrinology. 2018 Sep 1;159(9):3259–67.

305. Sódar BW, Kittel Á, Pálóczi K, Vukman KV, Osteikoetxea X, Szabó-Taylor K, et al. Low-density lipoprotein mimics blood plasma-derived exosomes and microvesicles during isolation and detection. Sci Rep. 2016 Jul;6(1):24316.

306. Karimi N, Cvjetkovic A, Jang SC, Crescitelli R, Hosseinpour Feizi MA, Nieuwland R, et al. Detailed analysis of the plasma extracellular vesicle proteome after separation from lipoproteins. Cell Mol Life Sci. 2018 Aug 1;75(15):2873–86.

307. Newman LA, Muller K, Rowland A. Circulating cell-specific extracellular vesicles as biomarkers for the diagnosis and monitoring of chronic liver diseases. Cell Mol Life Sci. 2022 Apr 10;79(5):232.

308. Madden LA, Vince RV, Sandström ME, Taylor L, McNaughton L, Laden G. Microparticle-associated vascular adhesion molecule-1 and tissue factor follow a circadian rhythm in healthy human subjects. Thromb Haemost. 2008;99(11):909–15.

309. Frühbeis C, Helmig S, Tug S, Simon P, Krämer-Albers EM. Physical exercise induces rapid release of small extracellular vesicles into the circulation. J Extracell Vesicles. 2015 Jan 1;4(1):28239.

310. György B, Pálóczi K, Kovács A, Barabás E, Bekő G, Várnai K, et al. Improved circulating microparticle analysis in acid-citrate dextrose (ACD) anticoagulant tube. Thromb Res. 2014 Feb 1;133(2):285–92.

311. Kapogiannis D, Eren E, Hunt JFV, Shardell M, Vogt NM, Johnson SC, et al. Plasma extracellular vesicles of neuronal and astrocytic origins: Biomarker carriers and pathogenic effectors in Alzheimer's disease. Alzheimers Dement. 2020;16(S2):e037317.

312. Eren E, Leoutsakos JM, Troncoso J, Lyketsos CG, Oh ES, Kapogiannis D. Neuronal-Derived EV Biomarkers Track Cognitive Decline in Alzheimer's Disease. Cells. 2022 Jan;11(3):436.

313. Labayen I. Prevention of Diabetes in Overweight/Obese Preadolescent Children Through a Family-based Intervention Program Including Supervised Exercise; the PREDIKID Study [Internet]. clinicaltrials.gov; 2020 Nov [cited 2022 Oct 25]. Report No.: NCT03027726. Available from: https://clinicaltrials.gov/ct2/show/NCT03027726

314. Muraoka S, Hirano M, Isoyama J, Nagayama S, Tomonaga T, Adachi J. Comprehensive proteomic profiling of plasma and serum phosphatidylserine-positive extracellular vesicles reveals tissue-specific proteins. iScience. 2022 Apr 15;25(4):104012.

315. Li Y, He X, Li Q, Lai H, Zhang H, Hu Z, et al. EV-origin: Enumerating the tissue-cellular origin of circulating extracellular vesicles using exLR profile. Comput Struct Biotechnol J. 2020;18:2851–9.

316. Sun X, Feng X, Wu X, Lu Y, Chen K, Ye Y. Fat Wasting Is Damaging: Role of Adipose Tissue in Cancer-Associated Cachexia. Front Cell Dev Biol. 2020;8.

317. Argilés JM, Stemmler B, López-Soriano FJ, Busquets S. Inter-tissue communication in cancer cachexia. Nat Rev Endocrinol. 2019 Jan;15(1):9–20.

318. Henriques F, Júnior MLB. Adipose Tissue Remodeling during Cancer-Associated Cachexia: Translational Features from Adipose Tissue Dysfunction. Immunometabolism. 2020 Sep 10;4(3).

319. Mori MA, Ludwig RG, Garcia-Martin R, Brandão BB, Kahn CR. Extracellular miRNAs: From Biomarkers to Mediators of Physiology and Disease. Cell Metab. 2019 Oct 1;30(4):656–73.

6 Appendix

A: Supplemental Data

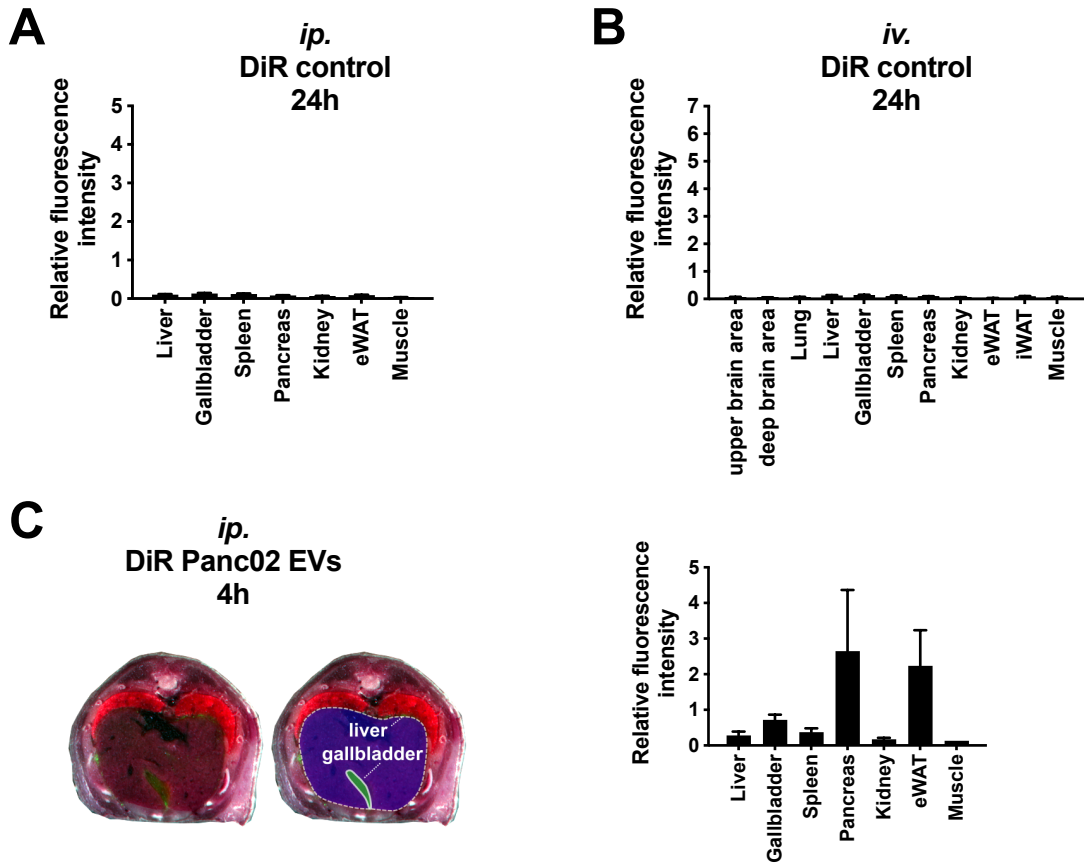

Figure S 1: Tissue specific uptake of ip. and iv. injected fluorescently labelled DiR controls and Panc02 EVs in mice. *Relative quantifications of fluorescence intensities between the target organs (A-C) and representative cross-sections of multiscale and multispectral images of the whole cryosliced mouse torso along the axial planes after colour and fluorescence image (C) of mice ip. injected with (**A**) DiR-control 24 h after ip. injection and (**B**) DiR-control 24 h after iv. injection. (**C**) shows images and quantification of mice ip. injected with DiR-labelled Panc02 EVs 4 h after injection. Images are shown as unlabelled (left) and overlaid with organ labels (right). Three representative slices per animal (n=2) were selected for quantification. Data represent organs with detectable signals only and are shown as mean ± SD.*

Table S 1: Significantly enriched KEGG pathways (p<0.05) of differing proteins isolated from eWAT EVs or eWAT tissue lysates from lean and DIO mice.

Pathway	eWAT EVs DIO vs. lean		eWAT lysate DIO vs. lean	
	p-value	# hits	p-value	# hits
Ribosome	5.22266E-09	34	1.61726E-06	17
Peroxisome	1.56047E-06	19	0.005882251	7
Alzheimer's disease	8.0422E-06	31	0.178933196	5
PPAR signalling pathways	3.44724E-05	18	0.150619456	4
Huntington's disease	8.19923E-05	29	0.180227182	5
Steroid hormone biosynthesis	0.000156762	8	0.378969583	1
Fatty acid metabolism	0.000163716	15	1	0
Citrate cycle (TCA cycle)	0.000275595	14	0.034229958	5
ECM-receptor interaction	0.000465711	16	1	0
Cell adhesion molecules (CAMs)	0.000783874	12	1	0
Protein processing in ER	0.000869557	23	0.1674602	3
Parkinson's disease	0.001099318	24		
Metabolic pathways	0.001343794	109	0.001026566	48
Small cell lung cancer	0.001515921	8	0.381285041	1
Hematopoietic cell lineage	0.002246284	10	1	0
Fat digestion and absorption	0.002592001	7	1	0
Renin-angiotensin system	0.002630528	8	0.37829517	1
Glycerophospholipid metabolism	0.002868735	11	1	0
Phagosome	0.002904001	23	0.029844672	1
Non-alcoholic fatty liver disease	0.002969891	19	0.155470112	2
Toxoplasmosis	0.00333598	10	0.33664478	1
Fatty acid biosynthesis	0.005479969	4	1	0
Steroid biosynthesis	0.005479969	4	1	0
Oxidative phosphorylation	0.005855414	22	0.08035104	2
Carbon metabolism	0.006625381	26	3.19501E-07	21
Serotonergic synapse	0.009493476	8	0.368170193	1
Hypertrophic cardiomyopathy (HCM)	0.009586977	11	0.266742894	1
Spliceosome	0.011455043	1	0.256557106	1
Arrhythmogenic right ventricular cardiomyopathy (ARVC)	0.011788334	10	0.317590898	1
Dilated cardiomyopathy	0.012258978	11	0.256557106	1
Amoebiasis	0.01241947	13	0.224788575	3
Viral myocarditis	0.0132738	8	0.361445398	1
Glycerolipid metabolism	0.014518014	9	0.33664478	1
Propanoate metabolism	0.018803839	9	0.151156474	3
RNA transport	0.019697404	1	0.287265221	1
Complement and coagulation cascades	0.020342625	5	0.001291138	11
Tryptophan metabolism	0.023410722	8	0.252880978	2
Cocaine addiction	0.025095709	4	1	0
Fatty acid degradation	0.027590937	11	0.271253294	2
Cardiac muscle contraction	0.028641077	10	1	0
Tuberculosis	0.029217271	13	0.227006026	2
Lysine degradation	0.029274429	7	0.235215428	2
Ascorbate and aldarate metabolism	0.03354544	5	1	0
Linoleic acid metabolism	0.036932042	2	1	0
Taste transduction	0.036932042	2	1	0
Thyroid hormone synthesis	0.037501979	7	1	0
Protein export	0.040590979	4	1	0
alpha-Linolenic acid metabolism	0.046288005	3	1	0
Amino sugar and nucleotide sugar metabolism	0.046337648	2	0.190504549	3
Biosynthesis of unsaturated fatty acids	0.046512246	5	1	0
Neurotrophin signalling pathway	0.047123933	1	0.345537309	1
Retinol metabolism	0.047622869	6	0.21306655	2
Antigen processing and presentation	0.049995734	9	1	0
Biosynthesis of amino acids	0.136934806	10	5.17066E-05	13
Aminoacyl-tRNA biosynthesis	1	0	0.000106873	7
Pertussis	0.196112642	5	0.001261694	7
Pentose phosphate pathway	0.189545637	3	0.002595702	6
Terpenoid backbone biosynthesis	0.281322171	1	0.003161081	4
Legionellosis	0.085355183	6	0.006812948	5
Fructose and mannose metabolism	0.175943982	3	0.014849994	5
Staphylococcus aureus infection	0.2101675	4	0.014849994	5
2-Oxocarboxylic acid metabolism	0.10967691	5	0.017888165	4
Folate biosynthesis	1	0	0.024416991	3
Central carbon metabolism in cancer	0.211244634	4	0.026085896	4
Glyoxylate and dicarboxylate metabolism	0.072217433	6	0.030771152	4
PI3K-Akt signalling pathway	0.060260827	5	0.033636687	1
Galactose metabolism	0.150038261	2	0.035819255	4
Arginine biosynthesis	1	0	0.038806438	3

B: Materials and laboratory eqipment

Chemicals and reagents

1-Step™ Ultra TMB-ELISA substrate	Thermo Fisher Scientific Inc., Waltham, MA, USA
Alexa Fluor 488 antibody (anti-mouse and anti-rat)	Dianova, Hamburg, Germany
Biotin	Sigma-Aldrich, St. Louis, MO, USA
BSA	Sigma-Aldrich, St. Louis, MO, USA
BSA fatty acid free	Sigma-Aldrich, St. Louis, MO, USA
BSA low endotoxin	Sigma-Aldrich, St. Louis, MO, USA
BSA standard (2 mg/ml)	Thermo Fisher Scientific Inc., Waltham, MA, USA
Clarity™ Western ECL Substrate	Bio-Rad Laboratories Inc., Hercules, CA, USA
Collagenase IV	Gibco, Waltham, MA, USA
Collagenase P	Roche, Basel, Switzerland
Collagen coating solution	Cell Applications, Inc., San Diego, CA, USA
cOmplete Mini Protease Inhibitor cocktail tablets (EDTA free)	Roche, Basel, Switzerland
Cortisol	Sigma-Aldrich, St. Louis, MO, USA
CpG oligonucleotides	TIB MOLBIOL, Berlin, Germany
CNBr-activated sepharose™ 4 fast flow	GE-Healthcare, Chicago, IL, USA
Cytochalasin D	Sigma-Aldrich, St. Louis, MO, USA
Dexamethasone	Sigma-Aldrich, St. Louis, MO, USA
DiR	Biotium, Fremont, CA, USA
DMSO	Carl Roth, Karlsruhe, Germany
EDTA	Lonza, Basel, Switzerland
ExoQuick®	System Biosciences, Palo Alto, CA, USA
FBS	Gibco, Waltham, MA, USA
Ficoll-Paque	GE-Healthcare, Chicago, IL, USA
Gentamicin	Gibco, Waltham, MA, USA
GW4869	Sigma-Aldrich, St. Louis, MO, USA
Halt™ Protease & Phosphatase Inhibitor Cocktail	Thermo Fisher Scientific Inc., Waltham, MA, USA
HBSS	Gibco, Waltham, MA, USA

HEPES	Gibco, Waltham, MA, USA
Hybridoma cloning factor	Capricorn Scientific GmbH, Ebsdorfergrund, Germany
Hypoxantin-aminopterin supplement	Thermo Fischer Scientific, Inc., Waltham, MA, USA
IBMX	Sigma-Aldrich, St. Louis, MO, USA
Insulin (human)	Sigma-Aldrich, St. Louis, MO, USA
Insulin (murine)	Sigma-Aldrich, St. Louis, MO, USA
Interferon gamma	R & D Systems, Minneapolis, MN, USA
Interleukin 4	R & D Systems, Minneapolis, MN, USA
Isoproterenol	Sigma-Aldrich, St. Louis, MO, USA
L-Glutamine	Gibco, Waltham, MA, USA
MEM non-essential amino acids	Gibco, Waltham, MA, USA
β-mercaptoethanol	Carl Roth, Karlsruhe, Germany
Normocin	InvivoGen, San Diego, CA, USA
NuPAGE™ LDS Sample Buffer	Thermo Fischer Scientific, Inc., Waltham, MA, USA
PageRuler™ prestained protein ladder	Thermo Fischer Scientific, Inc., Waltham, MA, USA
Pantothenate	Sigma-Aldrich, St. Louis, MO, USA
PBS	Gibco, Waltham, MA, USA
Penicillin/ Streptomycin	Gibco, Waltham, MA, USA
pHrodo™ BioParticles® Conjugates	Thermo Fischer Scientific, Inc., Waltham, MA, USA
Ponceau S	PanReac AppliChem, Glenview, IL, USA
Primer pairs	Sigma-Aldrich, St. Louis, MO, USA
QIAzol	Qiagen, Hilden, Germany
Rosiglitazone	Cayman Chemical, Ann Arbor, MI, USA
Skimmed milk powder	Sigma-Aldrich, St. Louis, MO, USA
Sodium pyruvate	Lonza, Basel, Switzerland
SYBR Green PCR Master Mix	Applied Biosystems, Waltham, MA, USA
TaqMan probes	Applied Biosystems, Waltham, MA, USA
TaqMan Universal PCR Master Mix	Applied Biosystems, Waltham, MA, USA
Transferrin	Gibco, Waltham, MA, USA
Triiodothyronine (T_3)	Sigma-Aldrich, St. Louis, MO, USA

Tris/Glycine/SDS-electrophoresis buffer	BioRad Laboratories, Inc., Hercules, CA, USA
TRIzol	Thermo Fisher Scientific Inc., Waltham, MA, USA
Trypsin-EDTA solution (0.05 %)	Gibco, Waltham, MA, USA
Uranyl acetate	Merck KGaA, Darmstadt, Germany

Cell culture media

DMEM/F-12 GlutaMAX™	Gibco, Waltham, MA, USA
DMEM high glucose (4.5 g/l), pyruvate (1 mM), L-glutamine (4 mM)	Gibco, Waltham, MA, USA
DMEM high glucose (4.5 g/l), GlutaMAX™ supplement, pyruvate (1 mM)	Gibco, Waltham, MA, USA
EGM™-2 Medium	Lonza, Basel, Switzerland
Human skeletal muscle cell differentiation medium	Cell Applications, Inc., San Diego, CA, USA
Human skeletal muscle cell growth medium	Cell Applications, Inc., San Diego, CA, USA
IMDM	Gibco, Waltham, MA, USA
McCoy's 5A medium	Gibco, Waltham, MA, USA
RPMI 1640 (ATCC Modification)	Gibco, Waltham, MA, USA

Kits and assays

BCA Protein Assay Reagent A and B	Thermo Fisher Scientific Inc., Waltham, MA, USA
5' Rapid amplification of cDNA ends (RACE)-PCR Kit	Invitrogen, Waltham, MA, USA
Ultra Sensitive Mouse Insulin ELISA Kit	Crystal Chem, Elk Grove Village, IL, USA
QuantiTect® Reverse Transcription Kit	Qiagen, Hilden, Germany
QIAquick® Gel Extraction Kit	Qiagen, Hilden, Germany
Rneasy® Mini Kit	Qiagen, Hilden, Germany

Laboratory equipment and consumables

Cell culture flasks (25 cm², 75 cm², 175 cm²)	Sarstedt, Nümbrecht, Germany
Cell culture plates (6, 12, 24 well)	Corning Inc., Corning, NY, USA
Cell culture plates glass bottom (96-well)	Greiner Bio-One, Kremsmünster, Austria
Criterion™ Blotter	BioRad Laboratories, Inc., Hercules, CA, USA
Criterion™ TGX™ 12% precast gel	BioRad Laboratories, Inc., Hercules, CA, USA
Criterion™ Vertical Electrophoresis Cell	BioRad Laboratories, Inc., Hercules, CA, USA
Cryotome CM 1950	Leica Microsystems, Wetzlar, Germany
Cryo tubes (CryoPure, 1.6 ml)	Sarstedt, Nümbrecht, Germany
EM grids, formvar- carbon coated, 200 mesh Copper	Plano GmbH, Wetzlar, Germany
Exo-spin™ columns	Cell Guidance Systems Ltd, Cambridge, UK
Freestyle Freedom Lite glucometer	Abbott, Chigaco, USA
Heated shaker Lab Companion SI-600	Jeiotech, Seoul, Korea
Heraeus™ Multifuge™ X3R Centrifuge	Thermo Fisher Scientific Inc., Waltham, MA, USA
iTEM software	Olympus Soft Imaging Solutions GmbH, Münster, Germany
Keyence BZ-9000E fluorescence microscope	Keyence Corporation, Osaka, Japan
Mastercycler® pro	Eppendorf, Hamburg, Germany
MicroAmp® Adhesive Film	Applied Biosystems, Waltham, MA, USA
Microvette EDTA-coated	Sarstedt, Nümbrecht, Germany
Monovette heparinized	Sarstedt, Nümbrecht, Germany
NanoDrop 2000 Spectrophotometer	Thermo Fisher Scientific Inc., Waltham, MA, USA
Nitrocellulose membrane (Whatman® Protran® BA85)	GE Healthcare, Chicago, IL, USA
Non-tissue culture treated petri dishes	Greiner Bio-One, Kremsmünster, Austria
Odyssey® Fc Imaging System	LI-COR, Inc., Lincoln, NE, USA
Optima™ MAX-XP ultracentrifuge	Beckman Coulter Inc., Brea, CA, USA
Optima™ L-70 ultracentrifuge	Beckman Coulter Inc., Brea, CA, USA
PCR plates (384 well)	Thermo Fisher Scientific Inc., Waltham, MA, USA
PCR- SoftStrips, 0.2 ml	Biozym Scientific, Oldendorf, Germany
PHERAStar FS microplate reader	BMG LABTECH GmbH, Ortenberg, Germany
Protein G-Sepharose 4 Fast Flow columns	GE Healthcare, Chicago, IL, USA

PVDF membrane Immobilon™-P, pore size 0.45 µm	Merck KGaA, Darmstadt, Germany
Reaction tubes (1.5, 2, 15, 50, 120 ml)	Sarstedt, Nümbrecht, Germany
Serological pipettes (5, 10, 25, 50 ml)	Sarstedt, Nümbrecht, Germany
Suspension dishes	Sarstedt, Nümbrecht, Germany
TC10™ automated cell counter	Bio-Rad Laboratories Inc., Hercules, CA, USA
Thermal shaker Thermomixer comfort	Eppendorf, Hamburg, Germany
TissueLyser	Qiagen, Hilden, Germany
Ultracentrifugation tubes	Beckman Coulter Inc., Brea, CA, USA
Ultrasonic Homogenizer 150 VT	BioLogics Inc., Manassas, VA, USA
V-bottom plate (96-well)	Thermo Fisher Scientific Inc., Waltham, MA, USA
ViiA™ 7 Real-Time PCR System	Applied Biosystems, Waltham, MA, USA
Whatman® Minifold I Dot-Blot System	GE Healthcare, Chicago, IL, USA
Zeiss Libra 120 Plus	Carl Zeiss NTS GmbH, Jena, Germany
Zetasizer Nano ZS	Malvern Instruments Ltd, Malvern, UK
ZetaView® Nanoparticle Tracking Analyzer PMX 110	Particle Metrix GmbH, Meerbusch, Germany

Acknowledgements

At this point, I would like to take the opportunity to express my gratitude to all the people who made this work and PhD thesis possible.

First and foremost, I want to thank Prof. Dr. Matthias Tschöp for giving me the great opportunity to do my PhD thesis at the IDO in this exceptional scientific surrounding and research environment. I am also deeply grateful to Prof. Dr. Paul Pfluger for taking over my official supervision and giving me the opportunity to finalize this thesis. Beyond, I want to thank Paul for his conceptional and scientific advice not only in the final phase but also during my whole PhD project.

I am deeply grateful to Prof. Dr. Kerstin Stemmer and Dr. Petra Kotzbeck for their outstanding supervision and continuous encouragement during my project. I would particularly like to thank Kerstin for her generous support over all the years, starting with acquiring funding of my PhD project, all the helpful discussions and scientific advice, and in the end for the support and encouragement to finalize and for proofreading the thesis. Thank you so much for being approachable for help and advice at any time!

A special thanks goes to Petra for her great support in numerous ways during my thesis. Thank you for your support inside and outside the lab, for all the helpful advice and for your time and encouragement. Thanks a lot for the austrian-bavarian connection 2.0!

A great thank you goes to the Metabolism and Cancer-group: Christina Neff and Fabio Zani (aka the unbeatable fantastic four), Peggy Dörfelt, Alexandra Harger, David Sailer and my new lab companion at UniA, Edward Milbank. Thanks a lot for your technical and personal support in the lab and office and for being not only colleagues but also friends.

I want to thank the whole IDO family for the help in various ways over all the years and the friendly and supportive working environment. I also want to thank Dr. Günter Müller for scientific advice in the EV field and for fruitful discussions. I would like to thank Aina Martin Medina for her friendly help with the DLS ZetaSizer measurements and Anett Selig for her great support with the islet isolation procedure.

A special thanks also goes to the fabulous Sugar Doctors. You showed me that being high class scientists and excellent musicians fits together perfectly and adds a beautiful colour to life. Thanks to you I was able to dive into a different world and get to know you not only on a professional level as outstanding scientists but also personally as awesome bandmates and friends. Thank you for all the great opportunities and fantastic moments you gave to me in and beyond science.

Finally, I want to thank my family, especially Veronika and Christoph. I am deeply grateful for your limitless support over all these years. You accompanied me through all the ups and downs of the lab life, helped me to overcome difficult phases and encouraged me again and again to finalize the thesis. A big hug for your never-ending care and love!

Eidesstattliche Erklärung

Ich, Michaela Bauer, erkläre an Eides statt, dass ich die bei der Fakultät für Medizin der TUM zur Promotionsprüfung vorgelegte Arbeit mit dem Titel

„The Role of Adipocyte-derived Extracellular Vesicles in Metabolic Diseases"

am Institut für Diabetes und Adipositas (Helmholtz Zentrum München) unter der Anleitung und Betreuung durch Prof. Dr. Pfluger ohne sonstige Hilfe erstellt und bei der Abfassung nur die gemäß § 7 Abs. 6 und 7 angegebenen Hilfsmittel benutzt habe.

Ich habe keine Organisation eingeschaltet, die gegen Entgelt Betreuer*innen für die Anfertigung von Dissertationen sucht, oder die mir obliegenden Pflichten hinsichtlich der Prüfungsleistungen für mich ganz oder teilweise erledigt.

Ich habe die Dissertation in dieser oder ähnlicher Form in keinem anderen Prüfungsverfahren als Prüfungsleistung vorgelegt.

Die Dissertation wurde noch nicht veröffentlicht.

Ich habe den angestrebten Doktorgrad noch nicht erworben und bin nicht in einem früheren Promotionsverfahren für den angestrebten Doktorgrad endgültig gescheitert.

Ich habe bisher an keiner Hochschule unter Vorlage einer Dissertation die Zulassung zur Promotion beantragt.

Ich habe keine Kenntnis über ein strafrechtliches Ermittlungsverfahren in Bezug auf wissenschaftsbezogene Straftaten gegen mich oder eine rechtskräftige strafrechtliche Verurteilung mit Wissenschaftsbezug.

Die öffentlich zugängliche Promotionsordnung sowie die Richtlinien zur Sicherung guter wissenschaftlicher Praxis und für den Umgang mit wissenschaftlichem Fehlverhalten der TUM sind mir bekannt, insbesondere habe ich die Bedeutung von § 27 PromO (Nichtigkeit der Promotion) und § 28 PromO (Entzug des Doktorgrades) zur Kenntnis genommen. Ich bin mir der Konsequenzen einer falschen Eidesstattlichen Erklärung bewusst.

Mit der Aufnahme meiner personenbezogenen Daten in die Alumni-Datei bei der TUM bin ich einverstanden.

Landshut, den 08.11.2022

Michaela Bauer

List of Publications

- Stemmer K, Kotzbeck P, Zani F, Bauer M, Neff C, Müller TD, Pfluger PT, Divanovic S. Thermoneutral housing is a critical factor for immune function and diet-induced obesity in C57BL/6 nude mice. International Journal of Obesity. 2014 39 (5), 791-797.

- Stemmer K, Zani F, Habegger KM, Neff C, Kotzbeck P, Bauer M, Yalamanchilli S, Lehti M, Martins PJF, Müller TD, Pfluger PT, Seeley RJ. FGF21 is not required for glucose homeostasis, ketosis and tumor suppression associated to ketogenic diets in mice. Diabetologia. 2015 58 (10), 2414-2423.

- Stemmer K, Tschöp MH, Bauer M, Zeidler R, Feederle R. Tissue-specific exosomes as biomarkers. International Patent Publication No.: WO2017/194499, International Publication Date: November 16, 2017.

- *Kulaj K, *Harger A, *Bauer M, *Caliskan ÖS, Gupta TK, Chiang D, Milbank E, Reber J, Karlas A, Kotzbeck P, Sailer DN, Volta F, Lutter D, Prakash S, Merl-Pham J, Ntziachristos V, Hauner H, Pfaffl MW, Tschöp MH, Müller TD, Hauck SM, Engel BD, Gerdes JM, Pfluger PT, Krahmer N, Stemmer K. Adipocyte-derived extracellular vesicles increase insulin secretion through transport of insulinotropic protein cargo. Nature Communications. 2023 14 (709).
  *equal contribution

Conference Presentations

- Bauer M, Kotzbeck P, Lutter D, Reber J, Merl-Pham J, Karlas A, Irmler M, Hauck SM, Tschöp MH, Stemmer K. Adipocyte exosomes as biomarkers for adipose tissue function and disease. Keystone Symposium New Therapeutics for Diabetes and Obesity, La Jolla, CA, 2016.

- Bauer M, Kotzbeck P, Lutter D, Reber J, Merl-Pham J, Karlas A, Irmler M, Hauck SM, Tschöp MH, Stemmer K. EV-based tissue communication and EVs as biomarkers in metabolic diseases. IGLD Symposium, Düsseldorf, 2017.